

# SENSITIVITY AND UNCERTAINTY ANALYSIS CAPABILITIES AND DATA IN SCALE

RADIATION PROTECTION

KEYWORDS: SCALE, sensitivity and uncertainty analysis, code and data validation

B. T. REARDEN,\* M. L. WILLIAMS, M. A. JESSEE, D. E. MUELLER,  
and D. A. WIARDA

Oak Ridge National Laboratory, Nuclear Science and Technology Division  
P.O. Box 2008, Building 5700, MS-6170, Oak Ridge, Tennessee 37831-6170

Received February 24, 2010

Accepted for Publication September 14, 2010

*In SCALE 6, the Tools for Sensitivity and UNcertainty Analysis Methodology Implementation (TSUNAMI) modules calculate the sensitivity of  $k_{eff}$  or reactivity differences to the neutron cross-section data on an energy-dependent, nuclide-reaction-specific basis. These sensitivity data are useful for uncertainty quantification, using the comprehensive neutron cross-section-covariance data in SCALE 6. Additional modules in SCALE 6 use the sensitivity and uncertainty data to produce correlation coef-*

*ficients and other relational parameters that quantify the similarity of benchmark experiments to application systems for code validation purposes. Bias and bias uncertainties are quantified using parametric trending analysis or data adjustment techniques, providing detailed assessments of sources of biases and their uncertainties and quantifying gaps in experimental data available for validation. An example application of these methods is presented for a generic burnup credit cask model.*

## I. INTRODUCTION

### I.A. Sensitivity Analysis and Uncertainty Quantification

Sensitivity analysis provides a unique insight into system performance in that the predicted response of the system to a change in some input process is quantified. Important processes can be identified as those that cause the largest changes in the response per unit change in the input. In neutron transport numerical simulations, two important responses are  $k_{eff}$  and reactivity, and their quantification requires many input parameters such as material compositions, system geometry, temperatures, and neutron cross-section data. Because of the complexity of nuclear data and its evaluation process, the response of neutron transport models to the cross-section data can provide valuable information to analysts. The SCALE 6 (Ref. 1) sensitivity and uncertainty (S/U) analysis sequences, known as the Tools for Sensitivity and UNcertainty Analysis Methodology Implementation (TSUNAMI) and developed at Oak Ridge National Laboratory (ORNL), quantify the predicted change in  $k_{eff}$  or reactivity differences due to changes in the energy-dependent, nuclide-reaction-specific cross-section data.

Where uncertainties in the neutron cross-section data are available, the sensitivity of the system to the cross-section data can be applied to propagate the uncertainties in the cross-section data to an uncertainty in the system response. Uncertainty quantification is useful for identifying potential sources of computational biases and highlighting parameters important to code validation.

### I.B. Validation of Codes and Data

Modern neutron transport codes, such as the KENO Monte Carlo codes<sup>2</sup> in the SCALE code system, can predict  $k_{eff}$  with a high degree of precision. Still, computational biases of a percent or more are often found when using these codes to model critical benchmark experiments. The primary source of this computational bias is believed to be errors in the cross-section data, as bounded by their uncertainties, which can be tabulated in cross-section-covariance data. To predict or bound the computational bias for a design system of interest, the "American National Standards for Nuclear Criticality Safety in Operations with Fissionable Material Outside Reactors," ANSI/ANS-8.1-1998 (Ref. 3), and the "American National Standard for Validation of Neutron Transport Methods for Nuclear Criticality Safety Calculations,"

\*E-mail: reardenb@ornl.gov

ANSI/ANS-8.24-2007 (Ref. 4), allow the use of calculations in the determination of subcritical limits for the design of fissionable material systems. The standards require validation of the analytical methods and data used in nuclear criticality safety calculations to quantify any computational bias and the uncertainty in the bias. The validation procedure must be conducted through comparison of the computed results with experimental data, and the design system for which the subcritical limit is established must fall within the area of applicability of the experiments chosen for validation. The ANS-8.1 standard defines the area (or areas) of applicability as “the limiting ranges of material compositions, geometric arrangements, neutron-energy spectra, and other relevant parameters (e.g., heterogeneity, leakage, interaction, absorption, etc.), within which the bias of a computational method is established.”

### I.C. TSUNAMI Techniques for Code Validation

The TSUNAMI software provides a unique means of determining the similarity of nuclear criticality experiments to safety applications.<sup>5</sup> The basis of the TSUNAMI validation techniques is the assumption that computational biases are primarily caused by errors in the cross-section data, the potential for which are quantified in cross-section-covariance data.

TSUNAMI provides two methods to establish the computational bias introduced through cross-section data. For the first method, instead of using one or more average physical parameters to characterize a system, TSUNAMI determines the uncertainty in  $k_{eff}$ , due to cross-section uncertainties, that is shared between two systems. This shared uncertainty in  $k_{eff}$  directly relates to the bias shared by the two systems. To accomplish this, the sensitivity of  $k_{eff}$  to each groupwise nuclide-reaction-specific cross section is computed for all systems considered in the analysis. Correlation coefficients are developed by propagating the uncertainties in neutron cross-section data to uncertainties in the computed neutron multiplication factor for experiments and safety applications through sensitivity coefficients. The bias in the experiments, as a function of correlated uncertainty with the intended application, is extrapolated to predict the bias and bias uncertainty in the target application. This correlation coefficient extrapolation method is useful where many experiments with uncertainties that are highly correlated to the target application are available.

For the second method, data adjustment or data assimilation techniques are applied to predict computational biases, and more general responses—including but not limited to  $k_{eff}$ —can be addressed.<sup>5</sup> This technique utilizes S/U data to identify a single set of adjustments to nuclear data and experimental responses, taking into account their correlated uncertainties, that will result in the computational models producing response values close to their experimental response value. Then,

the same data adjustments are used to predict an unbiased response (e.g.,  $k_{eff}$ ) value for the application and an uncertainty on the adjusted response value. The difference between the originally calculated response value and the new postadjustment response value represents the bias in the original calculation, and the uncertainty in the adjusted value represents the uncertainty in this bias. If experiments are available to validate the use of a particular nuclide in the application, the uncertainty of the bias for this nuclide may be reduced. If similar experiments are not available, the uncertainty in the bias for the given nuclide is high. Thus, with a complete set of experiments to validate important components in the application, a precise bias with a small uncertainty can be predicted. Where the experimental coverage is lacking, a bias can be predicted with an appropriately large uncertainty. The data assimilation method presents many advantages over other techniques in that biases can be projected from an agglomeration of benchmark experiments, each of which may represent only a small component of the bias of the target application. Also, contributors to the computational bias can be analyzed on an energy-dependent, nuclide-reaction-specific basis.

### I.D. The Tools of TSUNAMI

TSUNAMI is a suite of computational tools in which individual components each perform a specific task. These tools are introduced below and explained in detail in subsequent sections.

The TSUNAMI-1D and TSUNAMI-3D analysis sequences compute the sensitivity of  $k_{eff}$  to energy-dependent cross-section data for each reaction of each nuclide in a system model. The one-dimensional (1-D) transport calculations are performed with XSDRNPM, and the three-dimensional (3-D) calculations are performed with KENO V.a or KENO-VI (Ref. 2). The energy-dependent sensitivity data are stored in a sensitivity data file (SDF) for subsequent analysis. Additionally, the TSUNAMI-1D and TSUNAMI-3D sequences use the energy-dependent cross-section-covariance data to compute the uncertainty in each system's  $k_{eff}$  value due to the cross-section-covariance data.

TSAR (Tool for Sensitivity Analysis of Reactivity responses) computes the sensitivity of the reactivity change between two  $k_{eff}$  calculations, using SDFs from TSUNAMI-1D and/or TSUNAMI-3D. TSAR also computes the uncertainty in the reactivity difference due to the cross-section-covariance data.

TSUNAMI-IP (TSUNAMI Indices and Parameters) uses the SDFs generated from TSUNAMI-1D, TSUNAMI-3D, or TSAR for a series of systems to compute correlation coefficients that determine the amount of shared uncertainty between each target application and each benchmark experiment considered in the analysis. TSUNAMI-IP offers a wide range of options for more

detailed assessment of system-to-system similarity. Additionally, TSUNAMI-IP can generate input for the Upper Subcritical Limit STATistical Software<sup>6</sup> (USLSTATS) trending analysis and compute a penalty, or additional margin, needed for the gap analysis.

TSURFER (Tool for S/U Analysis of Response Functions Using Experimental Results) is a bias and bias uncertainty prediction tool that implements the generalized linear least-squares (GLLS) approach to data assimilation and cross-section data adjustment. The data adjustments produced by TSURFER are not used to produce adjusted cross-section data libraries for subsequent use; rather, they are used only to predict biases in application systems.

## II. SENSITIVITY ANALYSIS

Sensitivity coefficients are defined physically such that they represent the percentage effect on some system response because of a percentage change in an input parameter. For fissionable material systems, one of the appropriate responses is the system multiplication factor  $k_{eff}$ . The sensitivity coefficients are often presented as energy-dependent profiles, where the change in  $k_{eff}$  due to perturbations of the cross-section data is given as a function of incident neutron energy. These sensitivity profiles can be generated for each material in the system and may include various nuclear reactions (e.g., scatter, absorption, fission), as well as the neutron energy distribution from fission  $\chi$  and average number of neutrons emitted per fission  $\bar{\nu}$ .

### II.A. Direct Perturbation

The most basic means of obtaining sensitivity coefficients is through direct perturbation of the input data and interpretation of the resulting response change. With SCALE, it is straightforward to use direct perturbation to determine the sensitivity of  $k_{eff}$  to the density of a material or nuclide. The sensitivity of  $k_{eff}$  to the number density is equivalent to the sensitivity of  $k_{eff}$  to the total cross section, integrated over energy. For each sensitivity coefficient examined by direct perturbation, the  $k_{eff}$  of the system is computed first with the nominal values of the input quantities, then with the selected nominal input value increased by a certain percentage, and then with the nominal value decreased by the same percentage. The direct perturbation sensitivity coefficient of  $k_{eff}$  to some input value  $\alpha$  is computed as

$$S_{k,\alpha} = \frac{\alpha}{k} \times \frac{dk}{d\alpha} = \frac{\alpha}{k} \times \frac{k_{\alpha^+} - k_{\alpha^-}}{\alpha^+ - \alpha^-} , \quad (1)$$

where  $\alpha^+$  and  $\alpha^-$  represent the increased and decreased values, respectively, of the input quantity  $\alpha$ , and  $k_{\alpha^+}$  and  $k_{\alpha^-}$  represent the corresponding values of  $k_{eff}$ . When

direct perturbation calculations are performed using KENO, the Monte Carlo statistical uncertainties in the computed values of  $k_{eff}$  are propagated to uncertainties in direct perturbation sensitivity coefficients, assuming the values are uncorrelated, using standard error propagation techniques such as<sup>7</sup>

$$\sigma_s = \left( \left( \frac{(\sigma_{k^+}^2 + \sigma_{k^-}^2)}{(k^+ - k^-)^2} + \frac{\sigma_k^2}{k^2} \right) \times \left( \frac{k^+ - k^-}{k} \right)^2 \right)^{1/2} \times \frac{\alpha}{\alpha^+ - \alpha^-} . \quad (2)$$

Additionally, multiple perturbations can be performed and linear regression techniques can be employed. The slope of the linear regression through the normalized perturbed  $k_{eff}$  values as a function of the normalized perturbations represents the sensitivity coefficient.

### II.B. Adjoint-Based Eigenvalue Sensitivity Analysis Theory

The explicit sensitivity coefficients in the TSUNAMI-1D and TSUNAMI-3D sequences are calculated using the well-established adjoint-based perturbation theory approach.<sup>8-11</sup> The sensitivity coefficients produced with these techniques give the sensitivity of the computed  $k_{eff}$  to a particular component of the groupwise cross-section data.

The full derivation of the general procedure is not given here; however, the specific theory for the generation of  $k_{eff}$  sensitivities is presented below.

The steady-state Boltzmann transport equation can be written in the form

$$[A - \lambda B]\phi = 0 , \quad (3)$$

where

$\phi$  = neutron flux

$\lambda$  = eigenvalues where the largest eigenvalue is  $1/k_{eff}$

$A$  = operator that represents all of the transport equation except for the fission term

$B$  = operator that represents the fission term of the transport equation.

Defining perturbed transport operators and the perturbed eigenvalues as

$$A' = A + \delta A ,$$

$$B' = B + \delta B ,$$

and

$$\lambda' = \lambda + \delta \lambda , \quad (4)$$

where  $\delta A$  and  $\delta B$  represent small linear perturbations in their corresponding transport operators and  $\delta\lambda$  represents the resulting change in the eigenvalues, the perturbed transport equation can be written in the form

$$[A' - \lambda'B']\phi' = 0 \quad (5)$$

The equation adjoint to Eq. (3) is

$$[A^\dagger - \lambda B^\dagger]\phi^\dagger = 0 \quad (6)$$

where  $\phi^\dagger$  is the adjoint flux and has a special physical significance as the “importance” of the particles within the system, and  $A^\dagger$  and  $B^\dagger$  are the adjoint operators corresponding to  $A$  and  $B$ .

Multiplying Eq. (5) by  $\phi^\dagger$  and integrating over all phase-space yields

$$\langle \phi^\dagger (A' - \lambda'B') \phi' \rangle = 0 \quad (7)$$

where  $\langle \rangle$  represents integration over all phase-space (volume, energy, and direction).

Expanding Eq. (7) in terms of Eq. (4) yields

$$\langle \phi^\dagger (A - \lambda B + \delta A - \lambda \delta B - B \delta \lambda - \delta \lambda \delta B) \phi' \rangle = 0 \quad (8)$$

Using the property of adjointness [i.e.,  $\langle \phi^\dagger (A - \lambda B) \phi' \rangle = \langle \phi' (A^\dagger - \lambda^\dagger B^\dagger) \phi^\dagger \rangle$ ] and Eq. (6) to reduce the number of terms yields

$$\langle \phi^\dagger (\delta A - \lambda \delta B - B \delta \lambda - \delta \lambda \delta B) \phi' \rangle = 0 \quad (9)$$

Equation (9) is further simplified by ignoring the second-order perturbation term ( $\delta \lambda \delta B$ ) and substituting  $\phi'$  with  $\phi$ , indicating that the perturbations in the transport operators do not cause significant perturbations in the flux solution. The eigenvalue perturbation becomes

$$\frac{\delta \lambda}{\lambda} = \frac{\langle \phi^\dagger (\delta A - \lambda \delta B) \phi \rangle}{\langle \phi^\dagger (\lambda B) \phi \rangle} \quad (10)$$

Substituting the perturbation terms with partial derivatives with respect to a macroscopic cross section  $\Sigma$  of the transport operator at some point in phase-space  $\vec{r}$ , the relative sensitivity of  $\lambda$  becomes

$$\frac{\delta \lambda}{\lambda} = \frac{\left\langle \phi^\dagger(\vec{\xi}) \left( \frac{\partial A[\Sigma(\vec{\xi})]}{\partial \Sigma(\vec{r})} - \lambda \frac{\partial B[\Sigma(\vec{\xi})]}{\partial \Sigma(\vec{r})} \right) \phi(\vec{\xi}) \right\rangle}{\langle \phi^\dagger(\vec{\xi}) \lambda B[\Sigma(\vec{\xi})] \phi(\vec{\xi}) \rangle} \quad (11)$$

where  $\vec{\xi}$  is the phase-space vector and the brackets (i.e.,  $\langle \rangle$ ) indicate integration over space, direction, and energy variables.

Note that since  $\lambda = 1/k$ , then  $\partial \lambda / \lambda = -\partial k / k$ , where  $k = k_{eff}$ , the sensitivity of  $k$  due to a small perturbation in a macroscopic cross section  $\Sigma$  of the transport operator at some point in phase-space can be expressed as

$$S_{k, \Sigma(\vec{r})} \equiv \frac{\Sigma(\vec{r})}{k} \frac{\partial k}{\partial \Sigma(\vec{r})} = -\frac{\Sigma(\vec{r})}{k} \frac{\left\langle \phi^\dagger(\vec{\xi}) \left( \frac{\partial A[\Sigma(\vec{\xi})]}{\partial \Sigma(\vec{r})} - \frac{1}{k} \frac{\partial B[\Sigma(\vec{\xi})]}{\partial \Sigma(\vec{r})} \right) \phi(\vec{\xi}) \right\rangle}{\left\langle \phi^\dagger(\vec{\xi}) \frac{1}{k^2} B[\Sigma(\vec{\xi})] \phi(\vec{\xi}) \right\rangle} \quad (12)$$

The  $k$  sensitivity for individual cross sections can be obtained from Eq. (12) using the discrete-ordinates form of the transport equation and analytic derivatives of the transport operators with respect to each cross section of interest. In doing so, the phase-space vector  $\vec{\xi}$  has been replaced by indices representing discretization in space, energy, and angular moment. Here, sensitivity coefficients for reaction  $x$ , isotope  $i$ , energy group  $g$ , and computational region  $z$  are represented, and energy-integrated coefficients are obtained by summing the groupwise coefficients over all energy groups.

The computational form of each sensitivity coefficient is expressed with the volume-integrated product of the forward and adjoint flux moments as

$$P_{g, g', z}^\ell = V_z \sum_{j=L_{\ell-1}}^{L_\ell} \tilde{\phi}_{g', z}^{\dagger j} \tilde{\phi}_{g, z}^j \quad (13)$$

where

$\tilde{\phi}_{g, z}^j = j$ 'th real-valued spherical harmonics forward flux component for energy group  $g$  and region  $z$

$\tilde{\phi}_{g', z}^{\dagger j} = j$ 'th real-valued spherical harmonics adjoint flux component for energy group  $g'$  and region  $z$

$\ell =$  Legendre order

$L_\ell =$  index of real-valued flux moments corresponding to the desired Legendre order of expansion

$V_z =$  volume of region  $z$ .

For calculations where the fluxes are not accumulated over a spatial mesh, the flux product is computed with Eq. (13), where the fluxes represent the average flux in each user-defined spatial zone  $z$ . For calculations where fluxes are computed on a spatial mesh, the flux product for each material region is computed as

$$P_{g,g',z}^\ell = \sum_j \sum_m \tilde{\phi}_{g',z_m}^{ij} \tilde{\phi}_{g,z_m}^j V_{z_m}, \quad (14)$$

where

$m$  = flux meshes that occur in region  $z$

$z_m$  = fluxes computed in mesh  $m$  of region  $z$

$V_{z_m}$  = volume of mesh  $m$  in region  $z$ .

A common denominator for all sensitivity coefficients,  $D$ , is expressed as

$$D = \frac{1}{k} \sum_{i=1}^I \sum_{z=1}^R V_z \sum_{g=1}^G (\bar{\nu}_{g,z}^i \Sigma_{f,g,z}^i \phi_{g,z}) \sum_{g'=1}^G (\chi_{g',z}^i \phi_{g',z}^\dagger), \quad (15)$$

where

$\chi_{g',z}^i$  = average fraction of fission neutrons emitted into energy group  $g'$  from fission of isotope  $i$  in region  $z$

$\bar{\nu}_{g,z}^i$  = average number of fission neutrons emitted from fission of isotope  $i$  in region  $z$  in energy group  $g$

$\Sigma_{f,g,z}^i$  = macroscopic cross section for fission of isotope  $i$  in region  $z$  and energy group  $g$

$I$  = number of isotopes in the system model

$R$  = number of computational regions in the system model

$G$  = number of neutron energy groups in the system model.

Once the flux products are computed for each material region or zone, the sensitivity coefficients for each reaction type can be computed as follows.

1. *Capture reaction sensitivity (nonfission, nonscattering)*: The sensitivity of  $k_{eff}$  to nonfission, nonscattering absorption cross sections  $[(n, \gamma), (n, \alpha), (n, p), \text{etc.}]$  and can be expressed as

$$S_{x,g,z}^i = \frac{-\Sigma_{x,g,z}^i \sum_{\ell=0}^{ISCT} (2\ell + 1) P_{g,g,z}^\ell}{D}, \quad (16)$$

where

$\Sigma_{x,g,z}^i$  = macroscopic cross section for reaction  $x$  of isotope  $i$ , from energy group  $g$  in region  $z$

$ISCT$  = highest Legendre order of scattering used in the sensitivity calculations.

2. *Fission reaction sensitivity*: The sensitivity of  $k_{eff}$  to the fission cross section is expressed as

$$S_{f,g,z}^i = \frac{1}{D} \left[ \left( \frac{1}{k} \bar{\nu}_{g,z}^i \Sigma_{f,g,z}^i \chi_{g',z}^i - \Sigma_{f,g,z}^i \right) P_{g,g,z}^0 + \sum_{\substack{g'=1 \\ g \neq g'}}^G \frac{1}{k} \bar{\nu}_{g,z}^i \Sigma_{f,g,z}^i \chi_{g',z}^i P_{g,g',z}^0 - \Sigma_{f,g,z}^i \sum_{\ell=1}^{ISCT} (2\ell + 1) P_{g,g,z}^\ell \right]. \quad (17)$$

3. *Scattering reaction sensitivity*: The sensitivity of  $k_{eff}$  to scattering cross sections [elastic, inelastic, and  $(n, 2n)$  reactions] is expressed as

$$S_{x,g,z}^i = \frac{1}{D} \left( \sum_{\ell=0}^{ISCT} \left\{ (\Sigma_{x,g \rightarrow g,z}^{\ell,i} - (2\ell + 1) \Sigma_{x,g,z}^i) P_{g,g,z}^\ell + \sum_{\substack{g'=1 \\ g' \neq g}}^G \Sigma_{x,g \rightarrow g',z}^{\ell,i} P_{g,g',z}^\ell \right\} \right), \quad (18)$$

where  $\Sigma_{x,g \rightarrow g',z}^{\ell,i}$  =  $\ell$ 'th moment of the transfer cross section for reaction  $x$  of isotope  $i$ , from energy group  $g'$  to energy group  $g$  in region  $z$ .

4. *Total reaction sensitivity*: The sensitivity of  $k_{eff}$  to the total cross section is expressed as

$$S_{t,g,z}^i = \frac{1}{D} \left[ \left( \Sigma_{s,g \rightarrow g,z}^{0,i} + \frac{1}{k} \bar{\nu}_{g,z}^i \Sigma_{f,g,z}^i \chi_{g',z}^i - \Sigma_{t,g,z}^i \right) P_{g,g,z}^0 + \sum_{\substack{g'=1 \\ g \neq g'}}^G \left( \Sigma_{s,g \rightarrow g',z}^{0,i} + \frac{1}{k} \bar{\nu}_{g,z}^i \Sigma_{f,g,z}^i \chi_{g',z}^i \right) P_{g,g',z}^0 + \left\{ \sum_{\ell=1}^{ISCT} (\Sigma_{s,g \rightarrow g,z}^{\ell,i} - (2\ell + 1) \Sigma_{t,g,z}^i) P_{g,g,z}^\ell + \sum_{\substack{g'=1 \\ g' \neq g}}^G \Sigma_{s,g \rightarrow g',z}^{\ell,i} P_{g,g',z}^\ell \right\} \right]. \quad (19)$$

5.  $\bar{\nu}$  Sensitivity: The sensitivity of  $k_{eff}$  to  $\bar{\nu}$  is expressed as

$$S_{\bar{\nu},g,z}^i = \frac{\frac{1}{k} \sum_{g'=1}^G \bar{\nu}_{g',z}^i \sum_{f,g,z}^i \chi_{g',z}^i P_{g,g',z}^0}{D} . \quad (20)$$

6.  $\chi$  Sensitivity: The sensitivity of  $k_{eff}$  to the fission spectrum  $\chi$  is optionally expressed in one of two forms. The traditional form, the so-called unconstrained  $\chi$  sensitivity, is expressed as

$$S_{\chi,g,z}^i = \frac{\frac{1}{k} \sum_{g'=1}^G \bar{\nu}_{g',z}^i \sum_{f,g',z}^i \chi_{g',z}^i P_{g',g',z}^0}{D} . \quad (21)$$

Using the unconstrained  $\chi$  of Eq. (21), the sensitivity coefficients sum to 1.0 when added over all energy groups and nuclides. However, since the fission spectrum probability distribution for any nuclide must by definition sum to 1.0 over all energy groups, the sensitivity of  $k_{eff}$  to the fission spectrum should sum to 0.0, as any change in fission spectrum in any group must be compensated by changes in other groups to maintain the constraint that all values sum to 1.0. The constrained  $\chi$  calculation was first developed for the SAGEP code<sup>12</sup> and is implemented as the default option in TSUNAMI as

$$\tilde{S}_{\chi,g,z}^i = S_{\chi,g,z}^i - \chi_{g,z}^i \sum_{g'=1}^G S_{\chi,g',z}^i . \quad (22)$$

### II.C. Implicit Effect of Resonance Self-Shielding Calculations

The methodology to calculate the sensitivity coefficients, as presented in Sec. II.B, was developed for fast reactor applications in which the effect of resonance self-shielding in the multigroup cross-section data is minimal. To provide an accurate estimation of the sensitivity coefficients for systems in which resonance self-shielding is important, the sensitivity coefficients require additional terms to account for the first-order implicit effect of perturbations in the material number densities or nuclear data upon the shielded groupwise macroscopic cross-section data.<sup>13</sup> For example, in a water-moderated, low-enriched-uranium system, the resonance self-shielded cross section for  $^{238}\text{U}(n, \gamma)$  is dependent on the moderation of neutrons by  $^1\text{H}$ . Thus, the sensitivity of  $k_{eff}$  to  $^1\text{H}$  elastic scattering has an implicit component introduced by its influence on the resonance self-shielded cross section for  $^{238}\text{U}(n, \gamma)$ , which leads to a change in  $k_{eff}$  for the system.

For cross-section data process  $y$  of nuclide  $j$  in energy group  $h$  expressed as  $\Sigma_{y,h}^j$ , which is sensitive to perturbations in process  $x$  in energy group  $g$  for nuclide  $i$  expressed as  $\Sigma_{x,g}^i$ , the complete sensitivity of  $k_{eff}$  due to

perturbations of  $\Sigma_{x,g}^i$  can be defined using the chain rule for derivatives as

$$\begin{aligned} (S_{k,\Sigma_{x,g}^i})_{complete} &= \frac{\Sigma_{x,g}^i}{k} \frac{dk}{d\Sigma_{x,g}^i} \\ &= \frac{\Sigma_{x,g}^i}{k} \frac{\partial k}{\partial \Sigma_{x,g}^i} + \sum_j \sum_h \frac{\Sigma_{y,h}^j}{k} \frac{\partial k}{\partial \Sigma_{y,h}^j} \times \frac{\Sigma_{x,g}^i}{\Sigma_{y,h}^j} \frac{\partial \Sigma_{y,h}^j}{\partial \Sigma_{x,g}^i} \\ &= S_{k,\Sigma_{x,g}^i} + \sum_j \sum_h S_{k,\Sigma_{y,h}^j} S_{\Sigma_{y,h}^j,\Sigma_{x,g}^i} , \end{aligned} \quad (23)$$

where the sensitivity coefficients with respect to  $k_{eff}$  are the explicit components as computed in Sec. II.B, with the region subscript  $z$  omitted, and  $j$  and  $h$  are varied to include all processes that are influenced by the value of  $\Sigma_{x,g}^i$ .

In SCALE 6, full-range Bondarenko factors are available in the ENDF/B-VI and ENDF/B-VII multi-group cross-section libraries, and implicit terms are computed with a sensitivity version of BONAMI, called BONAMIST. For LATTICECELL calculations, some implicit terms are propagated through the Dancoff factor. In this case, the sensitivities of the Dancoff factors for each zone of the BONAMI model to each nuclide are computed. As with other SCALE sequences, the TSUNAMI-1D and TSUNAMI-3D resonance self-shielded cross sections in the resolved energy range are computed with CENTRM and PMC, but the implicit sensitivities in all energy ranges are computed with BONAMIST.

Because the sensitivity of a response to a material number density is equivalent to the sensitivity of the same response to the corresponding total macroscopic cross section, the computation of the implicit sensitivity coefficients can be based on the sensitivity to the input material number densities, which reduces the number of terms that must be carried through the BONAMIST calculation. The implicit sensitivity of  $k_{eff}$  to the total cross section of nuclide  $i$  is

$$\begin{aligned} (S_{k,\Sigma_{T,g}^i})_{implicit} &= \sum_j \sum_y \sum_h \frac{\Sigma_{y,h}^j}{k} \frac{\partial k}{\partial \Sigma_{y,h}^j} \times \frac{\Sigma_{T,g}^i}{\Sigma_{y,h}^j} \frac{\partial \Sigma_{y,h}^j}{\partial \Sigma_{T,g}^i} \times \frac{\Sigma_{T,g}^i}{\Sigma_{T,g}^i} \frac{\partial \Sigma_{T,g}^i}{\partial \Sigma_{T,g}^i} \\ &= \sum_j \sum_y \sum_h S_{k,\Sigma_{y,h}^j} S_{\Sigma_{y,h}^j,\Sigma_{T,g}^i} S_{\Sigma_{T,g}^i,\Sigma_{T,g}^i} \\ &= \sum_j \sum_y \sum_h S_{k,\Sigma_{y,h}^j} S_{\Sigma_{y,h}^j,N^i} S_{\Sigma_{T,g}^i,\Sigma_{T,g}^i} , \end{aligned} \quad (24)$$

where  $j$  and  $y$  are varied to include all processes that are sensitive to  $N^i$ , the number density of the  $i$ 'th nuclide.

Additionally, the energy group for the implicit sensitivity,  $g$ , is varied over all energies. The sensitivity of the total macroscopic cross section to the groupwise macroscopic total cross section to the groupwise macroscopic total cross section  $S_{\Sigma_T^i, \Sigma_T^i, g}$  is simply 1.0. For the Dancoff factors calculated by SCALE and input to BONAMIST, an additional term is necessary to account for the sensitivity of the Dancoff factor for a given region of the BONAMI model, denoted here as  $C_m$ . The chain rule for derivatives can again be used to propagate this sensitivity to a  $k_{eff}$  sensitivity. The implicit sensitivity of  $k_{eff}$  to the input number densities in this case is

$$\begin{aligned}
 (S_{k, \Sigma_T^i, k})_{implicit} &= \sum_m \sum_j \sum_y \sum_h \frac{\Sigma_{y,h}^j}{k} \frac{\partial k}{\partial \Sigma_{y,h}^j} \times \frac{C_m}{\Sigma_{y,h}^j} \frac{\partial \Sigma_{y,h}^j}{\partial C_m} \\
 &\times \frac{\Sigma_T^i}{C_m} \frac{\partial C_m}{\partial \Sigma_T^i} \times \frac{\Sigma_{T,g}^i}{\Sigma_T^i} \frac{\partial \Sigma_T^i}{\partial \Sigma_{T,g}^i} \\
 &= \sum_m \sum_j \sum_y \sum_h S_{k, \Sigma_{y,h}^j} S_{\Sigma_{y,h}^j, C_m} S_{C_m, \Sigma_T^i} S_{\Sigma_T^i, \Sigma_{T,g}^i} \\
 &= \sum_m \sum_j \sum_y \sum_h S_{k, \Sigma_{y,h}^j} S_{\Sigma_{y,h}^j, C_m} S_{C_m, N^i} S_{\Sigma_T^i, \Sigma_{T,g}^i}, \quad (25)
 \end{aligned}$$

where  $m$  is varied to include all Dancoff factors in the resonance self-shielding calculation. The calculation of the implicit sensitivity of a total cross section requires the sum of the implicit quantities computed in Eqs. (24) and (25), if Dancoff factors are used.

To compute the implicit portion of sensitivity coefficients for reactions,  $x$ , other than total, an additional term must be employed. With the implicit sensitivity of  $k_{eff}$  to the total cross section computed, the chain rule for derivatives is again applied to propagate the sensitivity of  $k_{eff}$  to the total cross section to the sensitivity of  $k_{eff}$  to some other process. This is accomplished using the sensitivity of the total cross section to the particular processes, computed from the unshielded cross-section data as

$$(S_{k, \Sigma_{x,g}^i})_{implicit} = \left( \frac{\Sigma_{T,g}^i}{k} \frac{\partial k}{\partial \Sigma_{T,g}^i} \right)_{implicit} \times \left( \frac{\Sigma_{x,g}^i}{\Sigma_{T,g}^i} \frac{\partial \Sigma_{T,g}^i}{\partial \Sigma_{x,g}^i} \right). \quad (26)$$

#### II.D. Complete Sensitivity Coefficient

With the implicit sensitivities properly computed, the complete sensitivity coefficient by group can be computed as the sum of the explicit and implicit terms as

$$(S_{k, \Sigma_{x,g}^i})_{complete} = (S_{k, \Sigma_{x,g}^i})_{explicit} + (S_{k, \Sigma_{x,g}^i})_{implicit}. \quad (27)$$

When a Monte Carlo transport solution is used to produce sensitivity coefficients, uncertainties in the forward and adjoint flux solutions and the value of  $k_{eff}$  are propagated to the final sensitivity results using standard error propagation techniques.<sup>14</sup> The forward and adjoint fluxes are treated as uncorrelated to each other. Also, the groupwise values of each flux solution are treated as uncorrelated. The flux moments within each group are treated as fully correlated. The quantification of true correlations would be costly in terms of storage and processing in the Monte Carlo simulation. Although the current method provides an adequate assessment of the statistical uncertainty in the sensitivity coefficients, a more robust technique may be implemented in the future.

#### II.E. Summary of Sensitivity Coefficients Calculated by TSUNAMI

Sensitivity coefficients are calculated for the sensitivity of  $k_{eff}$  to the reactions listed in Table I, if appropriate cross-section data are available. The Evaluated Nuclear Data File (ENDF) MT identifier for each of these sensitivity types is also given.<sup>15</sup> The MT of zero assigned to scattering is arbitrary, as a sum of scattering reactions does not exist in the ENDF specification.

#### II.F. One-Dimensional Sensitivity Analysis Sequence

TSUNAMI-1D is a SCALE control module that facilitates the application of sensitivity and uncertainty theory to criticality safety analysis using 1-D models by performing all necessary steps to compute sensitivity coefficients from a single input file. The data computed with TSUNAMI-1D are the sensitivity of  $k_{eff}$  to each

TABLE I  
Sensitivity Types Computed by TSUNAMI-1D  
and TSUNAMI-3D

MT	Reaction	TSUNAMI Identifier
0	Sum of scattering	Scatter
1	Total	Total
2	Elastic scattering	Elastic
4	Inelastic scattering	n, n'
16	n, 2n	n, 2n
18	Fission	Fission
101	Neutron disappearance	Capture
102	n, $\gamma$	n, gamma
103	n, p	n, p
104	n, d	n, d
105	n, t	n, t
106	n, $^3\text{He}$	n, he-3
107	n, $\alpha$	n, alpha
452	$\bar{\nu}$	Nubar
1018	$\chi$	chi

constituent cross-section data component used in the calculation. TSUNAMI-1D provides automated, problem-dependent cross sections using the same methods and input as the SCALE criticality safety sequences. Additionally, TSUNAMI-1D computes the implicit terms of the sensitivity coefficients during the resonance self-shielding calculation.

After the cross sections are processed, TSUNAMI-1D performs two XSDRNPM criticality calculations, one forward and one adjoint, where TSUNAMI-1D assigns spatial zones for the neutron transport calculations, automatically subdividing the user-input geometry. Finally, the sequence calls the Sensitivity Analysis Module for SCALE (SAMS), where the flux moment product terms are computed from angular fluxes and the sensitivity coefficients are computed as shown by Eqs. (15) through (22). SAMS prints energy-integrated sensitivity coefficients to the SCALE output file and generates a SDF containing the energy-dependent sensitivity coefficients.

### II.G. Three-Dimensional Sensitivity Analysis Sequences

TSUNAMI-3D is a SCALE control module that facilitates the application of sensitivity and uncertainty theory to criticality safety analysis using 3-D Monte Carlo models by performing all necessary steps to compute sensitivity coefficients from a single input file. Like TSUNAMI-1D, the data computed with TSUNAMI-3D are the sensitivities of  $k_{eff}$  to each constituent cross-section data component used in the calculation. TSUNAMI-3D also provides automated, problem-dependent cross sections using the same methods and input as the SCALE criticality safety sequences but with implicit terms also included.

After the cross sections are processed, TSUNAMI-3D performs two KENO criticality calculations, one forward and one adjoint, to compute the energy and spatially dependent flux solutions and their angular moments. The user must provide adequately fine spatial resolution of the flux solutions to allow for appropriate folding of the forward and adjoint solutions. This is accomplished either by manually entering geometry divisions or by using the automated meshing features of KENO developed specifically for this purpose. The calculation of angular flux moments with Monte Carlo techniques has been previously described,<sup>16</sup> and the mesh flux accumulator is described in another paper in this special issue.<sup>2</sup> The TSUNAMI-3D sequences provide for separate control of the forward and adjoint calculations to independently specify the number of particles per generation, the number of generations, the number of generations skipped before accumulating data, and the desired convergence criteria for each calculation.

The analyst's selection of modeling strategies and TSUNAMI-3D input parameters can significantly affect the sensitivity profiles generated by TSUNAMI-3D. Erroneous implicit sensitivity coefficients may result if

the cross-section resonance self-shielding model (e.g., lattice cell, multiregion, or infinite homogeneous) is inconsistent with the use of the material in the KENO model. Thus, the importance of performing a thorough set of direct perturbation calculations to verify the accuracy of the TSUNAMI-3D sensitivity data cannot be overemphasized.

Finally, the sequences call SAMS where the flux moment product terms are computed and the sensitivity coefficients are computed as shown by Eqs. (15) through (22). SAMS also computes the uncertainty in the sensitivity coefficients introduced by uncertainties in the Monte Carlo calculations. SAMS prints energy-integrated sensitivity coefficients and their uncertainties to the SCALE output file and generates a SDF containing the energy-dependent sensitivity coefficients and their uncertainties.

### II.H. Reactivity Sensitivity Coefficients

The TSUNAMI-1D and TSUNAMI-3D control modules in SCALE compute multigroup sensitivity coefficients for  $k_{eff}$ , the reciprocal of the  $\lambda$ -eigenvalue of the neutron transport equation for a multiplying medium. The TSAR module in SCALE performs sensitivity calculations for responses represented by the difference of two eigenvalues. These types of responses are often of interest in reactor physics applications. For example, TSAR can compute data sensitivities and uncertainties of reactivity responses such as control rod worths, fuel and moderator temperature coefficients, and void coefficients for two defined states of a power reactor.<sup>17</sup> Another potential application is in the analysis of critical benchmark experiments for nuclear data testing and validation studies. Data and methods deficiencies can introduce a computational bias manifested as a trend in calculated critical eigenvalues versus experiment parameters. TSAR can be applied to the difference in the computed eigenvalues of two benchmarks to establish the sensitivity of the bias trend to various nuclear data used in the calculations.

TSAR builds upon capabilities of other TSUNAMI modules. The TSUNAMI-1D or TSUNAMI-3D sequences are first used to calculate sensitivities for the multiplication factors of the reference and altered states of the reactor, respectively. TSAR reads the SDFs produced by TSUNAMI  $k_{eff}$  calculations and uses them to compute relative or absolute sensitivities of an eigenvalue-difference response. The reactivity sensitivities are written to an output file and to a reactivity SDF for subsequent applications or visualization.

A detailed description of the sensitivity methodology for reactivity responses is given in Ref. 18; thus, only a brief overview is presented here. The  $\lambda$ -eigenvalue form of the neutron transport equation for a multiplying medium is given by Eq. (3). It is assumed that the system is initially in a well-defined state 1 having a  $\lambda$ -eigenvalue of  $\lambda_1$ . The reactivity for state 1 is defined as  $\rho_1 = 1 - \lambda_1$ .

Suppose that changes in  $A$  and/or  $B$  transport operators transformed the original system into a new, distinct configuration designated as state 2, with the  $\lambda$ -eigenvalue of  $\lambda_2$  and static reactivity of  $\rho_2 = 1 - \lambda_2$ . For example, the configuration change could be caused by moving a control rod or by voiding of the coolant. The reactivity insertion/withdrawal associated with the designated change in conditions is defined as

$$\rho_{1 \rightarrow 2} = \rho_2 - \rho_1 = \lambda_1 - \lambda_2, \quad (28)$$

which defines the eigenvalue-difference (i.e., reactivity) response addressed by TSAR.

Where the relative  $k_{eff}$ -sensitivity coefficient for an arbitrary data parameter  $\alpha$  appearing in the transport equation, including all explicit and implicit effects, is expressed as

$$S_{k,\alpha} = \frac{\partial k/k}{\partial \alpha/\alpha} = - \frac{\partial \lambda/\lambda}{\partial \alpha/\alpha}, \quad (29)$$

an analogous expression defines the relative sensitivity coefficient of the reactivity response:

$$S_{\rho,\alpha} = \frac{\partial \rho_{1 \rightarrow 2} / \rho_{1 \rightarrow 2}}{\partial \alpha / \alpha}. \quad (30)$$

Unlike the multiplication factor, the reactivity response can be negative. This can be a source of confusion when interpreting the relative sensitivity coefficient; hence, by convention TSAR defines sensitivities relative to the absolute value of the reactivity; thus,

$$S_{\rho,\alpha} \rightarrow \frac{\partial \rho_{1 \rightarrow 2} / |\rho_{1 \rightarrow 2}|}{\partial \alpha / \alpha}. \quad (31)$$

In this way, a positive value for the relative sensitivity coefficient means that increasing the value of  $\alpha$  always increases the value of the reactivity (i.e., a positive  $\rho$  becomes more positive, and a negative  $\rho$  becomes less negative). Conversely, a negative relative sensitivity coefficient means that increasing  $\alpha$  always decreases the reactivity (i.e., a positive  $\rho$  becomes less positive, and a negative  $\rho$  becomes more negative). This convention is used in TSAR for all relative quantities involving the reactivity.

From the definitions in Eqs. (28) and (29), Eq. (31) is simplified to the following expression used in TSAR:

$$S_{\rho,\alpha} = \frac{\lambda_2 S_{k_2,\alpha} - \lambda_1 S_{k_1,\alpha}}{|\rho_{1 \rightarrow 2}|}, \quad (32)$$

where  $S_{k_1,\alpha}$  and  $S_{k_2,\alpha}$  are the  $k$  sensitivities for the two states.

In cases where the net reactivity change is very small, the denominator of Eq. (32) approaches zero; thus, the relative sensitivity coefficient can increase without bound. The analysis of replacement critical experiments—

where one or more materials are exchanged between configurations, but criticality is maintained with other controls—provides  $k_{eff}$  values near 1.0 for both  $k_1$  and  $k_2$ . For this reason TSAR provides an input option to compute absolute rather than relative sensitivity coefficients. Absolute quantities are indicated here by the presence of a tilde ( $\sim$ ), while relative quantities have no tilde. The absolute sensitivity coefficient is defined in TSAR as the absolute change in the reactivity, expressed in pcm (percent-milli, or  $10^{-5}$  in  $k_{eff}$ ), due to a fractional change in data. Absolute reactivity difference sensitivity coefficients are expressed as

$$\tilde{S}_{\rho,\alpha} = \lambda_2 S_{k_2,\alpha} - \lambda_1 S_{k_1,\alpha} \times 10^5. \quad (33)$$

Prior to executing TSAR, it is necessary to perform TSUNAMI-1D or TSUNAMI-3D calculations for each state, in order to generate the relative  $k$ -sensitivity coefficients. These are written in SDFs and saved for input to TSAR. TSAR reads the two previously prepared files and uses them to evaluate Eq. (32) or (33) for the reactivity sensitivities. The  $\rho$  sensitivities are then output to another SDF. Because the complete sensitivities calculated by TSUNAMI-1D or TSUNAMI-3D include implicit effects associated with resonance self-shielding, the reactivity sensitivities also account for these effects, which can be significant.

### III. UNCERTAINTY ANALYSIS

Uncertainty analysis involves the assessment of the potential impact on an evaluated result due to the use of inexact or inaccurate quantities or techniques in its determination. In the validation of codes and data for nuclear safety analysis, there are two primary types of uncertainties: uncertainties in the computed responses (e.g.,  $k_{eff}$ ) and uncertainties in evaluated benchmark experiments.

For uncertainties in input quantities used in the determination of evaluated results, the uncertainty in the input quantity is propagated to an uncertainty in the result through the sensitivity coefficients that quantify the expected change in the result due to a change in an input quantity.

For example, the relative change in a computed or experimentally evaluated  $k_{eff}$  due to an arbitrary relative variation or uncertainty in parameter  $\alpha$  is

$$\frac{\Delta k}{k} \sim S_{k,\alpha} \frac{\Delta \alpha}{\alpha}. \quad (34)$$

In Eq. (34), the quantification is approximate because the sensitivity coefficients are typically computed to first-order accuracy.

#### III.A. Sources of Response Uncertainty

Transport calculations of responses such as the neutron multiplication factor inherently have biases and

uncertainties due to several factors that can be grouped into three classes:

1. *Class A*: numerical approximations in the transport code
2. *Class B*: system modeling approximations
3. *Class C*: input data uncertainties.

### III.A.1. *Class-A Uncertainties (Numerical)*

Class-A uncertainties are sometimes referred to as “methods uncertainties.” In Monte Carlo calculations these may be caused by imperfections in random number generation routines, approximations in techniques for scoring neutron multiplication (e.g., incomplete convergence of fission source distribution, neglect of correlations between generations, etc.), and biases from algorithms used to represent nuclear data and to sample probability distributions, as well as the basic statistical uncertainty that is fundamental to the Monte Carlo method. Deterministic methods have uncertainties from using finite space-energy-direction meshes, truncated (rather than infinite) expansions of functions, incomplete convergence of iterations, and especially self-shielding approximations for the multigroup cross sections. Computational benchmark studies often can establish a reasonable upper limit for these effects, which may be judged either as negligible or as requiring some conservative bias to be applied to the application calculations. Here, it is assumed that class-A uncertainties in the calculated response can be made acceptably small (e.g., by running more histories or refining mesh sizes) or at least have been previously quantified and can be bounded by a margin applied to the computation. Hence, class-A uncertainties are considered as systematic tolerance and are not further addressed here.

### III.A.2. *Class-B Uncertainties (Modeling/Experimental)*

Class-B uncertainties occur because the mathematical model used in the transport computations of an application or an experimental response does not correspond exactly to the “true” system. The response uncertainty caused by modeling effects may either be associated with (a) direct computational simplifications such as omitting or homogenizing some components in the calculation model or (b) fundamental uncertainties in the material compositions, densities, and dimensions of the experiment. The former are systematic uncertainties similar in effect to class-A numerical uncertainties and may be addressed in the same manner—that is, by bounding the magnitude of the uncertainty through the applied safety margins. However, the latter are true random uncertainties that in theory have probability distributions and can be addressed.

Even “clean” critical benchmark experiments have uncertainties in the nominal system parameters—fuel enrichment, impurities, densities, critical dimensions, and numerous other components—that may lead to discrepancies in the measured and calculated responses for the system. The impact of these uncertainties is designated as the “experimental uncertainty” in the response, since this uncertainty will be present even if no simplifications or approximations are made in the model used for the transport computation. The terminology is sometimes a source of confusion. For example, the measured  $k_{eff}$  in a critical experiment usually is known to be unity with a very small uncertainty associated with the long but finite stable period. While there is little doubt about  $k_{eff}$  for a critical experiment, there may be considerable uncertainty in the system parameter values describing the benchmark configuration. This contribution to the modeling uncertainty could be justifiably considered either “experimental” (because system parameters such as material compositions and dimensions are specified by the experimentalists) or “computational” (because uncertainties in the system parameters affect the calculation model), but here they are designated as experimental uncertainties. In any case, the uncertainty in each system parameter must be propagated to an uncertainty in the measured response. For a  $k_{eff}$  response, this may be done experimentally by physically varying the system parameter and measuring the reactivity effect or, more commonly, by performing auxiliary transport calculations to determine the eigenvalue variation.

The response uncertainty components associated with the respective modeling uncertainties in system parameters determine the overall experimental uncertainty. Many benchmark experiment descriptions in the “International Handbook of Evaluated Criticality Safety Benchmark Experiments”<sup>19</sup> (IHECSBE) include information about uncertainties in the system parameters and their estimated impact on the multiplication factor. The standard deviations in  $k_{eff}$  due to uncertainties in various system parameters are assigned by the benchmark evaluators based on published or archived experiment descriptions, and sometimes on other considerations.

A complication in specifying experimental uncertainties is how to treat correlations among the experiments. Response correlations in two benchmark experiments may be caused by factors such as the use of the same fuel pins and container tank, as well as common instrumentation (same detectors, hydrometers, etc.). For example, if two different experiments use the same fuel material, then it is not reasonable to conclude that the enrichment in one is too high while the other is too low, even if both differences fall within the specified standard deviation. Reference 20 has shown that these correlations may not be negligible when applying validation techniques to a set of benchmark experiments. Only a limited amount of experiment correlation data has been published, but more is expected in future revisions to the IHECSBE.

### III.A.3. Class-C Uncertainties (Nuclear Data)

In many applications, the major source of uncertainty in the calculated response is due to uncertainties in evaluated nuclear data such as microscopic cross sections, fission spectra ( $\chi$ ), neutron yield ( $\bar{\nu}$ ), and scattering distributions that are contained in cross-section evaluations such as ENDF/B. These arise from uncertainties in experimental nuclear data measurements, as well as from uncertainties in the evaluation process itself, which in general combine differential experimental information with nuclear physics theory to generate the basic data in compilations like ENDF/B. Class-C uncertainties are governed by probability distributions. The actual probabilities are unknown, but the evaluated data values are assumed to represent the mean of the distribution, and the evaluated variance represents a measure of the distribution width. Correlations as well as uncertainties in nuclear data can have a significant impact on the overall uncertainty in the calculated response; thus, it is important to include covariances as well as variances in the uncertainty analysis. The uncertainties in fundamental nuclear data also impact resonance self-shielding of multigroup cross-section values, further contributing to the response uncertainty.<sup>13</sup> In TSUNAMI-1D and TSUNAMI-3D, the effects of implicit changes in self-shielded cross sections are included in the overall response sensitivity coefficients rather than in the covariance data, so that the fundamental data uncertainties are isolated from problem-specific effects.<sup>21</sup>

Covariance information is currently limited in the number of nuclides for which data are available in all evaluated nuclear data compilations such as ENDF/B. A more complete library of multigroup uncertainties has been created for SCALE using data from a variety of sources, including ENDF/B-VI and ENDF/B-VII, JENDL-3.1, and approximate covariances based on uncertainties in measured integral data and nuclear model calculations, as described in Sec. IV.

### III.B. Uncertainty Theory

Given uncertainty information for the cross sections for all nuclides and reaction processes that are important to the system of interest, it is possible to estimate the uncertainty in the calculated system response due to these data uncertainties.

The nuclear data parameters are represented by the vector  $\alpha$ , the elements of which are  $(\alpha_{x,g}^i)$ , where  $i$  is varied over all isotopes,  $x$  is varied over all reactions for each isotope, and  $g$  is varied over all energy groups. If  $M$  is the number of nuclide-reaction pairs  $\times$  the number of energy groups (i.e., the number of elements in  $\alpha$ ), the symmetric  $M \times M$  matrix containing the relative variances (diagonal elements) and relative covariances (off-diagonal elements) in the nuclear data is  $\mathbf{C}_{\alpha\alpha}$ . The elements of  $\mathbf{C}_{\alpha\alpha}$  are

$$(\mathbf{C}_{\alpha_{x,g}^i \alpha_{y,g'}^j}) = \frac{\text{COV}(\alpha_{x,g}^i, \alpha_{y,g'}^j)}{\alpha_{x,g}^i \alpha_{y,g'}^j}, \quad (35)$$

where  $i$  and  $j$  are varied over all isotopes,  $x$  and  $y$  are varied over all reactions for each isotope, and  $g$  and  $g'$  are varied over all energy groups. Additionally,

$$\text{COV}(\alpha_{x,g}^i, \alpha_{y,g'}^j) = \langle \delta\alpha_{x,g}^i \delta\alpha_{y,g'}^j \rangle, \quad (36)$$

where  $\delta\alpha_{x,g}^i$  and  $\delta\alpha_{y,g'}^j$  represent the difference between the values and expectation values of the nuclear data parameters and  $\langle \rangle$  represents integration over the ranges of  $\alpha_{x,g}^i$  and  $\alpha_{y,g'}^j$  weighted with a probability density function.

The vector containing relative sensitivities of the calculated response  $k$ , which could be  $k_{\text{eff}}$ , reactivity, or some other response, to the  $\alpha$  parameters is represented by  $\mathbf{S}_{k_n}$ , where each element is

$$\mathbf{S}_{k_n} \equiv \left[ \frac{\alpha_m}{k_n} \frac{\partial k_n}{\partial \alpha_m} \right], \quad m = 1, 2, \dots, M, \quad (37)$$

and  $n$  identifies the system considered and  $M$  is the number of nuclear data parameters for which sensitivity coefficients are computed, consolidating all combinations of nuclides, reactions, and energy groups into a single index.

For the purposes of TSUNAMI uncertainty calculation, the  $\alpha_m$  parameters are simply the groupwise cross-section data. If a particular material is present in more than one material region, the sensitivity coefficients for all regions are summed prior to creating the  $\mathbf{S}_{k_n}$  vector.

The variance for the  $k_{\text{eff}}$  value of system  $n$  is given as

$$\sigma_{k_n}^2 = \mathbf{S}_{k_n} \mathbf{C}_{\alpha\alpha} \mathbf{S}_{k_n}^T, \quad (38)$$

where  $T$  indicates a transpose.

The covariance in the response due to the energy correlations of two particular processes can be assessed by examining a subset of the elements of  $\mathbf{C}_{\alpha\alpha}$ , where  $i, j, x$ , and  $y$  are held constant. If  $G$  is the number of energy groups, the covariance data for a particular process are represented as the  $G \times G$  matrix  $\mathbf{C}_{\alpha_x^i \alpha_y^j}$ , and the groupwise sensitivity vectors of length  $G$  for the processes are represented as  $\mathbf{S}_{k_n, \alpha_x^i}$  and  $\mathbf{S}_{k_n, \alpha_y^j}$ . The relative covariance in the response due to the particular process or processes is given as

$$\sigma_{k_n, x, y}^2 = \mathbf{S}_{k_n, \alpha_x^i} \mathbf{C}_{\alpha_x^i \alpha_y^j} \mathbf{S}_{k_n, \alpha_y^j}^T. \quad (39)$$

In actuality, the COVERX-formatted<sup>22</sup> data file read by TSUNAMI represents the covariance data in the form of multiple  $\mathbf{C}_{\alpha_x^i \alpha_y^j}$  matrices. Thus, although commonly used for its mathematical convenience,  $\mathbf{C}_{\alpha\alpha}$  does not exist as a continuous matrix. In the COVERX format, if  $\mathbf{C}_{\alpha_x^i \alpha_y^j}$

is present on the data file with  $i \neq j$  and/or  $x \neq y$ , then the transpose matrix  $C_{\alpha_j \alpha_x^i}$  is not present. Thus, using each matrix on the COVERX file only once, an upper (or lower) triangular  $C_{\alpha\alpha}$  matrix could be constructed, but not a full matrix.

In TSUNAMI, the value of  $\sigma_{k_n}^2$  is calculated by first determining the values of the variances or covariance as in Eq. (39) for all processes in the system under consideration, excluding the total reaction. The total reaction is excluded because it is the sum of the other processes and its inclusion would increase the variance from its actual value. The value of  $\sigma_{k_n}^2$  is then computed as the sum of the variances [diagonal elements of  $C_{\alpha\alpha}$  plus twice the sum of the covariances (off-diagonal elements of  $C_{\alpha\alpha}$ )]. The standard deviation of  $k_{eff}$  is simply the square root of  $\sigma_{k_n}^2$ . If  $S_{k_n}$  is defined in terms of absolute sensitivities, then the absolute response uncertainty due to a relative cross-section uncertainty results.

Uncertainties due to the cross-section-covariance data are computed in the TSUNAMI-1D and TSUNAMI-3D sequences, TSAR, TSUNAMI-IP, and TSURFER.

#### IV. CROSS-SECTION-COVARIANCE DATA

The TSUNAMI tools that perform uncertainty analysis require reasonable estimates for nuclear data uncertainties. Historically, the lack of sufficient covariance information in nuclear data files such as ENDF/B has limited the usefulness of available S/U computation tools like TSUNAMI.

Nevertheless, S/U analysis has proceeded in some cases even with this impairment. Omitted uncertainty data are treated effectively as having zero uncertainty, causing the calculated uncertainty in integral responses to be underestimated. This deficiency is sometimes acceptable, with the recognition that the computed uncertainty represents a lower bound. A more serious problem may occur in applications data adjustment tools like TSURFER. If a response is sensitive to some nuclide/reaction with no available covariance information, then the TSURFER calculation may adjust other data to compensate for the effect of the omitted information. This can lead to nonphysical data modifications. In some instances the omitted covariance data cause an inconsistency manifested as an excessive chi-square value, but this is not always the case. To circumvent these problems, both TSUNAMI modules have options to input values for missing covariances. While this approach provides more flexibility, the user is still confronted with the question of what uncertainty values to use.

The SCALE 6 cross-section-covariance library is a single comprehensive library with a total of 401 materials in the SCALE 44-energy-group structure. The SCALE covariance library data correspond to 44-group relative uncertainties assembled from a variety of sources, including evaluations from ENDF/B-VII, ENDF/B-VI,

JENDL-3.1, and more than 300 approximated uncertainties from a collaborative project performed by Brookhaven National Laboratory (BNL), Los Alamos National Laboratory (LANL), and ORNL.

Because SCALE includes separate multigroup cross-section libraries processed from ENDF/B-V, ENDF/B-VI.8, and ENDF/B-VII.0, the application of a single generic covariance library to all multigroup cross-section libraries obviously raises questions about consistency with any given data evaluation. In reality much of the approximate uncertainty data in the library is based on simplifying approximations that do not depend on specific ENDF evaluations and thus can be applied to all cross-section libraries, within the limitations of the assumed methodology. In other cases where a covariance evaluation has been taken from a specific nuclear data file (e.g., ENDF/B-VII, ENDF/B-VI, or JENDL-3.3), it is assumed that the same relative (rather than absolute) uncertainties can be applied to all cross-section libraries, even if these are not strictly consistent with the nuclear data evaluations. This may be questionable for some older evaluations in the ENDF/B-V data, but it should be reasonable for the SCALE ENDF/B-VI and ENDF/B-VII cross-section libraries. The assumption is partially justified by the fact that different evaluations often use many of the same experimental measurements, since there is a limited amount of this information available. Also, because most important nuclear data are now known rather well, newer evaluations in many instances correspond to rather modest variations from previous ones and are expected to lie within the earlier uncertainties. As shown by Fig. 1, the nuclear data evaluations from ENDF/B-VII, ENDF/B-VI, JEF-3.1, and JENDL-3.3 tend to agree well. Similar results are found for many types of cross sections; thus, it seems reasonable to assume that the uncertainties in these data are similar.

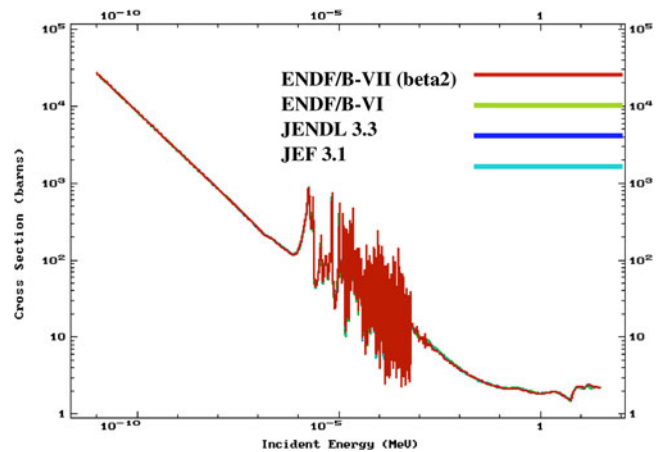


Fig. 1.  $^{233}\text{U}$  fission comparison between ENDF/B-VII (beta 2), ENDF/B-VI, JENDL-3.3, and JEF-3.1.

It should be noted that there is no inherently true uncertainty that can be defined unambiguously for nuclear data. For example, in theory, two independent evaluations could produce similar nuclear data with much different uncertainties. While differences in nuclear data evaluations have direct impact on calculations that can be affirmed by comparisons with benchmark experiments, it is more difficult to quantify the reliability of uncertainty estimates. In general, the SCALE covariance library should be viewed as a best-estimate assessment of data uncertainties based upon the specific methodologies described in Secs. IV.A through IV.D. This methodology is certainly not unique, and it can be argued that other approaches could have been used. Nevertheless, it is felt that the SCALE covariance library is a reasonable representation of the nuclear data uncertainties, given the current lack of information.

#### IV.A. Evaluated Covariances from Nuclear Data Files

A rigorous, modern evaluation of nuclear data typically utilizes a regression algorithm that adjusts parameters in a nuclear physics model (e.g., Reich-Moore resonance formula, optical model, etc.) to fit a set of differential experimental measurements that have various sources of statistical and systematic uncertainties.<sup>23</sup> Information from the regression analysis of the model parameters can be propagated to uncertainties and correlations in the evaluated differential data. In this manner the differential nuclear data and covariances are consistent and coupled together by an evaluation process. Unfortunately, only a relatively few cross-section evaluations have produced high-fidelity covariances in this rigorous manner. All other nuclear data uncertainties must be estimated from approximations in which the uncertainty assessment may be decoupled from the original evaluation procedure.

#### IV.B. Approximate Covariance Data

At the other end of the spectrum from high-fidelity data, low-fidelity (lo-fi) covariances are defined to be those that are estimated independently of a specific data evaluation. The approximate covariance data in SCALE are based on results from a collaborative project funded by the Department of Energy Nuclear Criticality Safety Program to generate lo-fi covariances over the energy range from  $10^{-5}$  eV to 20 MeV for materials without covariances in ENDF/B-VII.0. Nuclear data experts at BNL, LANL, and ORNL devised simple procedures to estimate data uncertainties in the absence of high-fidelity covariance evaluations. The result of this project is a set of covariance data in ENDF/B file 33 format that can be processed into multigroup covariances.<sup>24</sup> In this documentation, these data are called the “BLO” (BNL-LANL-ORNL) uncertainty data, which were generated as described below.

ORNL used uncertainties in integral experiment measurements of thermal cross sections, resonance integrals, and potential cross sections to approximate the standard deviations of capture, fission, and elastic scattering reactions for the thermal (<0.5 eV) and resonance ranges (0.5 eV to 5 keV). Full energy correlation was assumed for the covariances within each of these respective ranges.<sup>21,25</sup> The integral measurement uncertainty values were tabulated by Mughabghab in the *Atlas of Neutron Resonances: Resonance Parameters and Thermal Cross Sections*.<sup>26</sup> The lo-fi relative uncertainty is computed as the absolute uncertainty in the integral parameter (i.e., thermal cross section or resonance integral) taken from the *Atlas*, divided by the average of the measured parameter and the calculated value computed from ENDF/B-VII differential data:

$$U = \frac{\Delta_I}{0.5 \times (X_I + X_D)} , \quad (40)$$

where

$U$  = relative lo-fi uncertainty included in SCALE

$\Delta_I$  = absolute uncertainty in the integral measurement, obtained from Mughabghab

$X_I, X_D$  = measured and computed (from ENDF/B differential data) integral parameter values, respectively.

In some cases the integral measurement value from the Mughabghab *Atlas*<sup>26</sup> and the corresponding value computed from the ENDF/B-VII differential evaluation are inconsistent—defined here as having a difference  $>2\sigma$  in the measured and computed integral parameters. In these cases, the lo-fi relative standard deviation is defined as half the difference, relative to the average of the measured and calculated values:

$$U = \frac{|X_I - X_D|}{X_I + X_D} ; \quad \text{for } |X_I - X_D| > 2\Delta_I . \quad (41)$$

In some instances, this expression may exceed 100%. For these cases, a 100% uncertainty was assigned. Also, the *Atlas* does not include uncertainties in integral measurements for a few isotopes, which typically are not of great interest for most applications. The integral uncertainty was defined as a 5 in the least significant digit for these materials.

Both BNL and LANL provided estimates in the fast energy range from 5 keV to 20 MeV for covariances of capture, fission, elastic, inelastic, ( $n, 2n$ ) cross sections, and prompt  $\bar{\nu}$ . BNL used optical model calculations with estimated uncertainties in model parameters to compute covariances in the fast range for about 300 structural isotopes, fission products, and nonfissionable heavy nuclei. Estimated uncertainties in model parameters were

based on previous work and expert judgment.<sup>27</sup> Covariances for 14 actinide isotopes were obtained from earlier work done by BNL for Subgroup-26 (SG-26).<sup>28</sup> The SG-26 actinide covariances cover the full energy range, including thermal, resonance, and fast regions. Thermal data uncertainties tend to be overestimated by the SG-26 approach, which is based on propagating resonance parameter uncertainties; therefore, the thermal data covariances are represented by ORNL's integral uncertainty technique.

Additionally, LANL produced covariances in the fast range for another 47 actinide materials. The LANL actinide covariances were based on empirical estimates of nuclear reaction models.<sup>29</sup> Full energy range covariances were also produced by LANL for 16 light isotopes ranging from hydrogen to fluorine.<sup>30</sup> These included high-fidelity covariances from R-matrix analyses for  $^1\text{H}$ ,  $^6\text{Li}$ , and  $^{10}\text{B}$ , along with lo-fi uncertainties for the other materials, based on approximations such as least-squares fitting to experimental data, statistical model calculations at higher energies, or sometimes simply best-judgment estimation.<sup>24</sup>

#### IV.C. Modifications to Covariance Data

In generating earlier covariance libraries for SCALE 5.1, a number of obvious omissions or inconsistencies were identified and corrected in the ENDF/B-VI covariance evaluations, and these modifications are retained in the current SCALE covariance library. Two modifications were also made to the ENDF/B-VII evaluated  $\bar{\nu}$  covariances. These  $\bar{\nu}$  uncertainties are believed to be more realistic. The ENDF/B-VII.0  $^{235}\text{U}$  thermal  $\bar{\nu}$  uncertainty of 0.71% was revised to the JENDL-3.3 value of 0.31%. In addition, the thermal  $\bar{\nu}$  uncertainty in the pre-released ENDF/B-VII.1  $^{233}\text{U}$  evaluation was modified to the value in a recent ORNL data evaluation.<sup>31</sup> This ORNL  $^{233}\text{U}$  cross-section evaluation also provided the thermal and resonance cross sections for the pre-released ENDF/B-VII.1 data.

Several modifications were also made to the uncertainties obtained from the BLO data. The energy boundary between the thermal and resonance covariance blocks was modified from 0.5 to 0.625 eV to coincide with a 44-group boundary. The BLO lo-fi data do not include thermal or resonance range uncertainties for isotope reactions that do not have integral uncertainties given in the Mughabghab text. These occur mainly for relatively unimportant data such as elastic cross sections of several fission products. In these cases the uncertainties were estimated by different approaches. For example, the thermal data uncertainty was sometimes used to represent the epithermal uncertainty if it was not available in the Mughabghab tabulation, and sometimes the high-energy uncertainty was extended to lower energies. The BLO thermal uncertainties for  $^1\text{H}$  capture and elastic and for  $^{16}\text{O}$  elastic were modified to the JENDL-3.3 values of 0.5% and 0.1%, respectively. Similarly, the uncertainty

in the  $^{10}\text{B}(n, \alpha)$  thermal cross section was modified to the ENDF/B-VI value of  $\sim 0.2\%$ , since this is more consistent with the Mughabghab integral uncertainty. The uncertainty in the  $^{149}\text{Sm}$  resonance capture integral is not provided in the 2006 edition of Mughabghab's text; therefore, it was set to the value of 5.7%, which was obtained from an earlier tabulation by Mughabghab.<sup>32</sup>

#### IV.D. Covariance Data for Fission Spectra

The methodology used to construct multigroup fission spectrum ( $\chi$ ) covariance matrices is described in Ref. 33. In this approach, the fission spectrum is represented as either a Watt or Maxwellian distribution. These energy distributions are widely used to represent fission spectra and have been commonly employed in many ENDF/B evaluations. For example, Watt and Maxwellian expressions were used almost exclusively to describe fission spectra in ENDF/B-V and also for many ENDF/B-VI evaluations. More recent evaluations for some important fissionable nuclides have replaced the simple Watt and Maxwellian analytical expressions by distributions such as the Madland-Nix spectrum obtained from more phenomenological nuclear fission models. However, it is assumed here that uncertainties based on an appropriate Watt or Maxwellian representation of the fission spectrum can be transferred to the actual fission spectra contained in the different multigroup cross-section libraries.

#### IV.E. Contents of the SCALE 6 Covariance Library

Covariance data were processed with the ORNL PUFF-IV code<sup>22</sup> to generate the production library distributed with SCALE 6. The SCALE covariance library provides uncertainty data in the 44-group uncertainty data for a total of 401 materials, including some duplication for materials with multiple thermal scattering kernels.

The contents of the SCALE 6 covariance library are summarized in Table II, where the following nomenclature is used:

1. *ENDF/B-VII.0*: evaluated covariance data released with ENDF/B-VII.0
2. *ENDF/B-VII-p*: recently evaluated data proposed for future release of ENDF/B-VII.1
3. *ENDF/B-VI*: evaluated covariance data released with ENDF/B-VI
4. *JENDL-3.3*: evaluated covariance data in JENDL-3.3
5. *BLO approximate data*: lo-fi covariances from BLO project
6. *BLO LANL evaluation*: LANL R-matrix evaluation from BLO project
7. *SG-26*: approximate covariances from WPEC Subgroup-26.

TABLE II  
Sources of Covariance Data in the SCALE 6 Covariance Library

Data Source	Materials
ENDF/B-VII.0	152,154–158,160Gd, 191,193Ir, 7Li, 99Tc, 232Th
ENDF/B-VII-p	197Au, 209Bi, 59Co, 23Na, 93Nb, 58Ni, 239Pu, 48Ti, 233,235,238U, V
ENDF/B-VI	27Al, 241Am, C, C-graphite, 50,52–54Cr, 65Cu, 156Dy, 54,56–58Fe, In, 55Mn, 60–62,64Ni, 206–208Pb, 242Pu, 185,187Re, 45Sc, Si, 28–30Si, 89Y
JENDL-3.3	11B, 240,241Pu
JENDL-3.3+BLO	16O
SG-26	234,236U, 242,242m Am, 242–245Cm, 237Np, 238Pu
BLO LANL evaluation +JENDL-3.3	10B, 1H, H-ZrH, H-poly, Hfreegas
BLO LANL evaluation	6Li
BLO approximate data	225–227Ac, 107,109,110m,111Ag, 243,244,244m Am, 36,38,40Ar, 74,75As, 130,132,133,135–138,140Ba, 7,9Be, Bebound, 249,250Bk, 79,81Br, Ca, 40,42–44,46,48Ca, Cd, 106,108,110–114,115m,116Cd, 136,138,139–144Ce, 249–254Cf, Cl, 35,37Cl, 241,246–250Cm, 58,58mCo, 133–137Cs, 63Cu, 158,160–164Dy, 162,64,166–168,170Er, 253–255Es, 151–157Eu, 19F, 255Fm, Ga, 69,71Ga, 153Gd, 70,72–74,76Ge, 2,3H, Dfreegas, 3,4He, Hf, 174,176–180Hf, 196,198–202,204Hg, 165Ho, 127,129–131,135I, 113,115In, K, 39–41K, 78,80,82–86Kr, 138–140La, 175,176Lu, Mg, 24–26Mg, Mo, 92,97–100Mo, 14,15N, 94,95Nb, 142–148,150Nd, 59Ni, 235,236,238,239Np, 17O, 31P, 231–233Pa, 204Pb, 102,104–108,110Pd, 147,148,148m,149,151Pm, 141–143Pr, 236,237,243,244,246Pu, 85–87Rb, 103,105Rh, 96,98–106Ru, S, 32–34,36S, 121,123–126Sb, 74,76–80,82Se, 144,147–154Sm, 112–120,122–125Sn, 84,86–90Sr, 181,182Ta, 159,160Tb, 120,122–126,127m,128,129m,130Te, 227–230,233,234Th, Ti, 46,47,49,50Ti, 232,237,239–241U, W, 182–184,186W, 123,124,126,128–136Xe, 90,91Y, Zr, 90–96Zr

Figures 2 and 3 show examples of covariance data in the SCALE-6 library. Figure 2 is a high-fidelity ENDF/B-VII evaluation for  $^{235}\text{U}$  fission, while Fig. 3 shows BLO approximate data for fission product  $^{149}\text{Sm}(n, \gamma)$ .

## V. USE OF SENSITIVITY AND UNCERTAINTY DATA IN SIMILARITY ASSESSMENT

When using robust 3-D neutron transport techniques to predict the criticality of a system, the most likely sources of computational bias are errors in the nuclear data. The basis of the TSUNAMI validation techniques is that computational biases are primarily caused by errors in the cross-section data, which are quantified and bounded by the cross-section-covariance data. For criticality code validation,  $k_{eff}$  sensitivity data are computed for the targeted application systems as well as relevant benchmark criticality experiments. The similarity of a benchmark experiment and an application system is quantified using sensitivity and uncertainty analysis techniques described in this section.

### V.A. Comparison of Sensitivity Profiles

It is often instructive to examine the energy-dependent sensitivity data for the application system and bench-

mark experiments to visually identify important features in the sensitivity data. The Javapeño data-plotting package of SCALE 6 provides convenient interactive plotting of the sensitivity data from multiple data files. The VIBE package of SCALE 6 provides the ability to group collapse the sensitivity data, then sort and filter the collapsed data in a tabular form to identify benchmark experiments with sensitivity data most similar to the application system.

### V.B. Nuclide-Reaction-Specific Integral Index $g$

A sensitivity-based integral index denoted  $g$ , sometimes referred to as “little  $g$ ,” is based on the coverage of the sensitivity of the application system  $a$  by a given benchmark experiment  $e$  for a single nuclide-reaction pair. It is defined in terms of the normalized differences of the groupwise sensitivity coefficients for a particular nuclide  $i$  and reaction  $x$  summed over all energy groups  $j$  as

$$g_x^i = 1 - \frac{\sum_j (S_{x,j}^{a,i} - S_{x,j}^{e,i})}{\sum_j S_{x,j}^{a,i}}, \quad (42)$$

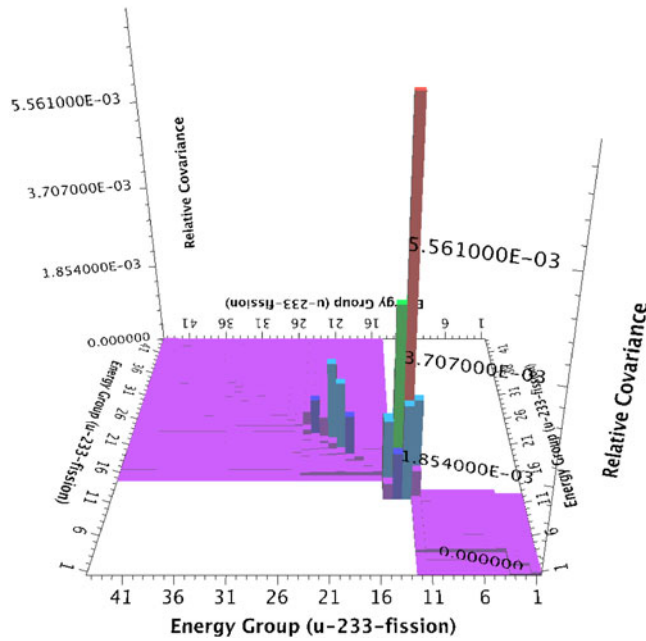


Fig. 2. ENDF/B-VII.0 covariance data for <sup>233</sup>U fission.

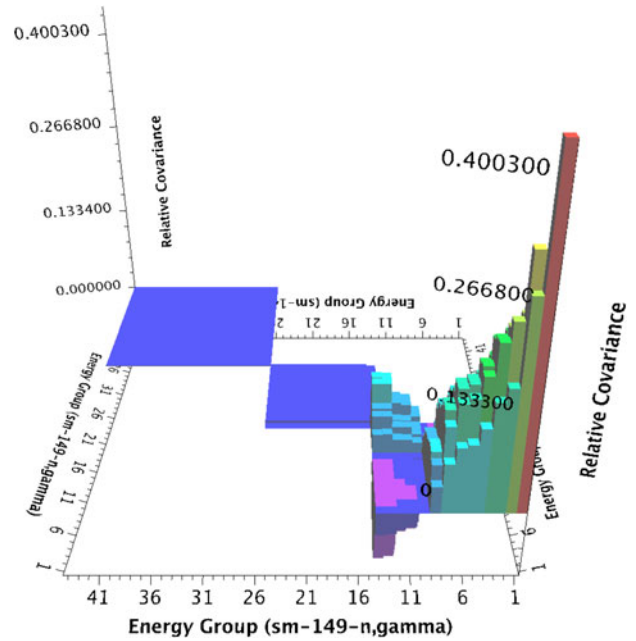


Fig. 3. BLO covariance data for <sup>149</sup>Sm(*n*,  $\gamma$ ).

where

$$S_{x,j}^{e,i} = \begin{cases} S_{x,j}^{e,i} , & \text{where } |S_{x,j}^{a,i}| \geq |S_{x,j}^{e,i}| \\ & \text{and } \frac{S_{x,j}^{a,i}}{|S_{x,j}^{a,i}|} = \frac{S_{x,j}^{e,i}}{|S_{x,j}^{e,i}|} \\ S_{x,j}^{a,i} , & \text{where } |S_{x,j}^{a,i}| < |S_{x,j}^{e,i}| \\ & \text{and } \frac{S_{x,j}^{a,i}}{|S_{x,j}^{a,i}|} = \frac{S_{x,j}^{e,i}}{|S_{x,j}^{e,i}|} \\ 0 , & \text{otherwise ,} \end{cases}$$

and the *j* summation is performed over all energy groups.

The definition of  $S_{x,j}^{e,i}$  restricts the coverage of the application by the experiment to the portion of the experiment’s sensitivity coefficient that does not exceed that of the application in magnitude. Additionally, the application’s sensitivity coefficient and that of the experiment must have the same sign. The *g* index is useful where the experiment sensitivity has a lower magnitude than that of the application in that it assesses the extent to which the benchmark experiment does not adequately test the cross section to the extent it is used in the application. The *g* index is normalized such that a *g* value of 1 indicates complete coverage of the application by the experiment for the particular nuclide-reaction pair. A *g* value of zero indicates no coverage of the application by the experiment for the particular nuclide-reaction pair. Even if the sensitivity of the benchmark experiment ex-

ceeds that of the application, the index will not exceed 1.0.

### V.C. Integral Correlation Coefficients

Since computational biases are primarily caused by errors in the cross-section data, as bounded by the cross-section-covariance data, a more rigorous approach to assessing the similarity of two systems for purposes of bias determination is the use of uncertainty analysis to quantify the shared uncertainty between two systems.<sup>5</sup> Coupling the sensitivity data from both systems with the cross-section-covariance data, the shared uncertainties between two systems can be represented by a correlation coefficient. This correlation coefficient index, denoted as  $c_k$ , measures the similarity of the systems in terms of related uncertainty.

The mathematical development of the integral index  $c_k$  is presented here based on the development given in Ref. 5. We define  $S_k$  to include the  $k_{eff}$  sensitivities of *N* different systems to the cross-section data  $\alpha$ ,

$$S_k \equiv \left[ \frac{\alpha_m}{k_n} \frac{\partial k_n}{\partial \alpha_m} \right] ,$$

$$n = 1, 2, \dots, N ; \quad m = 1, 2, \dots, M , \quad (43)$$

where *M* is the number of nuclear data parameters. The uncertainty matrix for all the system  $k_{eff}$  values  $C_{kk}$  is given as

$$C_{kk} = S_k C_{\alpha\alpha} S_k^T . \quad (44)$$

Here,  $\mathbf{S}_k$  is an  $N \times M$  matrix,  $\mathbf{C}_{\alpha\alpha}$  is an  $M \times M$  matrix, and the resulting  $\mathbf{C}_{kk}$  matrix is of dimensions  $N \times N$ . The diagonal elements of the  $\mathbf{C}_{kk}$  are the relative variance values  $\sigma_{k_n}^2$  for each of the systems under consideration, and the off-diagonal elements are the relative covariances between a given application system  $a$  and a given benchmark experiment  $e$ , represented as  $\sigma_{k_{ae}}^2$ . Correlation coefficients provide a common means of normalizing shared uncertainties. The correlation coefficient is defined by dividing the covariance terms by the corresponding standard deviations as

$$c_k = \frac{\sigma_{k_{ae}}^2}{(\sigma_{k_a} \sigma_{k_e})}, \quad (45)$$

such that the single  $c_k$  value represents the correlation of uncertainties between an application and experiment.

These correlations are primarily due to the fact that the uncertainties in the calculated  $k_{eff}$  values for two different systems are related, since they contain the same materials. Cross-section uncertainties propagate to all systems containing these materials. Systems with the same materials and similar spectra would be correlated, while systems with different materials or spectra would not be correlated. The interpretation of the correlation coefficient is as follows: A value of 0.0 represents no correlation between the systems, a value of 1.0 represents full correlation between the systems, and a value of  $-1.0$  represents a full anticorrelation.

#### V.D. Nuclide-Reaction-Specific Correlation Coefficients

It is sometimes desirable to assess the similarity of systems in terms of the shared uncertainties for a single nuclide-reaction pair. The individual  $c_k$  is similar to system-wide  $c_k$  from Eq. (45), except that it is normalized between  $-1$  and  $1$  for each for a particular nuclide  $i$  and reaction  $x$  as

$$c_{k_{ae},(i-x)}^{individual} = \frac{\sigma_{k_{ae},(i-x)}^2}{(\sigma_{k_a,(i-x)} \sigma_{k_e,(i-x)})}, \quad (46)$$

where

$\sigma_{k_{ae},(i-x)}^2$  = covariance between application  $a$  and experiment  $e$  due to the specified nuclide-reaction pairs

$\sigma_{k_a,(i-x)}^2$  = standard deviation in  $k_{eff}$  for the application due to the specified nuclide-reaction pair

$\sigma_{k_e,(i-x)}^2$  = standard deviation in  $k_{eff}$  for the experiment due to the specified nuclide-reaction pair.

Note that individual  $c_k$  values are only computed for the same nuclide-reaction pair in the application and the experiment. Although cross-reaction and cross-nuclide

covariance data are available, the cross-relationship has no physical interpretation for assessing the similarity of systems for a specific nuclide-reaction pair.

## VI. BIAS ASSESSMENT WITH TRENDING ANALYSIS

Because the uncertainty in  $k_{eff}$  due to cross-section data uncertainties is directly related to potential computational bias, the  $c_k$  coefficient quantifies the similarity of the two systems in terms of common sources of bias. Where many benchmarks similar to the application are available to quantify all potential sources of bias, linear regression and extrapolation techniques can be applied to determine bias and bias uncertainty values for an application. The USLSTATS code can be applied to determine the computational bias, bias uncertainty, and upper subcritical limit (USL) based on trends in calculated  $k_{eff}$  values as a function of their similarity to the application as determined by the integral index  $c_k$ . A linear regression of the ratio of computed-to-measured  $k_{eff}$  values as a function of  $c_k$  is extrapolated to a value 1.0, which is the  $c_k$  value generated when the application is compared to itself. Thus, the value of the regression line at  $c_k$  of 1.0 is the predicted calculated-to-measured ratio of the application system, from which the computational bias is determined. The statistical analysis techniques of USLSTATS are applied to determine a confidence band in the extrapolated value, which then becomes the uncertainty in the computational bias.

Where analytical methods are used to predict the criticality condition of a design system, the American National Standard ANSI/ANS-8.17-1984 (R1997) (Ref. 34) requires that the calculated multiplication factor  $k_s$  not exceed a maximum allowable value established as

$$k_s \leq k_c - \Delta k_s - \Delta k_c - \Delta k_m, \quad (47)$$

where

$k_s$  = calculated allowable maximum multiplication factor  $k_{eff}$  of the system being evaluated for normal or credible abnormal conditions or events

$k_c$  = mean  $k_{eff}$  that results from the calculation of the benchmark criticality experiments using a particular computational method. If the calculated  $k_{eff}$  values for the criticality experiments exhibit a trend with a parameter, then  $k_c$  shall be determined by extrapolation on the basis of a best fit to the calculated values. The criticality experiments used as benchmarks in computing  $k_c$  should have physical compositions, configurations, and nuclear characteristics (including reflectors) similar to those of the system being evaluated

$\Delta k_s$  = allowance for statistical or convergence uncertainties, or both in the computation of  $k_s$ ; material and fabrication tolerances; and uncertainties due to limitations in the geometric or material representations used in the computational method

$\Delta k_c$  = margin for uncertainty in  $k_c$ , which includes allowance for uncertainties in the critical experiments; statistical or convergence uncertainties, or both, in the computation of  $k_c$ ; uncertainties due to extrapolation of  $k_c$  outside the range of experimental data; and uncertainties due to limitations in the geometrical or material representations used in the computational method

$\Delta k_m$  = additional margin to ensure the subcriticality of  $k_s$ .

Consistent with the requirements of ANSI/ANS-8.17-1984 (R1997), a criticality code is typically validated against a suite of critical experiments to define a USL for design systems. According to the standard, the computed  $k_{eff}$  value of a design system (i.e.,  $k_s$ ) should not exceed the maximum acceptable value. This is expressed as

$$k_s + 2\sigma \leq USL = 1.00 + \beta - \Delta\beta - \Delta k_m, \quad (48)$$

where  $\sigma$  is the standard deviation of the computed value  $k_s$ , and  $\beta$  and  $\Delta\beta$  represent the computational bias and uncertainty in the bias, respectively.<sup>35</sup> For critical experiments, the computational bias is the difference between the mean value of  $k_{eff}$  calculated for the critical experiments,  $k_c$ , and 1.0 (i.e.,  $\beta = k_c - 1.0$ ). In practice, certain critical experiments may exhibit calculated  $k_{eff}$  values  $> 1.0$ , leading to a positive bias and reducing the required

subcritical margin for the design system. However, regulatory impositions typically have not allowed for a positive computational bias; thus,  $\beta$  is either negative or zero in practice. The quantity  $\Delta k_m$  is often referred to as an administrative margin and commonly assigned a value between 2 and 5% in  $k_{eff}$  (e.g.,  $\Delta k_m = 0.05$ ), depending on the application and regulatory guidance.

Two commonly used approaches for the calculation of the USL based on a suite of criticality experiments covering a particular area of applicability are the confidence band with administrative margin, referred to as USL<sub>1</sub>, and the single-sided uniform-width closed-interval approach, also called the lower tolerance band method, referred to as USL<sub>2</sub> (Ref. 6). The statistical analysis commonly used in the computation of USL<sub>1</sub> and USL<sub>2</sub> is only valid within the range of applicability of the chosen trending parameter. However, the approach applied with TSUNAMI always requires at least some extrapolation. As USL<sub>2</sub> is by definition a closed-interval approach, it is never suitable for extrapolation. However, the USL<sub>1</sub> approach can be appropriately defined for extrapolation as presented below and implemented in the SCALE 6 version of USLSTATS.

**VI.A. Correlation Coefficient Trending**

The USL<sub>1</sub> in Ref. 6 applies a statistical calculation of the bias and its uncertainty plus an optional additional margin to a linear fit of critical experiment benchmark data. This approach is illustrated in Fig. 4, where the additional margin is set to 0.02, or 2%,  $\Delta k/k$ . In this figure, the blue-dashed  $k(x)$  line (color online) represents a linear regression fit to a set of calculations based on the calculated-to-experiment (C/E) ratio of  $k_{eff}$  results from critical experiments. The relative bias in the

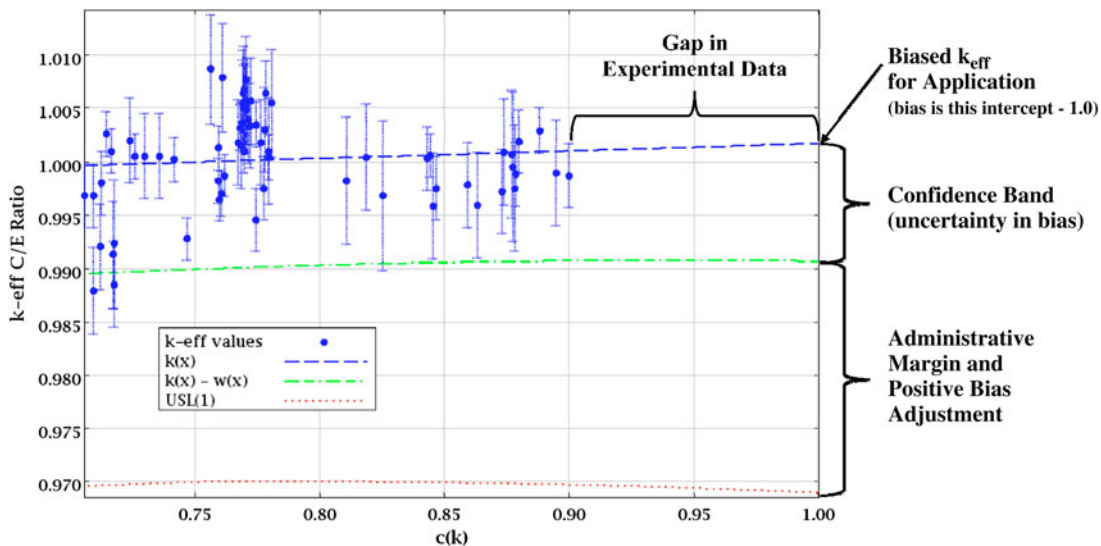


Fig. 4. Illustration of correlation coefficient trending with USL<sub>1</sub> and penalty.

application ( $\Delta k/k$ ) is given as  $k(x) - 1$ , evaluated at  $c_k = 1.0$ . The green-dashed line represents the lower confidence band for a single additional calculation, a quadratic expression defined below. The width of this band is determined statistically based on the existing data and a specified level of confidence; the greater the standard deviation in the data or the larger the confidence desired, the larger the band width will be. This confidence band  $w(x)$  accounts for uncertainties in the experiments and the calculational approach as well as the dispersion of the data points and is therefore a statistical basis for  $\Delta\beta$ , the uncertainty in the value of  $\beta$ . With a  $(1 - \gamma_1)$  confidence level,  $w(x)$  is defined as

$$w(x) = t_{1-\gamma_1, s_p} \left[ 1 + \frac{1}{n} + \frac{(x - \bar{x})^2}{\sum_{i=1, n} (x_i - \bar{x})^2} \right]^{1/2}, \quad (49)$$

where

- $n$  = number of critical calculations used in establishing  $k(x)$
- $t_{1-\gamma_1}$  = Student's t-distribution statistic for  $1 - \gamma_1$  and  $n - 2$  degrees of freedom
- $\bar{x}$  = mean value of the independent variable  $x$  in the set of calculations
- $s_p$  = pooled standard deviation for the set of criticality calculations.

The pooled standard deviation is obtained from the pooled variance ( $s_p = \sqrt{s_p^2}$ ), where  $s_p^2$  is given as

$$s_p^2 = s_{k(x)}^2 + s_w^2, \quad (50)$$

where  $s_{k(x)}^2$  is the variance (or mean square error) of the regression fit and is given by

$$s_{k(x)}^2 = \frac{1}{(n - 2)} \left[ \sum_{i=1, n} (k_i - \bar{k})^2 \frac{\left\{ \sum_{i=1, n} (x_i - \bar{x})(k_i - \bar{k}) \right\}^2}{\sum_{i=1, n} (x_i - \bar{x})^2} \right], \quad (51)$$

and  $s_w^2$  is the within-variance of the data:

$$s_w^2 = \frac{1}{n} \sum_{i=1, n} \sigma_i^2, \quad (52)$$

where  $\sigma_i$  is the standard deviation associated with  $k_i$ , which could be due to Monte Carlo calculations.

Note that the function  $w(x)$  is a curvilinear function that will increase in width as a function of extrapolation from the data. Typically,  $w(x)$  is determined at a 95% confidence level.

The red-dashed line (color online) in Fig. 4 represents  $USL_1$ , which discounts any positive bias and

cludes the administrative margin. The value of  $USL_1$  as a function of the trending parameter  $x$  is defined as

$$USL_1(x) = \begin{cases} 1 - \Delta k_m - w(x) + \beta(x), & \beta(x) < 0 \\ 1 - \Delta k_m - w(x), & \beta(x) \geq 0. \end{cases} \quad (53)$$

The value of  $USL_1$  for the application is determined by evaluating Eq. (53) with  $x = 1.0$ .

The data used in the  $USL_1$  determination must pass a normality test before statistical analyses are applied. USLSTATS provides a simple  $\chi^2$  test for normality using five equal-probability bins. Because the current normality test is so simple, data sets that may pass other normality tests may fail the USLSTATS normality test. If the data are shown to be normal by some other means, the statistical treatments of USLSTATS can still be valid, even though the data failed the internal test.

### VI.B. Gap Analysis Using TSUNAMI Penalty Assessment

The set of critical experiments used as benchmarks in the computation of  $\beta$  should be representative of the composition, configuration, and nuclear characteristics of the application system. However, ANSI/ANS-8.1 (Ref. 3) allows that the range of applicability may be extended beyond the range of conditions represented by the benchmark experiments by extrapolating the trends established for the bias. When the extrapolation is large relative to the range of data, the calculational method applied should be supplemented by other methods to better estimate the extrapolated bias. Note that "large" is not defined by the ANSI standard.

A method is available in TSUNAMI-IP to assess an additional margin to subcriticality, or penalty, where sufficient experiments are not available to provide complete coverage for a particular application. The gap between the best-available experiment and the application is illustrated in Fig. 4, where the  $c_k$  value of the best-matching experiment is 0.90, indicating that 10% of the cross-section uncertainty in the application is different from that in the closest matching experiment. Although the statistical treatment of USLSTATS accounts for trends in existing data, the lack of similarity indicates that some processes in the application may not be fully accounted for by the experiments included in the analysis. In this case, any possible change in the trend as  $c_k$  approaches 1.0 may not be bounded by a statistical analysis of the C/E values.

The TSUNAMI gap analysis technique quantifies an additional uncertainty component that can be added to the administrative margin to provide an added measure of safety for application systems where validation coverage is lacking. The penalty calculation is based on the criteria for coverage explained in Sec. V.B for the integral index  $g$ . The TSUNAMI penalty calculation

quantifies the uncertainty in the application that remains after the best-available coverage from qualified experiments has been applied. As this form of gap analysis is intended as a supplement to  $c_k$  trending analysis, any experiment used in the penalty assessment calculation must pass a qualification test to determine global similarity of the experiment, based on  $c_k$ . Thus, only experiments that exhibit a certain degree of similarity to the application, and thus an expected relevant influence on the trending analysis, can be considered in the penalty calculation. Additionally, a sufficient number of similar experiments are required before any penalty assessment is produced by TSUNAMI-IP.

To compute the penalty, a vector of the minimum differences in the sensitivity coefficients,  $\mathbf{Z}_a$ , for the application with respect to all experiments can be obtained as

$$\mathbf{Z}_a \equiv [Z_{x,j}^{a,n}] , \quad n = 1, \dots, N, x = 1, \dots, X, j = 1, \dots , \quad (54)$$

where

$$Z_{x,j}^{a,n} = S_{x,j}^{a,n} - C_{x,j}^{a,n} ,$$

where  $C_{x,j}^{a,n}$  is a composite of the best-available sensitivity data from all experiments and is defined as

$$C_{x,j}^{a,n} = S_{x,j}^{e',n} \text{ for the experiment that satisfies } \min |S_{x,j}^{a,n} - S_{x,j}^{e',n}|, e' = 1, \dots, E ,$$

$n$  = number of nuclides in the application system

$x$  = number of reactions for each nuclide

$j$  = number of energy groups

$e$  = number of experiments meeting the qualification tests.

Once  $\mathbf{Z}_a$  is computed, the portion of the sensitivity of the application that is not covered by the experiments can be used to propagate the uncertainty in the cross-section data to a relative uncertainty in  $k_{eff}$  as

$$\Delta k_{eff}/k_{eff} = \sqrt{\mathbf{Z}_a \mathbf{C}_{\alpha\alpha} \mathbf{Z}_a^T} . \quad (55)$$

In the above equation, the elements of  $\mathbf{Z}_a$  are each expressed in terms of  $(\Delta k_{eff}/k_{eff})/(\Delta\sigma/\sigma)$ , and the elements of  $\mathbf{C}_{\alpha\alpha}$  are expressed in terms of relative variances or covariances as  $(\Delta\sigma/\sigma)^2$ , so that the final penalty is expressed as a relative uncertainty in  $k_{eff}$ ,  $\Delta k_{eff}/k_{eff}$ . This relative uncertainty in  $k_{eff}$  due to the gap in experimental coverage can be used to increase the safety margin to provide for extrapolation beyond the range of applicability of available experiments.

## VII. BIAS ASSESSMENT WITH DATA ADJUSTMENT TECHNIQUES

A new capability for SCALE 6 allows the prediction of computational biases with the nuclear data adjustment tool TSURFER, which is based on a generalized linear least-squares approach.<sup>5</sup> The data adjustments in TSURFER are not used to produce adjusted cross-section data libraries for subsequent use; rather, they are used only to predict biases in application systems. As TSURFER is a general-purpose tool, a computed quantity for which a bias is predicted is referred to as a response. A response is often  $k_{eff}$  but in general could be a reactivity, a reaction rate ratio, or any other quantity of interest that can be both measured in benchmark experiments and calculated through numerical simulation using multigroup cross-section data. TSURFER identifies a single set of adjustments to nuclear data and experimental values, all bounded by their uncertainties, that will result in the computational models all producing response values close to their experimental response value. Then the same data adjustments are used to predict an unbiased response value for the application and an uncertainty on the adjusted response value. The difference between the originally calculated response value and the new postadjustment response value represents the bias in the original calculation, and the uncertainty in the adjusted value represents the uncertainty in this bias. If similar experiments are available to validate the use of a particular nuclide in the application, the uncertainty of the bias for this nuclide is reduced. In TSURFER, experiments that are dissimilar from the application can still provide useful information for bias assessment if at least one material demonstrates similar sensitivities to those of the application. If similar experiments are not available to validate a particular nuclide, a high uncertainty in the bias for the given nuclide will result. Thus, with a complete set of experiments to validate important components in the application, a precise bias with a small uncertainty can be predicted. Where the experimental coverage is lacking, a bias can be predicted with an appropriately large uncertainty. As users gain experience with TSURFER, it may become a preferred tool for rigorous bias and bias uncertainty determination, particularly for applications for which nearly identical critical experiments are not available. However, the results of TSURFER analyses rely on the availability of quality uncertainty and correlation data for both nuclear data and benchmark experiments.

### VII.A. TSURFER Computational Methodology

TSURFER applies a GLLS technique to produce the adjusted cross-section values that are used for bias prediction. A recent detailed derivation of the GLLS formalism is given in Ref. 5. The general formalism

allows cross correlations between the initial integral experiment measurements and the original nuclear data, such as would be present if the calculations used a previously “adjusted” library of nuclear data. Since this is not normally done in SCALE, correlations between the benchmark experiment measurements and the cross-section data in the multigroup libraries are not considered in the TSURFER code; therefore, the GLLS equations presented here are somewhat simplified compared to the more general expressions in Ref. 5.

At present, the SCALE cross-section-covariance data files characterize nuclear data uncertainties in terms of relative covariances. Therefore, the initial development that follows is for relative, rather than absolute, response sensitivity and uncertainty parameters. It is then shown how to express the quantities in absolute form for reactivity analysis and mixed relative-absolute form for combined  $k_{eff}$  and reactivity analysis.

The methodology consists of calculating values for a set of  $I$  integral responses ( $k_{eff}$ , reactivity differences, reaction rates, etc.), some of which have been measured in selected benchmark experiments. Responses with no measured values are then selected as applications, whose biases will be predicted based on the measured quantities. The set of measured response values  $\{m_i; i = 1, 2, \dots, I\}$  can be arranged into an  $I$ -dimension column vector designated as  $\mathbf{m}$ . By convention the (unknown) experimental values corresponding to applications are represented by the corresponding calculated values. As discussed in Sec. III.A.2, the measured integral responses have uncertainties—possibly correlated—due to uncertainties in the system parameter specifications. The  $I \times I$  covariance matrix describing the relative experimental uncertainties is defined to be  $\mathbf{C}_{mm}$ .

Experimental uncertainties are typically defined in the description of benchmark experiments. Often the sources of the uncertainties are detailed, and the contribution to the overall uncertainty in the response value is described. These uncertainties are important to TSURFER analysis, as the reported benchmark response value is only as precise as techniques used in its evaluation allow. It makes little sense to adjust cross-section data to precisely match an imprecise response value. Therefore, TSURFER not only adjusts the cross-section data within their uncertainties but also adjusts the experimental values within their uncertainties, constrained by their correlations.

Discrepancies between the calculated and measured responses are defined by the  $I$  dimensional column vector

$$\mathbf{d} = \left\{ d_i = \frac{k_i(\boldsymbol{\alpha}) - m_i}{k_i(\boldsymbol{\alpha})}, \quad i = 1, \dots, I \right\}, \quad (56)$$

where  $k_i(\boldsymbol{\alpha})$  is the computed  $k_{eff}$  value for system  $i$  using the prior, unadjusted, cross-section data  $\boldsymbol{\alpha}$ , and  $m_i$  is the measured  $k_{eff}$  of system  $i$ . In TSURFER the components of  $\mathbf{d}$  corresponding to application responses are set to

zero because applications have no measured values. Using the standard formula for propagation of error and assuming no correlations between  $k$  and  $m$ , the relative uncertainty matrix for the discrepancy vector  $\mathbf{d}$  can be expressed as the  $I \times I$  matrix:

$$\begin{aligned} \mathbf{C}_{dd} &= \mathbf{C}_{kk} + \mathbf{F}_{m/k} \mathbf{C}_{mm} \mathbf{F}_{m/k} \\ &= \mathbf{S}_k \mathbf{C}_{\alpha\alpha} \mathbf{S}_k^T + \mathbf{F}_{m/k} \mathbf{C}_{mm} \mathbf{F}_{m/k}, \end{aligned} \quad (57)$$

where  $\mathbf{F}_{m/k}$  is an  $I \times I$  diagonal matrix containing  $m/k$  factors, that is, E/C factors (ratio of experimental to calculated response values). The inverse of the matrix  $\mathbf{C}_{dd}$  appears in several expressions presented later in this section.

The goal of the GLLS method is to vary the nuclear data ( $\boldsymbol{\alpha} \rightarrow \boldsymbol{\alpha}'$ ) and the measured integral responses ( $\mathbf{m} \rightarrow \mathbf{m}'$ ), such that they are most consistent with their respective uncertainty matrices,  $\mathbf{C}_{\alpha\alpha}$  and  $\mathbf{C}_{mm}$ . This is done by minimizing chi-square, expressed as

$$\begin{aligned} \chi^2 &= \left[ \frac{\boldsymbol{\alpha}' - \boldsymbol{\alpha}}{\boldsymbol{\alpha}} \right]^T \mathbf{C}_{\alpha\alpha}^{-1} \left[ \frac{\boldsymbol{\alpha}' - \boldsymbol{\alpha}}{\boldsymbol{\alpha}} \right] \\ &\quad + \left[ \frac{\mathbf{m}' - \mathbf{m}}{\mathbf{m}} \right]^T \mathbf{C}_{mm}^{-1} \left[ \frac{\mathbf{m}' - \mathbf{m}}{\mathbf{m}} \right], \\ &= [\Delta\boldsymbol{\alpha}]^T \mathbf{C}_{\alpha\alpha}^{-1} [\Delta\boldsymbol{\alpha}] + [\Delta\mathbf{m}]^T \mathbf{C}_{mm}^{-1} [\Delta\mathbf{m}], \end{aligned} \quad (58)$$

where  $\Delta\alpha_i = (\alpha'_i - \alpha_i)/\alpha_i$  and  $\Delta m_i = (m'_i - m_i)/m_i$ . Equation (58) is rearranged to give

$$\begin{aligned} \chi^2 &= [\boldsymbol{\sigma}_\alpha^{-1} \Delta\boldsymbol{\alpha}]^T \mathbf{R}_{\alpha\alpha}^{-1} [\boldsymbol{\sigma}_\alpha^{-1} \Delta\boldsymbol{\alpha}] \\ &\quad + [\boldsymbol{\sigma}_m^{-1} \Delta\mathbf{m}]^T \mathbf{R}_{mm}^{-1} [\boldsymbol{\sigma}_m^{-1} \Delta\mathbf{m}]. \end{aligned} \quad (59)$$

Equation (59) expresses the variations in the nuclear data and measured responses in units of their respective standard deviations, that is,  $[\boldsymbol{\sigma}_\alpha^{-1} \Delta\boldsymbol{\alpha}]$  and  $[\boldsymbol{\sigma}_m^{-1} \Delta\mathbf{m}]$ .

Chi-square is a quadratic form indicating the squared magnitude of the combined data variations with respect to their uncertainties. This is easily seen for the simple case in which  $[\mathbf{R}_{\alpha\alpha}]^{-1}$  and  $[\mathbf{R}_{mm}]^{-1}$  are identity matrices, so that Eq. (59) reduces to just the diagonal contributions:

$$\chi^2 \rightarrow \sum_{n=1}^M \left( \frac{\alpha'_n - \alpha_n}{\tilde{\sigma}_{\alpha_n}} \right)^2 + \sum_{i=1}^I \left( \frac{m'_i - m_i}{\tilde{\sigma}_{m_i}} \right)^2. \quad (60)$$

The first term on the right side of Eq. (60) is equal to the sum of the squares of the individual nuclear data variations expressed in units of their standard deviations, while the second term represents a similar quantity for the measured integral responses. In the general case where correlations exist, the inverse matrices in Eq. (59) are not diagonal, and the value of chi-square must be evaluated using the indicated matrix multiplication.

Thus, it can be seen that the GLLS method determines adjustments in the nuclear data and experimental measurements that (a) make the calculated and measured responses agree [i.e.,  $\mathbf{k}' = \mathbf{k}'(\boldsymbol{\alpha}') = \mathbf{m}'$ , within the limitations of first-order sensitivity theory] and (b) minimize Eq. (60) so that the adjustments are most consistent with the data uncertainties. Although many possible combinations of data variations may make  $k' = m'$ , there is a unique set that also minimizes  $\chi^2$ .

The following variations minimize Eq. (60), subject to the constraint  $\mathbf{k}'(\boldsymbol{\alpha}') = \mathbf{m}'$  and the linearity condition  $[\Delta\mathbf{k}] = \mathbf{S}_{\mathbf{k}\boldsymbol{\alpha}}[\Delta\boldsymbol{\alpha}]$  where  $\Delta k_i = (k'_i - k_i)/k_i$ :

$$\Delta\boldsymbol{\alpha} = -[\mathbf{C}_{\boldsymbol{\alpha}\boldsymbol{\alpha}}\mathbf{S}_{\mathbf{k}\boldsymbol{\alpha}}^T\mathbf{C}_{\mathbf{d}\mathbf{d}}^{-1}]\mathbf{d} \quad (61)$$

and

$$\Delta\mathbf{m} = [\mathbf{C}_{\mathbf{m}\mathbf{m}}\mathbf{F}_{\mathbf{m}/\mathbf{k}}\mathbf{C}_{\mathbf{d}\mathbf{d}}^{-1}]\mathbf{d} . \quad (62)$$

In the above equations the initial response discrepancy vector  $\mathbf{d}$  is operated on by the transformation matrix in square brackets to obtain the desired variations in nuclear data and integral measurements; thus, it is the discrepancy components that drive the adjustments. If the linearity assumption is valid, then the changes in the calculated responses are found to be

$$\Delta k = F_{m/k}\Delta m - d = S_k\Delta\alpha . \quad (63)$$

Equation (63) relates the adjustments in calculated responses, measured responses, and nuclear data.

As previously discussed, consolidation of the calculated and measured responses reduces the prior uncertainties for  $\boldsymbol{\alpha}$ ,  $\mathbf{m}$ , and  $\mathbf{k}$  because additional knowledge has been incorporated. This is indicated by their modified covariance matrices  $\mathbf{C}_{\boldsymbol{\alpha}'\boldsymbol{\alpha}'}$ ,  $\mathbf{C}_{\mathbf{m}'\mathbf{m}'}$ ,  $\mathbf{C}_{\mathbf{k}'\mathbf{k}'}$ , respectively, given by

$$\mathbf{C}_{\boldsymbol{\alpha}'\boldsymbol{\alpha}'} = \mathbf{C}_{\boldsymbol{\alpha}\boldsymbol{\alpha}} - [\mathbf{C}_{\boldsymbol{\alpha}\boldsymbol{\alpha}}\mathbf{S}_{\mathbf{k}}^T\mathbf{C}_{\mathbf{d}\mathbf{d}}^{-1}\mathbf{S}_{\mathbf{k}}\mathbf{C}_{\boldsymbol{\alpha}\boldsymbol{\alpha}}] , \quad (64)$$

$$\mathbf{C}_{\mathbf{m}'\mathbf{m}'} = \mathbf{C}_{\mathbf{m}\mathbf{m}} - [\mathbf{C}_{\mathbf{m}\mathbf{m}}\mathbf{F}_{\mathbf{m}/\mathbf{k}}\mathbf{C}_{\mathbf{d}\mathbf{d}}^{-1}\mathbf{F}_{\mathbf{m}/\mathbf{k}}\mathbf{C}_{\mathbf{m}\mathbf{m}}] , \quad (65)$$

and

$$\mathbf{C}_{\mathbf{k}'\mathbf{k}'} = \mathbf{C}_{\mathbf{k}\mathbf{k}} - [\mathbf{C}_{\mathbf{k}\mathbf{k}}\mathbf{C}_{\mathbf{d}\mathbf{d}}^{-1}\mathbf{C}_{\mathbf{k}\mathbf{k}}] . \quad (66)$$

If all the responses on the TSURFER input are relative formatted, then the adjusted data and response values edited by TSURFER are obtained from Eqs. (61), (62), and (63), while the square roots of diagonal elements in Eqs. (64) and (65) correspond to the relative values for adjusted uncertainties in the nuclear data and in the experiment responses, respectively.

The adjustment formulas must be modified slightly to be consistent with the absolute-formatted responses. In the following expressions, absolute response covariance and response sensitivity data are denoted by a tilde:

$$\tilde{\mathbf{d}} = \mathbf{k}(\boldsymbol{\alpha}) - \mathbf{m} , \quad (67)$$

$$\tilde{\mathbf{C}}_{\mathbf{d}\mathbf{d}} = \tilde{\mathbf{C}}_{\mathbf{k}\mathbf{k}} + \mathbf{C}_{\mathbf{m}\mathbf{m}} = \tilde{\mathbf{S}}_{\mathbf{k}}\mathbf{C}_{\boldsymbol{\alpha}\boldsymbol{\alpha}}\tilde{\mathbf{S}}_{\mathbf{k}}^T + \tilde{\mathbf{C}}_{\mathbf{m}\mathbf{m}} , \quad (68)$$

$$\Delta\tilde{\boldsymbol{\alpha}} = \boldsymbol{\alpha}' - \boldsymbol{\alpha} = -[\mathbf{C}_{\boldsymbol{\alpha}\boldsymbol{\alpha}}\tilde{\mathbf{S}}_{\mathbf{k}}^T\tilde{\mathbf{C}}_{\mathbf{d}\mathbf{d}}^{-1}]\tilde{\mathbf{d}} , \quad (69)$$

$$\Delta\tilde{\mathbf{m}} = \mathbf{m}' - \mathbf{m} = [\tilde{\mathbf{C}}_{\mathbf{m}\mathbf{m}}\tilde{\mathbf{C}}_{\mathbf{d}\mathbf{d}}^{-1}]\tilde{\mathbf{d}} , \quad (70)$$

and

$$\Delta\tilde{\mathbf{k}} = \mathbf{k}' - \mathbf{k} = (\mathbf{m}' - \mathbf{m}) - \mathbf{d} = \mathbf{S}_{\mathbf{k}}(\boldsymbol{\alpha}' - \boldsymbol{\alpha}) . \quad (71)$$

The covariances for the posterior values of the nuclear data, in relative format, and measured responses, in absolute format, are given as

$$\mathbf{C}_{\boldsymbol{\alpha}'\boldsymbol{\alpha}'} = \mathbf{C}_{\boldsymbol{\alpha}\boldsymbol{\alpha}} - [\mathbf{C}_{\boldsymbol{\alpha}\boldsymbol{\alpha}}\tilde{\mathbf{S}}_{\mathbf{k}}^T\tilde{\mathbf{C}}_{\mathbf{d}\mathbf{d}}^{-1}[\tilde{\mathbf{S}}_{\mathbf{k}}\mathbf{C}_{\boldsymbol{\alpha}\boldsymbol{\alpha}}]] \quad (72)$$

and

$$\tilde{\mathbf{C}}_{\mathbf{m}'\mathbf{m}'} = \tilde{\mathbf{C}}_{\mathbf{m}\mathbf{m}} - [\tilde{\mathbf{C}}_{\mathbf{m}\mathbf{m}}\tilde{\mathbf{C}}_{\mathbf{d}\mathbf{d}}^{-1}\tilde{\mathbf{C}}_{\mathbf{m}\mathbf{m}}] . \quad (73)$$

If all input responses to TSURFER are absolute formatted, the adjusted data and response values edited by TSURFER are obtained from Eqs. (69), (70), and (71), while the square roots of diagonal elements in Eqs. (72) and (73) correspond to the values for adjusted uncertainties in the nuclear data and in the experiment responses, respectively.

The adjustment formulas again must be modified slightly given a set of mixed relative/absolute-formatted responses. In the following expressions, mixed response covariance and response sensitivity data are denoted by a caret, and  $\hat{\mathbf{F}}_{\mathbf{m}/\mathbf{k}}$  is an  $I \times I$  diagonal matrix containing  $m/k$  factors for relative-formatted responses or a value of one for absolute-formatted responses:

$$\hat{d}_i = \begin{cases} \frac{k(\boldsymbol{\alpha})_i - m_i}{k(\boldsymbol{\alpha})_i} & i\text{th response is relative formatted} \\ k(\boldsymbol{\alpha})_i - m_i & i\text{th response is absolute formatted} , \end{cases} \quad (74)$$

$$\Delta\hat{m}_i = \begin{cases} \frac{m'_i - m_i}{m_i} & \text{relative} \\ m'_i - m_i & \text{absolute} , \end{cases} \quad (75)$$

$$\Delta\hat{\mathbf{k}}_i = \begin{cases} \frac{\mathbf{k}'(\boldsymbol{\alpha}')_i - \mathbf{k}(\boldsymbol{\alpha})_i}{\mathbf{k}(\boldsymbol{\alpha})_i} & \text{relative} \\ \mathbf{k}(\boldsymbol{\alpha})_i - \mathbf{k}(\boldsymbol{\alpha})_i & \text{absolute} , \end{cases} \quad (76)$$

$$\begin{aligned} \hat{\mathbf{C}}_{\mathbf{d}\mathbf{d}}^{-1} &= \hat{\mathbf{C}}_{\mathbf{k}\mathbf{k}} + \hat{\mathbf{F}}_{\mathbf{m}/\mathbf{k}}\hat{\mathbf{C}}_{\mathbf{m}\mathbf{m}}\hat{\mathbf{F}}_{\mathbf{m}/\mathbf{k}} \\ &= \hat{\mathbf{S}}_{\mathbf{k}}\mathbf{C}_{\boldsymbol{\alpha}\boldsymbol{\alpha}}\hat{\mathbf{S}}_{\mathbf{k}}^T + \hat{\mathbf{F}}_{\mathbf{m}/\mathbf{k}}\hat{\mathbf{C}}_{\mathbf{m}\mathbf{m}}\hat{\mathbf{F}}_{\mathbf{m}/\mathbf{k}} , \end{aligned} \quad (77)$$

$$\Delta\hat{\boldsymbol{\alpha}} = -[\mathbf{C}_{\boldsymbol{\alpha}\boldsymbol{\alpha}}\hat{\mathbf{S}}_{\mathbf{k}}^T\hat{\mathbf{C}}_{\mathbf{d}\mathbf{d}}^{-1}]\hat{\mathbf{d}} , \quad (78)$$

$$\Delta\hat{\mathbf{m}} = [\hat{\mathbf{C}}_{\mathbf{m}\mathbf{m}}\hat{\mathbf{F}}_{\mathbf{m}/\mathbf{k}}\hat{\mathbf{C}}_{\mathbf{d}\mathbf{d}}^{-1}]\hat{\mathbf{d}} , \quad (79)$$

and

$$\Delta \hat{\mathbf{k}} = \hat{\mathbf{S}}_{\mathbf{k}} \Delta \hat{\boldsymbol{\alpha}} . \quad (80)$$

Covariances for the posterior values of the nuclear data and measured responses are given as

$$\mathbf{C}_{\boldsymbol{\alpha}'\boldsymbol{\alpha}'} = \mathbf{C}_{\boldsymbol{\alpha}\boldsymbol{\alpha}} - [\mathbf{C}_{\boldsymbol{\alpha}\boldsymbol{\alpha}} \hat{\mathbf{S}}_{\mathbf{k}}^T] \hat{\mathbf{C}}_{\mathbf{d}\mathbf{d}}^{-1} [\hat{\mathbf{S}}_{\mathbf{k}} \mathbf{C}_{\boldsymbol{\alpha}\boldsymbol{\alpha}}] \quad (81)$$

and

$$\hat{\mathbf{C}}_{\mathbf{m}'\mathbf{m}'} = \hat{\mathbf{C}}_{\mathbf{m}\mathbf{m}} - [\hat{\mathbf{C}}_{\mathbf{m}\mathbf{m}} \hat{\mathbf{F}}_{\mathbf{m}/\mathbf{k}} \hat{\mathbf{C}}_{\mathbf{d}\mathbf{d}}^{-1} \hat{\mathbf{F}}_{\mathbf{m}/\mathbf{k}} \hat{\mathbf{C}}_{\mathbf{m}\mathbf{m}}] . \quad (82)$$

If responses on the TSURFER input are both relative formatted and absolute formatted, the adjusted data and response values edited by TSURFER are obtained from Eqs. (78) and (79), while the square roots of diagonal elements in Eqs. (81) and (82) correspond to the relative or absolute values for adjusted uncertainties in the nuclear data and in the experiment responses, respectively.

### VII.B. Consistency Relations and Chi-Square Filtering

Using relative sensitivities, variations for  $\Delta \mathbf{m}$  and  $\Delta \boldsymbol{\alpha}$  defined by Eqs. (61) and (62) are those that give the smallest value of the quadratic form of  $\chi^2$ . This minimum  $\chi^2$  value is found by substituting Eqs. (61) and (62) into Eq. (58) as

$$\chi_{\min}^2 = \mathbf{d}^T \mathbf{C}_{\mathbf{d}\mathbf{d}}^{-1} \mathbf{d} = \mathbf{d}^T [\mathbf{C}_{\mathbf{k}\mathbf{k}} + \mathbf{F}_{\mathbf{m}/\mathbf{k}} \mathbf{C}_{\mathbf{m}\mathbf{m}} \mathbf{F}_{\mathbf{m}/\mathbf{k}}]^{-1} \mathbf{d} . \quad (83)$$

It is interesting to observe that the discrepancy vector  $\mathbf{d}$  defined by Eq. (74) does not depend upon adjustments in nuclear data or integral experiments and physically expresses a measure of the initial discrepancies ( $\mathbf{d}$ ) in all responses, compared to their combined calculation and experiment uncertainties ( $\mathbf{C}_{\mathbf{k}\mathbf{k}} + \mathbf{F}_{\mathbf{m}/\mathbf{k}} \mathbf{C}_{\mathbf{m}\mathbf{m}} \mathbf{F}_{\mathbf{m}/\mathbf{k}}$ ). Equation (83) can be viewed as an inherent limit on the consistency of the GLLS adjustment procedure. If the initial calculated and measured responses are not consistent with their stated uncertainties, then adjustments in nuclear data and experiment values obtained by TSURFER cannot be consistent either.

The TSURFER tool provides an option for  $\chi^2$  filtering to ensure that a given set of benchmark experiments is consistent, that is, that the input responses have an acceptable  $\chi_{\min}^2$  defined by Eq. (83). The code progressively removes individual experiments until the calculated  $\chi_{\min}^2$  is less than a user input threshold. Each iteration removes one experiment estimated to have the greatest impact on  $\chi^2$  per degree of freedom. The method used to assess individual contributions to  $\chi_{\min}^2$  is specified by the user from the options given below.

1. *Independent chi-square*: The consistency of the  $i$ 'th measured and calculated response values, disregarding any other integral response, is equal to the discrepancy in the measured and calculated value squared divided by the variance of the discrepancy of the  $i$ 'th response:

$$\chi_{ind,i}^2 = \frac{(k_i - m_i)^2}{s_{k_i}^2 + s_{m_i}^2} . \quad (84)$$

Equation (84) is strictly valid only when no correlations exist, but it may be a useful approximation to estimate the experiment having the greatest impact on chi-square per degree of freedom. Hence, this expression is called the independent chi-square approximation in TSURFER. This approximation executes quickly since no matrix inversions are required.

2. *Diagonal chi-square*: The diagonal chi-square approach uses diagonal values of the original inverse  $\mathbf{C}_{\mathbf{d}\mathbf{d}}$  matrix to estimate the experiment having the greatest impact on chi-square per degree of freedom:

$$\chi_{dia,i}^2 \equiv (k_i - m_i)^2 C_{dd}^{-1}(i, i) . \quad (85)$$

In this method the correlations in all responses are taken into account to some extent. The original  $\mathbf{C}_{\mathbf{d}\mathbf{d}}^{-1}$  is used in each iteration; therefore, the diagonal chi-square method requires only a single matrix inversion.

3. *Iterative-diagonal chi-square*: This approach is identical to the diagonal chi-square method except that an updated value of  $\mathbf{C}_{\mathbf{d}\mathbf{d}}^{-1}$  is computed for each iteration to reevaluate the total chi-square from Eq. (85). Thus, one matrix inversion is performed per iteration.

4. *Delta chi-square*: The most rigorous method to determine the impact of an individual response on the overall consistency is called the delta chi-square method in TSURFER. This method<sup>36</sup> calculates the change in chi-square whenever a particular response is omitted for the analysis; that is, omitting the  $i$ 'th response results in

$$\Delta \chi_i^2 = [\mathbf{d}^T \mathbf{C}_{\mathbf{d}\mathbf{d}}^{-1} \mathbf{d}] - [\mathbf{d}_{\neq i}^T (\mathbf{C}_{\mathbf{d}\mathbf{d}}^{\neq i})^{-1} \mathbf{d}_{\neq i}] , \quad (86)$$

where  $\mathbf{d}_{\neq i}$  and  $\mathbf{C}_{\mathbf{d}\mathbf{d}}^{\neq i}$  are, respectively, the discrepancy vector and discrepancy covariance with response  $i$  omitted. While Eq. (86) is the most rigorous method, it also requires the most computational effort. A matrix inversion must be performed for every omitted response in each iteration.

It has been observed that independent chi-square and diagonal chi-square options execute quickly but often eliminate more experiments than necessary to obtain the target chi-square value. The diagonal chi-square option is somewhat faster than the iterative-diagonal chi-square option but also sometimes omits more than the minimum number of experiments. The delta chi-square option is currently the default in TSURFER.

### VII.C. Expressions for Computational Bias

The computational bias is defined in TSURFER as the observed difference between a calculated and measured response. In conventional validation studies, such as those using USLSTATS, the expected bias in an

application response (for which there is no measurement, by definition) often is estimated as the sample mean of the biases for a set of benchmark experiments, and the uncertainty in the application bias is estimated by the sample standard deviation of the experimental biases.

The GLLS technique provides another method to compute the bias of an application response. The application response bias  $\beta_a$  is defined as the expected deviation of the original calculated response  $k_a$  from the best estimate of the measured response, which is unknown but has some probability distribution. Note that if the application response actually did have a prior measured value  $m_a$ , then the best estimate for the experiment value would be the final adjusted value  $m'_a$  obtained from the GLLS procedure. For this reason the notation  $m'_a$  is used here to represent the (unknown) best estimate for the application's projected measured response, so that

$$\beta_a = E[k_a - m'_a] , \quad (87)$$

where  $E$  is the expectation operator. The application's projected measured value can be expressed as  $m'_a = k_a(\alpha') - \delta m_a$ , where  $\delta m_a$  represents the difference between the best-computed response obtained with the adjusted data  $\alpha'$  and the expected value of the actual measurement. Therefore, Eq. (87) can be expressed as

$$\begin{aligned} \beta_a &= E[k_a - k_a(\alpha') + \delta m_a] \\ &= k_a - k_a(\alpha') + E[\delta m_a] . \end{aligned} \quad (88)$$

Recall that all experiment responses are sure to have  $\delta m_i = 0$ , because the GLLS procedure forces  $\mathbf{k}' = \mathbf{m}'$  within the approximation of first-order theory. However,  $\delta m_a (= k'_a - m'_a)$  for the application is not guaranteed to be zero, since there is no known measured value. Nevertheless, the application response calculated using the best cross sections  $\alpha'$  should approach the desired (unknown) measured value if a sufficient number of experiments similar to the application of interest are considered so that under these conditions  $E[\delta m_a] \rightarrow 0$  for the application as well.<sup>5</sup> More details concerning the suitable degree of similarity and the sufficient number of experiments necessary for convergence of the GLLS methodology are discussed in other publications.<sup>5</sup>

Assuming an adequate benchmark database such that  $E[\delta m_a] \sim 0$ , Eq. (88) simplifies to

$$\beta_a = k_a - k_a(\alpha') \sim -(k_a) \mathbf{S}_a^T \Delta \alpha \quad (89)$$

or, stated in absolute terms,

$$\beta_a = \sim -\tilde{\mathbf{S}}_a^T \Delta \alpha . \quad (90)$$

#### VII.D. Bias Uncertainty

In most cases some gaps exist in the benchmark database so that  $E[\delta m_a] \neq 0$ . In this case, the adjusted cross-section-covariance data from Eq. (81) are used to produce a postadjustment uncertainty, which is the uncertainty in

the adjusted response value, and thus the uncertainty in the computational bias. Similar to Eq. (38), the postadjustment uncertainty for the application is computed as

$$\sigma_{k_a}^2 = \mathbf{S}_a \mathbf{C}_{\alpha' \alpha'} \mathbf{S}_a^T , \quad (91)$$

and the uncertainty in the bias is

$$\Delta \beta_a = (\mathbf{S}_a \mathbf{C}_{\alpha' \alpha'} \mathbf{S}_a^T)^{1/2} . \quad (92)$$

The individual nuclide-reaction-specific contributors to the bias uncertainty can be computed from the individual processes that make up the postadjustment cross-section-covariance data. When folded with the application sensitivity data for the same processes, gaps in the benchmark database that contribute to the uncertainty in the bias are revealed.

## VIII. EXPERIMENT DESIGN

Where gaps in benchmark coverage are found, experiments can be optimized to fill the gaps using TSUNAMI techniques.<sup>37</sup> The techniques described in Sec. V for similarity assessment can be applied to proposed experiment designs to quantify their similarity to the targeted application. The comparisons can be based on the similarity of individual sensitivity profiles or in terms of global similarity using  $c_k$ .

In many cases, it is not practical to assemble a benchmark experiment that would produce a high  $c_k$  relative to a given application. In these cases, it may be possible to use reactivity experiments, where a single test material produces sensitivities in a similar spectrum as the application, and then carefully design a reference experiment without the test material. If the sensitivities for materials other than the test material are closely matched between the test experiment and the reference experiment, TSAR and TSURFER can be applied to extract the bias attributable only to the test material and project it to a bias for the same material in the application system.

## IX. EXAMPLE

The use of TSUNAMI for sensitivity analysis, uncertainty quantification, similarity assessment, and determination of computational bias and bias uncertainty is demonstrated in this section for a complex application system.

### IX.A. Demonstration Application

The demonstration application system is the GBC-32 burnup credit shipping cask model<sup>38,39</sup> shown in Fig. 5 with the top half and front right quarter removed. The cask has 20.3-cm-thick (8-in.-thick) steel sides, top, and bottom. The basket of the cask is formed from square

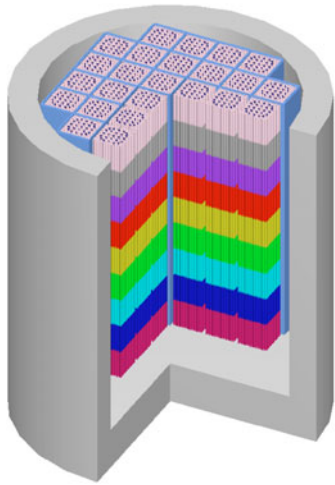


Fig. 5. Cut-away view of the GBC-32 cask model.

stainless steel tubes with a Boral plate between each pair of assemblies and on the outsides of each peripheral assembly. The cask is modeled as flooded with full density water and loaded with 32 Westinghouse  $17 \times 17$  optimized fuel assemblies having initial enrichment of 4 wt%  $^{235}\text{U}$  burned to 40 GWD/tonne U and cooled for 5 yr. The STARBUCS sequence of SCALE was used to generate 18 axial location-dependent burned fuel compositions. From the depletion calculations, fuel compositions for the following nuclides were retained for the criticality calculations:  $^{234}\text{U}$ ,  $^{235}\text{U}$ ,  $^{236}\text{U}$ ,  $^{238}\text{U}$ ,  $^{237}\text{Np}$ ,  $^{238}\text{Pu}$ ,  $^{239}\text{Pu}$ ,  $^{240}\text{Pu}$ ,  $^{241}\text{Pu}$ ,  $^{242}\text{Pu}$ ,  $^{241}\text{Am}$ ,  $^{243}\text{Am}$ ,  $^{95}\text{Mo}$ ,  $^{99}\text{Tc}$ ,  $^{101}\text{Ru}$ ,  $^{103}\text{Rh}$ ,  $^{109}\text{Ag}$ ,  $^{133}\text{Cs}$ ,  $^{147}\text{Sm}$ ,  $^{149}\text{Sm}$ ,  $^{150}\text{Sm}$ ,  $^{151}\text{Sm}$ ,  $^{152}\text{Sm}$ ,  $^{143}\text{Nd}$ ,  $^{145}\text{Nd}$ ,  $^{151}\text{Eu}$ ,  $^{153}\text{Eu}$ , and  $^{155}\text{Gd}$ . The fuel burnup calculations model the depletion of the  $^{235}\text{U}$  and the ingrowth of plutonium and selected fission product nuclides.

### IX.B. Sensitivity Analysis

Sensitivity data were generated for this model using TSUNAMI/KENO. The TSUNAMI parameters selected for this model are shown in Table III. Additionally, a variable spatial mesh was used for the flux accumulators, where the X- and Y-mesh planes were placed  $\sim 10$  cm apart through the outer regions of the cask, then with refined spacing ranging from  $\sim 0.7$  to 5 cm through the fueled and poisoned sections of the model to refine the solutions near individual components. The SCALE 6 ENDF/B-VII.0 calculation of the GBC-32 cask model produces a  $k_{eff}$  of  $0.9429 \pm 0.0005$ .

The TSUNAMI sensitivity results were verified with direct perturbation calculations, as described in Sec. II.A. The results shown in Table IV demonstrate good agreement between the TSUNAMI and direct perturbation results, with all results agreeing within  $< 1\sigma$ . For many of these comparisons, direct perturbation results were gen-

TABLE III  
TSUNAMI-3D-K5 Parameter Data  
for GBC-32 Model

Parameter	Description	Value
NPG	Number of particles per generation for the forward calculation	5 000
APG	Number of particles per generation for the adjoint calculation	20 000
GEN	Maximum number of generations for the forward calculation	10 100
AGN	Maximum number of generations for the adjoint calculation	10 100
NSK	Number of generations to skip before accumulating information for the forward calculation	100
ASK	Number of generations to skip before accumulating information for the adjoint case	100
SIG	Desired $k_{eff}$ convergence for the forward calculation	0.0005
ASG	Desired $k_{eff}$ convergence for the adjoint calculation	0.0005
PNM	Order of flux moment expansion	3

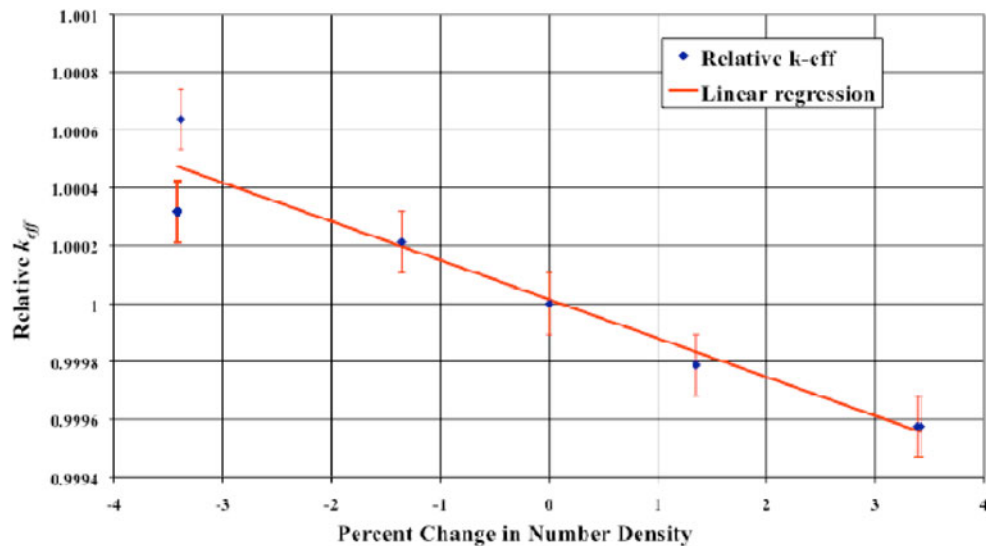
erated using a linear regression through the results of several different number density perturbations. This technique is illustrated in Fig. 6 for  $^{149}\text{Sm}$ , where the relative  $k_{eff}$  values represent the change in  $k_{eff}$  with respect to the unperturbed case and the error bars represent  $1\sigma$  in the Monte Carlo results. This example is interesting in that the sensitivity of  $k_{eff}$  to  $^{149}\text{Sm}$  is relatively small, and therefore larger changes in the number density are required to make statistically significant changes in  $k_{eff}$ . The number density changes of  $-3.42$  and  $-3.385\%$ , the  $k_{eff}$  values for which are expected to closely agree, differ from each other by  $> 1\sigma$  because of statistical variances in the Monte Carlo results. However, the regression line bisects the two data points, leading to acceptable agreement between the TSUNAMI and direct perturbation results. Had only one data point been selected, the results would not have agreed so closely, because the direct perturbation results would have appeared to be nonlinear.

Select energy-dependent sensitivity profiles, showing the sensitivity of  $k_{eff}$  to the cross-section data, for the GBC-32 cask model are shown in Fig. 7. Here, many interesting aspects of the physics of the system are revealed. As expected, the sensitivities for  $^{235}\text{U}$  and  $^{239}\text{Pu}$  are greatest at thermal energies. Although  $^1\text{H}$  elastic scattering has a smooth cross section as a function of energy, the sensitivity of  $k_{eff}$  to  $^1\text{H}$  elastic scattering reflects the structure of other nuclides. In the resonance region,  $k_{eff}$  demonstrates a positive sensitivity to  $^1\text{H}$  elastic scattering related to the escape probability from  $^{238}\text{U}$  and  $^{240}\text{Pu}$  resonances. A negative sensitivity to  $^1\text{H}$  elastic scattering occurs for the 0.67-eV fission resonance for  $^{239}\text{Pu}$ , where

TABLE IV

Comparison of TSUNAMI Sensitivities to Direct Perturbations Results

Isotope	TSUNAMI		Direct Perturbation		Difference	
	Sensitivity	Uncertainty (%)	Sensitivity	Uncertainty (%)	% $\Delta$ (Direct - TSUNAMI)/Direct	Standard Deviations Apart
$^{10}\text{B}$	-0.0317	0.24	-0.0318	-0.92	-0.3	0.3
$^1\text{H}$	0.2363	2.26	0.2414	10.85	-2.1	-0.2
$^{239}\text{Pu}$	0.0957	0.21	0.0959	7.28	-0.2	0.0
$^{240}\text{Pu}$	-0.0333	0.20	-0.0356	-14.14	-6.4	0.5
$^{149}\text{Sm}$	-0.0146	0.08	-0.0134	-11.18	9.0	-0.8
$^{235}\text{U}$	0.1656	0.17	0.1663	13.84	-0.4	0.0
$^{238}\text{U}$	-0.0889	0.30	-0.0924	-6.37	-3.8	0.6

Fig. 6. Relative  $k_{eff}$  values and linear regression for  $^{149}\text{Sm}$  direct perturbation.

scattering below this resonance decreases the probability of fission. A positive sensitivity is observed below this resonance, where further scattering results in an increased probability of thermal fission in  $^{235}\text{U}$  or  $^{239}\text{Pu}$ . Although  $^{10}\text{B}$  has a reactivity effect of several percent in this model, the sensitivity of  $k_{eff}$  to  $^{10}\text{B}$  is small. In the model, the black absorber panels will remain black even with several percent perturbations in the  $^{10}\text{B}$  content. For  $^{149}\text{Sm}$ , a small negative sensitivity is observed at thermal energies.

### IX.C. Uncertainty Analysis

As part of the TSUNAMI/KENO analysis sequence, the SCALE 6 covariance data are applied to the sensitiv-

ities of this model, quantifying an uncertainty due to cross-section-covariance data of  $0.52\% \Delta k/k$ . Thus, the computational bias of this model is expected to be consistent with a  $1\sigma$  uncertainty of  $0.52\% \Delta k/k$ . The top 25 individual contributions to the uncertainty from each covariance matrix are shown in Table V. The total uncertainty can be computed from individual values by adding the square of the values with positive signs and subtracting the square of the values with negative signs, then taking the square root. The negative values are the result of anticorrelations in the cross-section-covariance data. The largest contributors to uncertainty are the Pu and U processes, with the moderator, other actinides, structural materials, and fission products ranking one order of magnitude lower.

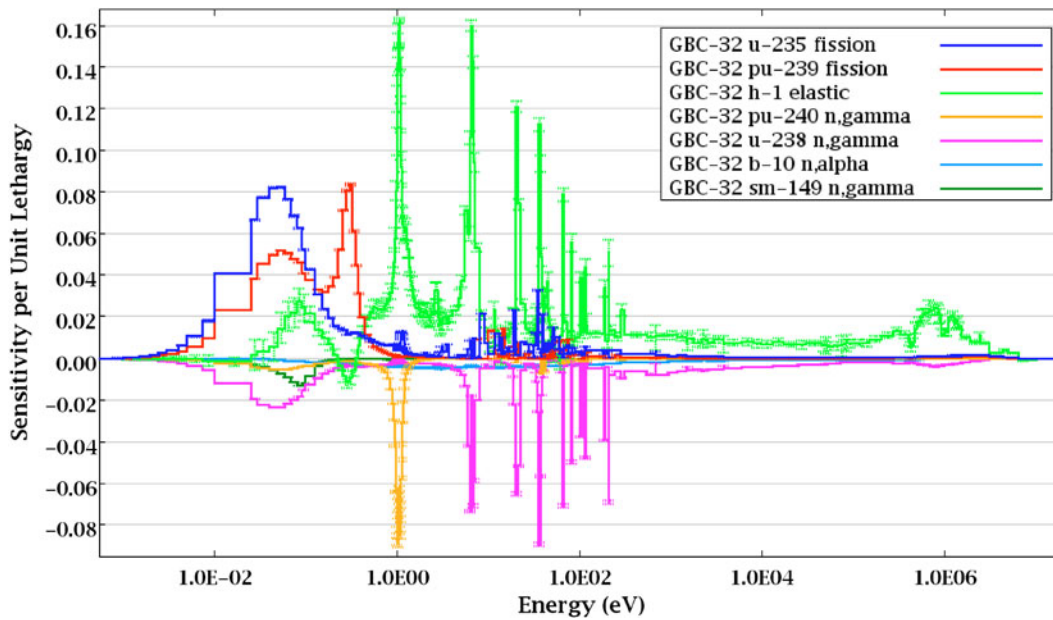


Fig. 7. Energy-dependent sensitivity of  $k_{eff}$  to select nuclides for GBC-32 cask model.

TABLE V

Uncertainty in  $k_{eff}$  of GBC-32 Due to Cross-Section Uncertainties

Covariance Matrix		Uncertainty % $\Delta k/k$
Nuclide-Reaction	Nuclide-Reaction	
$^{239}\text{Pu } \bar{p}$	$^{239}\text{Pu } \bar{p}$	3.61E-01 <sup>a</sup>
$^{238}\text{U } n, \gamma$	$^{238}\text{U } n, \gamma$	1.87E-01
$^{235}\text{U } \bar{p}$	$^{235}\text{U } \bar{p}$	1.57E-01
$^{239}\text{Pu}$ fission	$^{239}\text{Pu}$ fission	1.46E-01
$^{239}\text{Pu}$ fission	$^{239}\text{Pu } n, \gamma$	1.12E-01
$^{239}\text{Pu } n, \gamma$	$^{239}\text{Pu } n, \gamma$	9.68E-02
$^{235}\text{U } n, \gamma$	$^{235}\text{U } n, \gamma$	8.58E-02
$^{235}\text{U}$ fission	$^{235}\text{U}$ fission	7.27E-02
$^{235}\text{U}$ fission	$^{235}\text{U } n, \gamma$	6.88E-02
$^{238}\text{U } n, n'$	$^{238}\text{U } n, n'$	6.26E-02
$^{238}\text{U } \bar{p}$	$^{238}\text{U } \bar{p}$	6.24E-02
$^1\text{H}$ elastic	$^1\text{H}$ elastic	5.69E-02
$^{240}\text{Pu } n, \gamma$	$^{240}\text{Pu } n, \gamma$	4.49E-02
$^{238}\text{U}$ elastic	$^{238}\text{U } n, n'$	-4.22E-02
$^{56}\text{Fe}$ elastic	$^{56}\text{Fe}$ elastic	4.06E-02
$^{56}\text{Fe } n, \gamma$	$^{56}\text{Fe } n, \gamma$	3.70E-02
$^1\text{H } n, \gamma$	$^1\text{H } n, \gamma$	3.63E-02
$^{143}\text{Nd } n, \gamma$	$^{143}\text{Nd } n, \gamma$	3.48E-02
$^{16}\text{O}$ elastic	$^{16}\text{O}$ elastic	3.39E-02
$^{241}\text{Pu}$ fission	$^{241}\text{Pu}$ fission	2.67E-02
$^{90}\text{Zr}$ elastic	$^{90}\text{Zr}$ elastic	2.34E-02
$^{238}\text{U}$ elastic	$^{238}\text{U}$ elastic	2.18E-02
$^{92}\text{Zr } n, \gamma$	$^{92}\text{Zr } n, \gamma$	2.18E-02
$^{149}\text{Sm } n, \gamma$	$^{149}\text{Sm } n, \gamma$	2.16E-02
$^{103}\text{Rh } n, \gamma$	$^{103}\text{Rh } n, \gamma$	2.13E-02

<sup>a</sup>Read as  $3.61 \times 10^{-1}$ .

### IX.D. Critical Benchmark Experiments

It is desirable to identify benchmark experiments that can be used to quantify a bias, bias uncertainty, and upper subcritical limit for the GBC-32 cask model. For this task, sensitivity data are generated not only for application systems but also for each benchmark experiment examined for validation. A selection of critical experiments from the IHECSBE distributed through the International Criticality Safety Benchmark Evaluation Program<sup>40</sup> was included in this exercise. Experiments were included from evaluations HEU-MET-FAST-005 and -017; HEU-SOL-THERM-001 and -028; IEU-MET-FAST-002, -010, and -012; LEU-COMP-THERM-010, -17, -026, -042 and -049, -050, and -079; MIX-COMP-FAST-001; MIX-COMP-MIXED-001; MIX-COMP-THERM-002, -003, -004, -005, -006, -007, and -008; MIX-SOL-THERM-001, -002, -004, and -005; and PU-SOL-THERM-005. A total of 186 experiments were considered in this analysis. Many of these experiments are expected to demonstrate some similarity to the GBC-32 in terms of common U and Pu uncertainties. Others are expected to be dissimilar to the GBC-32. The ability of TSUNAMI to select similar experiments and reject dissimilar experiments will be demonstrated.

Sensitivity and uncertainty data were computed for each experiment using TSUNAMI with ENDF/B-VII.0 cross-section data. The benchmark  $k_{eff}$  values, benchmark  $k_{eff}$  uncertainties, and calculated  $k_{eff}$  values for each experiment are shown in Table VI. The uncertainties in the computed  $k_{eff}$  values due to the cross-section uncertainties are also included. Each  $k_{eff}$  value was computed with a Monte Carlo uncertainty of  $0.0005 \Delta k/k$  or less.

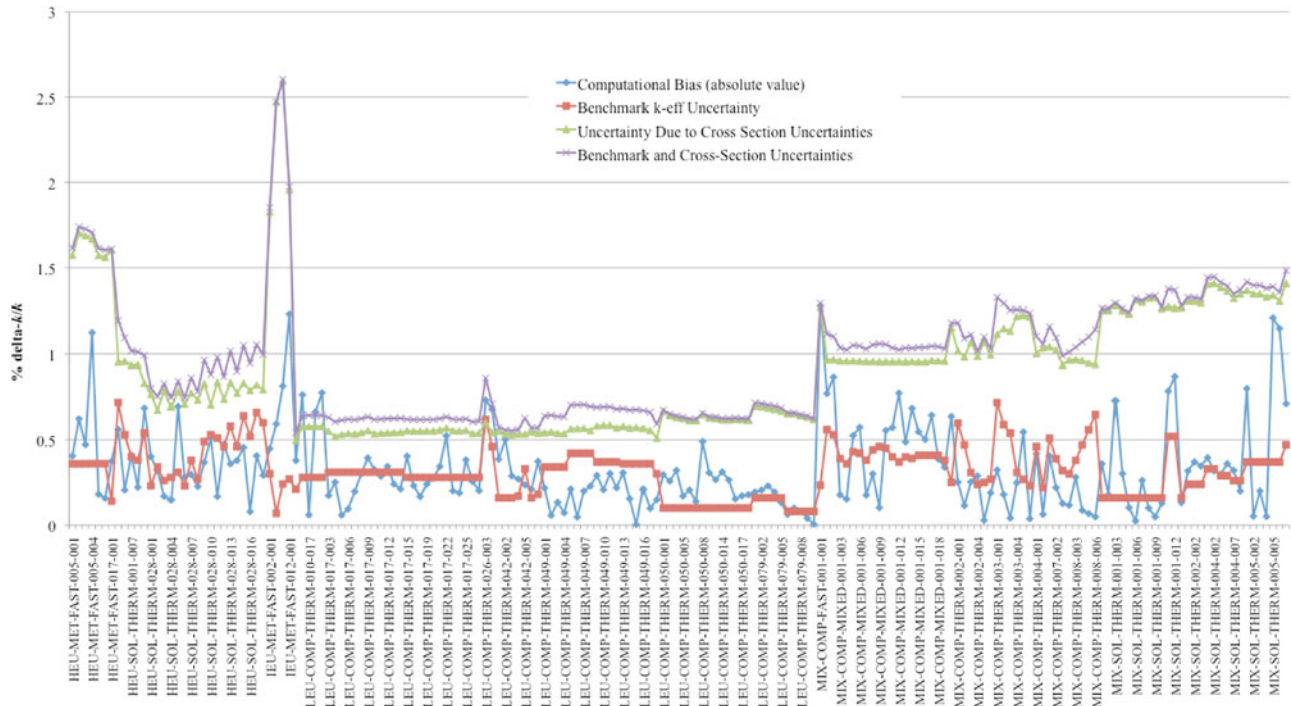


Fig. 8. Computational biases, benchmark  $k_{eff}$  uncertainties, and cross-section uncertainties for benchmark experiments.

The relative magnitudes of the computational bias for each benchmark are shown in Fig. 8, along with the benchmark  $k_{eff}$  uncertainties, cross-section uncertainties, and combined benchmark and cross-section uncertainties. For nearly all of these benchmarks, the combined benchmark and cross-section uncertainties bound the computational biases within  $1\sigma$ . All benchmarks are bounded by the combined uncertainties within  $2\sigma$ , demonstrating uncertainty quantification as a bounding estimate on computational bias.

### IX.E. Similarity Assessment

The similarity of each benchmark experiment to the GBC-32 cask was determined using the  $c_k$  correlation coefficient of TSUNAMI-IP, as shown in Table VI and Fig. 9. An experiment whose uncertainties on an energy-dependent basis are similar to those of the GBC-32 will have a high  $c_k$  value. In Table V, the largest sources of uncertainties are those for U and Pu isotopes and reactions. Experiments with sensitivities that are similar to those of the GBC-32 for U and Pu will be the most applicable for validation. Other processes are of secondary importance. Past studies have indicated that systems with  $c_k$  values of 0.9 and above are highly similar to the application, those with values of 0.8 to 0.9 are marginally similar, and those with values  $<0.8$  may not be similar in terms of computational bias.<sup>5</sup>

Examining the  $c_k$  values for the selected experiments, highly enriched uranium (HEU) systems do not

contain Pu, contain little  $^{238}\text{U}$ , and do not have similar sensitivities to those of the GBC-32 model, as quantified with  $c_k$  values  $<0.3$ . The intermediate enriched uranium (IEU) systems are not similar because of their fast spectrum, and some indicate a slightly negative  $c_k$  value due mainly to an interesting relationship between  $^{238}\text{U}$  inelastic scattering and its relationship with  $^{238}\text{U}$  fast fission for the IEU systems, which is beyond the scope of this paper. The low enriched uranium (LEU) systems do not contain Pu but will demonstrate some similarity to the GBC-32 for U processes, and their  $c_k$  values are  $\sim 0.5$ . Some mixed Pu and U experiments are moderately similar to the GBC-32 model, depending on the isotopic makeup of the mixed fuel and the spectra of the system. For example, the fast-spectra system MIX-COMP-FAST-001-001 has a  $c_k$  of 0.3. However, many MIX-COMP-THERM experiments have higher  $c_k$  values. Yet, none of the selected benchmarks demonstrate a  $c_k \geq 0.9$ , indicating that validation coverage may be lacking in some areas.

One of the highest  $c_k$  values is found for MIX-COMP-THERM-002-002, with a value of 0.8950. The experiment is a water-moderated lattice of fuel rods with natural  $\text{UO}_2$ -2.0 wt%  $\text{PuO}_2$  with 8%  $^{240}\text{Pu}$ . The moderator contains boric acid with 688-ppm boron in this benchmark. This configuration is somewhat different from that of the GBC-32, and differences in the sensitivity data realized, as shown in Fig. 10, where the integral value shown in the legend is the sum of the groupwise values for a given sensitivity profile, and the uncertainties shown are due to

TABLE VI  
Benchmark Experiments

Benchmark Experiment	Benchmark $k_{eff}$	Benchmark $k_{eff}$ Uncertainty (% $\Delta k/k$ )	Calculated $k_{eff}$	Uncertainty Due to Cross-Section Data (% $\Delta k/k$ )	$c_k$ with GBC-32
HEU-MET-FAST-005-001	1.0000	0.3600	0.9959	1.5744	0.0543
HEU-MET-FAST-005-002	1.0007	0.3597	0.9945	1.7019	0.0624
HEU-MET-FAST-005-003	0.9996	0.3601	0.9949	1.6884	0.0658
HEU-MET-FAST-005-004	0.9989	0.3604	0.9877	1.6684	0.0679
HEU-MET-FAST-005-005	0.9980	0.3607	0.9962	1.5719	0.0645
HEU-MET-FAST-005-006	0.9987	0.3605	0.9971	1.5622	0.0614
HEU-MET-FAST-017-001	0.9993	0.1401	0.9956	1.6032	0.0596
HEU-SOL-THERM-001-002	1.0021	0.7185	0.9965	0.9549	0.2250
HEU-SOL-THERM-001-004	1.0008	0.5296	0.9987	0.9571	0.2235
HEU-SOL-THERM-001-007	1.0008	0.3997	0.9967	0.9364	0.2325
HEU-SOL-THERM-001-008	0.9998	0.3801	0.9976	0.9383	0.2319
HEU-SOL-THERM-001-010	0.9993	0.5404	0.9924	0.8324	0.2568
HEU-SOL-THERM-028-001	1.0000	0.2300	0.9960	0.7674	0.2642
HEU-SOL-THERM-028-002	1.0000	0.3400	0.9968	0.6735	0.2910
HEU-SOL-THERM-028-003	1.0000	0.2600	0.9983	0.7869	0.2630
HEU-SOL-THERM-028-004	1.0000	0.2800	0.9985	0.6940	0.2857
HEU-SOL-THERM-028-005	1.0000	0.3100	0.9931	0.7839	0.2642
HEU-SOL-THERM-028-006	1.0000	0.2300	0.9972	0.7095	0.2821
HEU-SOL-THERM-028-007	1.0000	0.3800	0.9970	0.7749	0.2682
HEU-SOL-THERM-028-008	1.0000	0.2700	0.9977	0.7344	0.2769
HEU-SOL-THERM-028-009	1.0000	0.4900	0.9963	0.8299	0.2423
HEU-SOL-THERM-028-010	1.0000	0.5300	0.9949	0.7051	0.2721
HEU-SOL-THERM-028-011	1.0000	0.5100	0.9983	0.8370	0.2422
HEU-SOL-THERM-028-012	1.0000	0.4600	0.9953	0.7380	0.2630
HEU-SOL-THERM-028-013	1.0000	0.5800	0.9964	0.8355	0.2453
HEU-SOL-THERM-028-014	1.0000	0.4600	0.9962	0.7745	0.2561
HEU-SOL-THERM-028-015	1.0000	0.6400	1.0045	0.8325	0.2467
HEU-SOL-THERM-028-016	1.0000	0.5200	1.0008	0.7895	0.2543
HEU-SOL-THERM-028-017	1.0000	0.6600	0.9959	0.8217	0.2507
HEU-SOL-THERM-028-018	1.0000	0.6000	0.9971	0.7938	0.2538
IEU-MET-FAST-002-001	1.0000	0.3000	1.0045	1.8279	0.0102
IEU-MET-FAST-007-001	1.0045	0.0697	1.0105	2.4724	-0.0222
IEU-MET-FAST-010-001	0.9954	0.2411	1.0035	2.5931	-0.0214
IEU-MET-FAST-012-001	1.0007	0.2698	1.0130	1.9561	0.0336
LEU-COMP-THERM-010-005	1.0000	0.2100	0.9962	0.4982	0.5291
LEU-COMP-THERM-010-016	1.0000	0.2800	0.9924	0.5784	0.4874
LEU-COMP-THERM-010-017	1.0000	0.2800	0.9928	0.5793	0.4854
LEU-COMP-THERM-010-018	1.0000	0.2800	0.9934	0.5801	0.4840
LEU-COMP-THERM-010-019	1.0000	0.2800	0.9922	0.5786	0.4830
LEU-COMP-THERM-017-003	1.0000	0.3100	0.9935	0.5500	0.5167
LEU-COMP-THERM-017-004	1.0000	0.3100	0.9935	0.5204	0.5457
LEU-COMP-THERM-017-005	1.0000	0.3100	0.9937	0.5317	0.5386
LEU-COMP-THERM-017-006	1.0000	0.3100	0.9943	0.5376	0.5342
LEU-COMP-THERM-017-007	1.0000	0.3100	0.9933	0.5339	0.5341
LEU-COMP-THERM-017-008	1.0000	0.3100	0.9927	0.5421	0.5249
LEU-COMP-THERM-017-009	1.0000	0.3100	0.9916	0.5545	0.5152
LEU-COMP-THERM-017-010	1.0000	0.3100	0.9926	0.5355	0.5298
LEU-COMP-THERM-017-011	1.0000	0.3100	0.9935	0.5381	0.5275
LEU-COMP-THERM-017-012	1.0000	0.3100	0.9931	0.5417	0.5251
LEU-COMP-THERM-017-013	1.0000	0.3100	0.9930	0.5425	0.5233
LEU-COMP-THERM-017-014	1.0000	0.3100	0.9925	0.5440	0.5217

(Continued)

TABLE VI (Continued)

Benchmark Experiment	Benchmark $k_{eff}$	Benchmark $k_{eff}$ Uncertainty (% $\Delta k/k$ )	Calculated $k_{eff}$	Uncertainty Due to Cross-Section Data (% $\Delta k/k$ )	$c_k$ with GBC-32
LEU-COMP-THERM-017-015	1.0000	0.2800	0.9895	0.5533	0.5475
LEU-COMP-THERM-017-016	1.0000	0.2800	0.9911	0.5511	0.5471
LEU-COMP-THERM-017-017	1.0000	0.2800	0.9918	0.5511	0.5448
LEU-COMP-THERM-017-019	1.0000	0.2800	0.9903	0.5520	0.5425
LEU-COMP-THERM-017-020	1.0000	0.2800	0.9901	0.5519	0.5420
LEU-COMP-THERM-017-021	1.0000	0.2800	0.9886	0.5575	0.5389
LEU-COMP-THERM-017-022	1.0000	0.2800	0.9883	0.5695	0.5312
LEU-COMP-THERM-017-023	1.0000	0.2800	0.9943	0.5541	0.5377
LEU-COMP-THERM-017-024	1.0000	0.2800	0.9925	0.5522	0.5381
LEU-COMP-THERM-017-025	1.0000	0.2800	0.9896	0.5558	0.5367
LEU-COMP-THERM-017-028	1.0000	0.2800	0.9908	0.5370	0.5559
LEU-COMP-THERM-017-029	1.0000	0.2800	0.9908	0.5390	0.5525
LEU-COMP-THERM-026-003	1.0018	0.6189	0.9999	0.6004	0.4891
LEU-COMP-THERM-040-010	1.0000	0.4600	0.9932	0.5419	0.4744
LEU-COMP-THERM-042-001	1.0000	0.1600	0.9893	0.5504	0.5482
LEU-COMP-THERM-042-002	1.0000	0.1600	0.9904	0.5345	0.5531
LEU-COMP-THERM-042-003	1.0000	0.1600	0.9927	0.5294	0.5563
LEU-COMP-THERM-042-004	1.0000	0.1700	0.9927	0.5334	0.5546
LEU-COMP-THERM-042-005	1.0000	0.3300	0.9916	0.5327	0.5538
LEU-COMP-THERM-042-006	1.0000	0.1600	0.9927	0.5468	0.5463
LEU-COMP-THERM-042-007	1.0000	0.1800	0.9899	0.5394	0.5494
LEU-COMP-THERM-049-001	1.0000	0.3400	0.9978	0.5420	0.5211
LEU-COMP-THERM-049-002	1.0000	0.3400	0.9994	0.5464	0.5199
LEU-COMP-THERM-049-003	1.0000	0.3400	0.9987	0.5379	0.5230
LEU-COMP-THERM-049-004	1.0000	0.3400	0.9993	0.5361	0.5236
LEU-COMP-THERM-049-005	1.0000	0.4200	0.9979	0.5652	0.5115
LEU-COMP-THERM-049-006	1.0000	0.4200	0.9995	0.5659	0.5119
LEU-COMP-THERM-049-007	1.0000	0.4200	0.9980	0.5675	0.5098
LEU-COMP-THERM-049-008	1.0000	0.4200	0.9977	0.5545	0.5174
LEU-COMP-THERM-049-009	1.0000	0.3700	0.9971	0.5821	0.4998
LEU-COMP-THERM-049-010	1.0000	0.3700	0.9979	0.5854	0.4988
LEU-COMP-THERM-049-011	1.0000	0.3700	0.9970	0.5859	0.4982
LEU-COMP-THERM-049-012	1.0000	0.3700	0.9978	0.5702	0.5071
LEU-COMP-THERM-049-013	1.0000	0.3600	0.9969	0.5798	0.5048
LEU-COMP-THERM-049-014	1.0000	0.3600	0.9985	0.5692	0.5106
LEU-COMP-THERM-049-015	1.0000	0.3600	1.0000	0.5724	0.5086
LEU-COMP-THERM-049-016	1.0000	0.3600	0.9979	0.5663	0.5100
LEU-COMP-THERM-049-017	1.0000	0.3600	0.9990	0.5548	0.5169
LEU-COMP-THERM-049-018	1.0000	0.3000	1.0015	0.5104	0.5340
LEU-COMP-THERM-050-001	1.0004	0.1000	0.9974	0.6672	0.4316
LEU-COMP-THERM-050-003	1.0004	0.1000	0.9978	0.6428	0.4424
LEU-COMP-THERM-050-004	1.0004	0.1000	0.9972	0.6325	0.4464
LEU-COMP-THERM-050-005	1.0004	0.1000	0.9987	0.6242	0.4521
LEU-COMP-THERM-050-006	1.0004	0.1000	0.9983	0.6134	0.4562
LEU-COMP-THERM-050-007	1.0004	0.1000	0.9990	0.6135	0.4560
LEU-COMP-THERM-050-008	1.0004	0.1000	0.9955	0.6488	0.4412
LEU-COMP-THERM-050-012	1.0004	0.1000	0.9973	0.6281	0.4501
LEU-COMP-THERM-050-013	1.0004	0.1000	0.9977	0.6254	0.4515
LEU-COMP-THERM-050-014	1.0004	0.1000	0.9973	0.6167	0.4560
LEU-COMP-THERM-050-015	1.0004	0.1000	0.9978	0.6165	0.4561
LEU-COMP-THERM-050-016	1.0004	0.1000	0.9989	0.6194	0.4548
LEU-COMP-THERM-050-017	1.0004	0.1000	0.9987	0.6170	0.4557

(Continued)

TABLE VI (Continued)

Benchmark Experiment	Benchmark $k_{eff}$	Benchmark $k_{eff}$ Uncertainty (% $\Delta k/k$ )	Calculated $k_{eff}$	Uncertainty Due to Cross-Section Data (% $\Delta k/k$ )	$c_k$ with GBC-32
LEU-COMP-THERM-050-018	1.0004	0.1000	0.9986	0.6147	0.4569
LEU-COMP-THERM-079-001	0.9999	0.1600	0.9980	0.6986	0.4372
LEU-COMP-THERM-079-002	1.0002	0.1600	0.9982	0.6944	0.4389
LEU-COMP-THERM-079-003	1.0005	0.1600	0.9982	0.6856	0.4424
LEU-COMP-THERM-079-004	1.0004	0.1600	0.9985	0.6788	0.4457
LEU-COMP-THERM-079-005	1.0004	0.1600	0.9991	0.6678	0.4506
LEU-COMP-THERM-079-006	0.9994	0.0800	0.9988	0.6533	0.4243
LEU-COMP-THERM-079-007	1.0003	0.0800	0.9993	0.6526	0.4244
LEU-COMP-THERM-079-008	1.0008	0.0800	1.0000	0.6414	0.4291
LEU-COMP-THERM-079-009	1.0003	0.0800	0.9999	0.6331	0.4330
LEU-COMP-THERM-079-010	1.0009	0.0800	1.0009	0.6181	0.4401
MIX-COMP-FAST-001-001	0.9866	0.2331	0.9992	1.2713	0.2959
MIX-COMP-MIXED-001-001	0.9999	0.5601	0.9922	0.9653	0.7177
MIX-COMP-MIXED-001-002	0.9996	0.5302	0.9909	0.9666	0.7174
MIX-COMP-MIXED-001-003	1.0011	0.3896	1.0029	0.9598	0.7675
MIX-COMP-MIXED-001-004	1.0004	0.3599	1.0019	0.9584	0.7685
MIX-COMP-MIXED-001-005	1.0005	0.4298	1.0058	0.9590	0.7707
MIX-COMP-MIXED-001-006	0.9970	0.4213	1.0027	0.9575	0.7726
MIX-COMP-MIXED-001-007	0.9990	0.3804	1.0008	0.9557	0.7764
MIX-COMP-MIXED-001-008	0.9985	0.4407	1.0015	0.9567	0.7782
MIX-COMP-MIXED-001-009	1.0001	0.4600	1.0011	0.9548	0.7796
MIX-COMP-MIXED-001-010	0.9988	0.4505	1.0043	0.9553	0.7810
MIX-COMP-MIXED-001-011	0.9998	0.4001	1.0055	0.9551	0.7708
MIX-COMP-MIXED-001-012	0.9995	0.3702	1.0072	0.9559	0.7704
MIX-COMP-MIXED-001-013	1.0007	0.3997	1.0056	0.9546	0.7706
MIX-COMP-MIXED-001-014	0.9989	0.3904	1.0057	0.9566	0.7697
MIX-COMP-MIXED-001-015	1.0004	0.4098	1.0059	0.9542	0.7694
MIX-COMP-MIXED-001-016	1.0009	0.4096	1.0059	0.9539	0.7696
MIX-COMP-MIXED-001-017	1.0001	0.4100	1.0065	0.9616	0.7694
MIX-COMP-MIXED-001-018	1.0010	0.4096	1.0049	0.9593	0.7714
MIX-COMP-MIXED-001-019	1.0007	0.3797	1.0041	0.9576	0.7721
MIX-COMP-THERM-001-001	1.0000	0.2500	1.0064	1.1541	0.7784
MIX-COMP-THERM-002-001	1.0024	0.5986	0.9999	1.0191	0.8782
MIX-COMP-THERM-002-002	1.0009	0.4696	0.9998	0.9836	0.8950
MIX-COMP-THERM-002-003	1.0042	0.3087	1.0017	1.0684	0.8469
MIX-COMP-THERM-002-004	1.0024	0.2394	1.0053	0.9873	0.8881
MIX-COMP-THERM-002-005	1.0038	0.2491	1.0041	1.0698	0.8431
MIX-COMP-THERM-002-006	1.0029	0.2692	1.0048	0.9948	0.8797
MIX-COMP-THERM-003-001	1.0028	0.7180	0.9996	1.1152	0.8255
MIX-COMP-THERM-003-002	1.0019	0.5889	1.0001	1.1487	0.8110
MIX-COMP-THERM-003-003	1.0000	0.5400	1.0004	1.1332	0.8186
MIX-COMP-THERM-003-004	1.0027	0.3092	1.0002	1.2200	0.7775
MIX-COMP-THERM-003-005	1.0049	0.2687	0.9994	1.2258	0.7744
MIX-COMP-THERM-003-006	1.0000	0.2300	1.0004	1.2171	0.7795
MIX-COMP-THERM-004-001	1.0000	0.4600	0.9958	1.0022	0.8454
MIX-COMP-THERM-005-001	1.0008	0.2198	1.0014	1.0364	0.8443
MIX-COMP-THERM-006-001	1.0016	0.5092	0.9975	1.0422	0.8632
MIX-COMP-THERM-007-002	1.0024	0.3891	1.0002	1.0231	0.8594
MIX-COMP-THERM-008-001	0.9997	0.3201	0.9984	0.9364	0.8998
MIX-COMP-THERM-008-002	1.0008	0.2998	0.9996	0.9650	0.8785
MIX-COMP-THERM-008-003	1.0023	0.3791	0.9995	0.9674	0.8733
MIX-COMP-THERM-008-004	1.0015	0.4693	1.0024	0.9617	0.8739

(Continued)

TABLE VI (Continued)

Benchmark Experiment	Benchmark $k_{eff}$	Benchmark $k_{eff}$ Uncertainty (% $\Delta k/k$ )	Calculated $k_{eff}$	Uncertainty Due to Cross-Section Data (% $\Delta k/k$ )	$c_k$ with GBC-32
MIX-COMP-THERM-008-005	1.0022	0.5588	1.0029	0.9465	0.8770
MIX-COMP-THERM-008-006	1.0028	0.6482	1.0023	0.9405	0.8773
MIX-SOL-THERM-001-001	1.0000	0.1600	0.9964	1.2529	0.7599
MIX-SOL-THERM-001-002	1.0000	0.1600	0.9982	1.2530	0.7597
MIX-SOL-THERM-001-003	1.0000	0.1600	0.9927	1.2831	0.7468
MIX-SOL-THERM-001-004	1.0000	0.1600	0.9970	1.2523	0.7607
MIX-SOL-THERM-001-005	1.0000	0.1600	1.0010	1.2331	0.7697
MIX-SOL-THERM-001-006	1.0000	0.1600	1.0002	1.3101	0.7416
MIX-SOL-THERM-001-007	1.0000	0.1600	1.0026	1.2986	0.7146
MIX-SOL-THERM-001-008	1.0000	0.1600	1.0010	1.3228	0.7164
MIX-SOL-THERM-001-009	1.0000	0.1600	1.0005	1.3257	0.7258
MIX-SOL-THERM-001-010	1.0000	0.1600	1.0013	1.2635	0.7596
MIX-SOL-THERM-001-011	1.0000	0.5200	1.0079	1.2747	0.7613
MIX-SOL-THERM-001-012	1.0000	0.5200	1.0087	1.2665	0.7563
MIX-SOL-THERM-001-013	1.0000	0.1600	0.9987	1.2691	0.7619
MIX-SOL-THERM-002-001	1.0000	0.2400	1.0032	1.3054	0.7683
MIX-SOL-THERM-002-002	1.0000	0.2400	1.0037	1.3041	0.7691
MIX-SOL-THERM-002-003	1.0000	0.2400	1.0035	1.2938	0.7745
MIX-SOL-THERM-004-001	1.0000	0.3300	0.9960	1.4047	0.6977
MIX-SOL-THERM-004-002	1.0000	0.3300	0.9968	1.4091	0.7057
MIX-SOL-THERM-004-005	1.0000	0.2900	0.9970	1.3842	0.7027
MIX-SOL-THERM-004-006	1.0000	0.2900	0.9964	1.3626	0.6978
MIX-SOL-THERM-004-007	1.0000	0.2600	0.9968	1.3212	0.7094
MIX-SOL-THERM-004-008	1.0000	0.2600	0.9980	1.3469	0.7125
MIX-SOL-THERM-005-001	1.0000	0.3700	0.9920	1.3671	0.7122
MIX-SOL-THERM-005-002	1.0000	0.3700	1.0005	1.3470	0.7359
MIX-SOL-THERM-005-003	1.0000	0.3700	1.0020	1.3470	0.7242
MIX-SOL-THERM-005-004	1.0000	0.3700	1.0005	1.3287	0.7299
MIX-SOL-THERM-005-005	1.0000	0.3700	0.9879	1.3392	0.7095
MIX-SOL-THERM-005-006	1.0000	0.3700	0.9885	1.3048	0.7178
PU-SOL-THERM-005-005	1.0000	0.4700	1.0071	1.4077	0.6941

Monte Carlo statistical uncertainties. Although the shapes of the sensitivity profiles are similar, indicating the spectra of the systems are similar, the different U and Pu loadings for the systems lead to different magnitudes of sensitivities for  $^{235}\text{U}$  and  $^{239}\text{Pu}$  but similar shapes and magnitudes for  $^{238}\text{U}$ .

The TSUNAMI-IP integral index  $g$  was used to assess the nuclide-reaction-specific coverage of the GBC-32 by this experiment. The  $g$  values and energy-integrated sensitivities for fission, capture, and scatter for nuclide-reaction pairs with sensitivities of magnitude  $\geq 0.7$  are shown in Table VII. High values are observed for  $^{238}\text{U}$  and  $^{239}\text{Pu}$ , confirming that the experiment is at least as sensitive as the GBC-32 for these nuclides. The  $g$  values for  $^{235}\text{U}$  are lower because of the greater sensitivity of the GBC-32 for these processes.

#### IX.F. Bias Assessment with Trending Analysis

The  $c_k$  data were used in USLSTATS to produce a bias and bias uncertainty for the GBC-32 cask model based on the 68 benchmark experiments with  $c_k$  values  $\geq 0.70$ . The value of 0.70 was chosen to eliminate the influence of highly dissimilar experiments on the trending analysis yet still provide a statistically significant data sample. The USLSTATS calculations all used the input parameters below, and the data set passed the USLSTATS  $\chi^2$  normality test.

Proportion of population = 0.999

Confidence of fit = 0.950

Confidence on proportion = 0.950

Administrative margin = 0.00

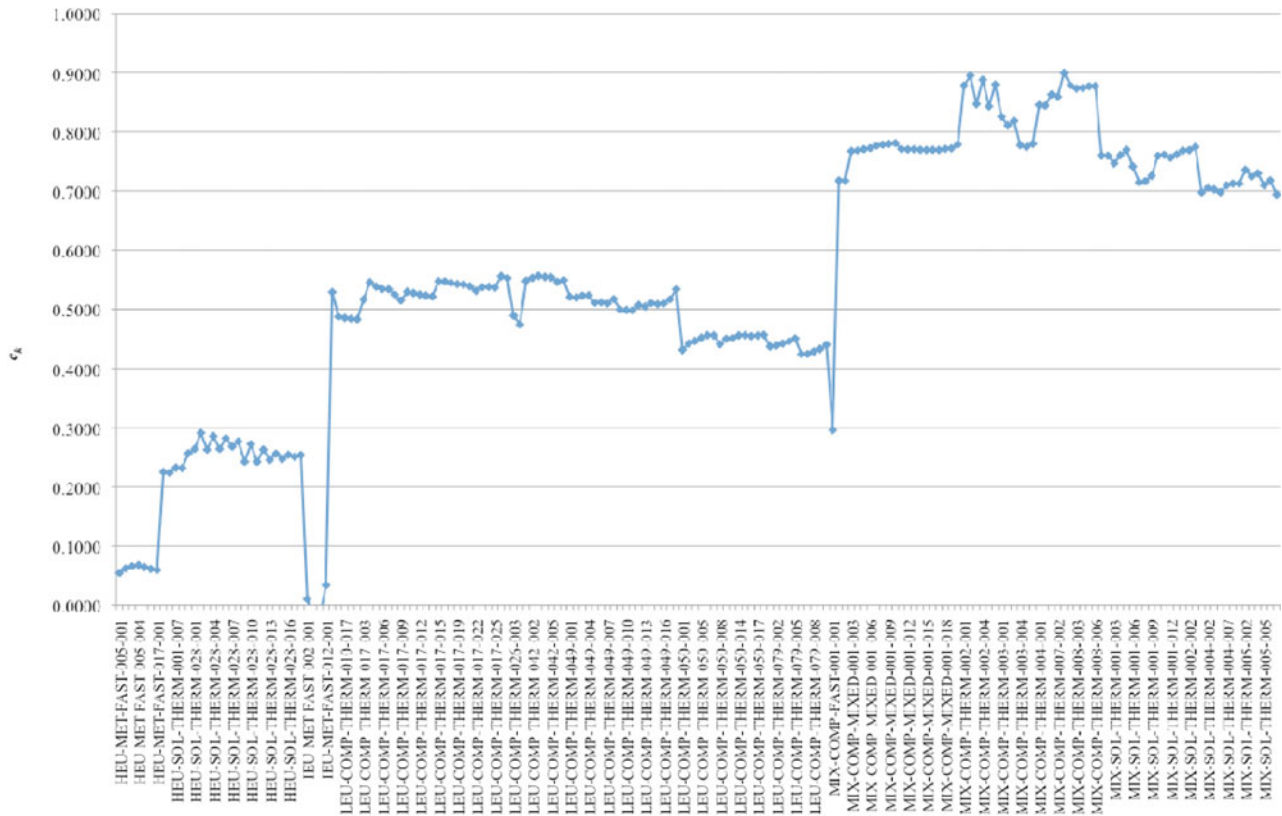


Fig. 9. The  $c_k$  values for benchmark experiments compared to GBC-32 cask model.

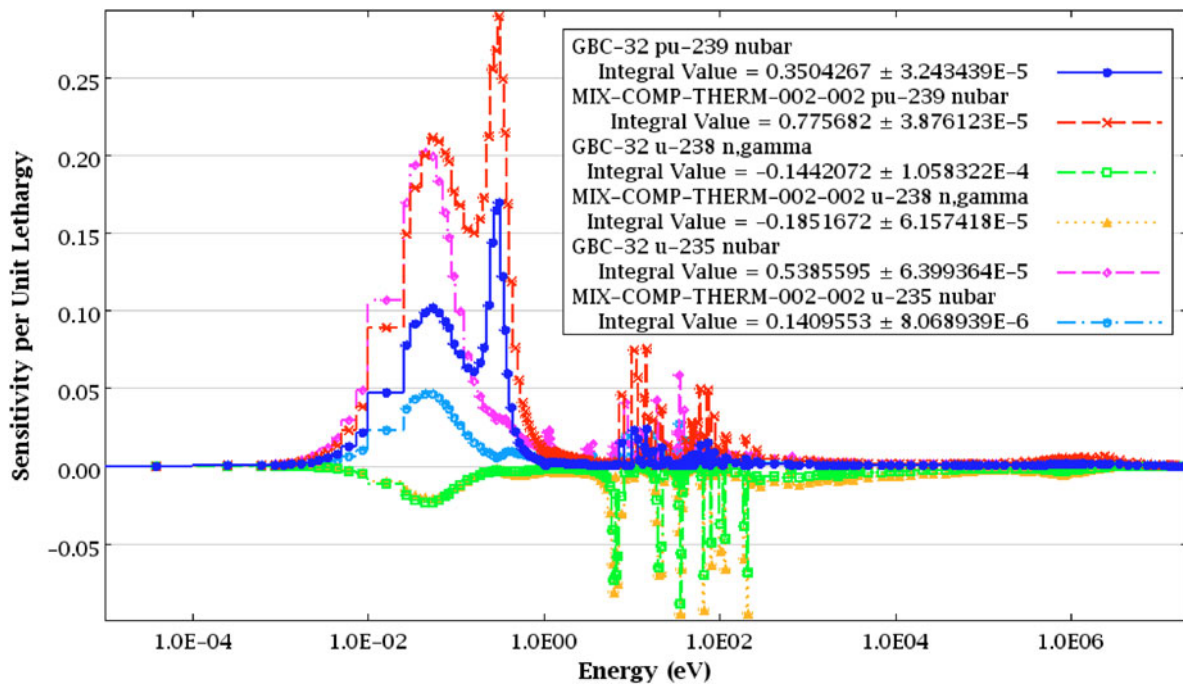


Fig. 10. Sensitivity profiles from GBC-32 and MIX-COMP-THERM-002-002.

TABLE VII

Nuclide-Reaction-Specific Sensitivities and Coverage of GBC-32 by MIX-COMP-THERM-002-002

Nuclide	Reaction	Sensitivity	<i>g</i>
<sup>1</sup> H	Capture	-7.27E-02 <sup>a</sup>	0.611
<sup>1</sup> H	Scatter	3.09E-01	0.811
<sup>10</sup> B	Capture	-3.17E-02	0.349
<sup>16</sup> O	Scatter	2.35E-02	0.916
<sup>56</sup> Fe	Scatter	1.32E-02	0.002
<sup>103</sup> Rh	Capture	-7.82E-03	0.000
<sup>143</sup> Nd	Capture	-1.03E-02	0.000
<sup>149</sup> Sm	Capture	-1.46E-02	0.000
<sup>235</sup> U	Fission	2.28E-01	0.227
<sup>235</sup> U	Capture	-6.30E-02	0.322
<sup>238</sup> U	Fission	3.57E-02	1.000
<sup>238</sup> U	Capture	-1.44E-01	0.957
<sup>238</sup> U	Scatter	1.96E-02	0.959
<sup>239</sup> Pu	Fission	1.80E-01	1.000
<sup>239</sup> Pu	Capture	-8.41E-02	1.000
<sup>240</sup> Pu	Capture	-3.38E-02	0.905
<sup>241</sup> Pu	Fission	2.99E-02	0.062
<sup>241</sup> Pu	Capture	-9.24E-03	0.079

<sup>a</sup>Read as  $-7.27 \times 10^{-2}$ .

Note that the choice of 0.00 for the administrative margin is selected to simplify this example calculation and may not represent an actual administrative margin selected for this type of analysis. The results of the analysis are plotted in Fig. 11 and summarized as follows:

Computational bias,  $\beta = 0.17\% \Delta k/k$

Uncertainty in the bias,  $\Delta\beta = 1.11\% \Delta k/k$

USL<sub>1</sub> = 0.989, disallowing the positive bias

In Fig. 11, the trend in bias from experiments with  $c_k$  values near 0.70 to those with  $c_k$  values approaching 0.90 exhibits a slight positive slope, resulting in the positive bias extrapolated to  $c_k = 1.0$ . The confidence band provides a 95% confidence interval that the application's bias will be within the band based on the statistical analysis.

**IX.G. Penalty Assessment**

Because there are no experiments with  $c_k \geq 0.9$ , an extrapolation occurs from  $c_k$  of  $\sim 0.90$  to 1.0, indicating that 10% of the uncertainty due to cross-section data, and thus up to 10% of the sources of computational bias, may not be included in the analysis. For this case, the penalty calculation of TSUNAMI-IP can be applied to examine sensitivities that are underrepresented in the benchmarks included in the trending analysis. Recall that the original uncertainty in  $k_{eff}$  due to all cross-section data was 0.52%  $\Delta k/k$ . Where the benchmarks with  $c_k \geq 0.70$  are included in the TSUNAMI-IP penalty calculation, the uncertainty remaining, due only to undercovered sensitivity data in the application, is 0.14%  $\Delta k/k$ . The top 25 sources of the penalty are listed according to covariance matrix in Table VIII. Comparing Table VIII with Table V, the many Pu processes shown as top sources of uncertainty are not present as sources of penalty, indicating that the

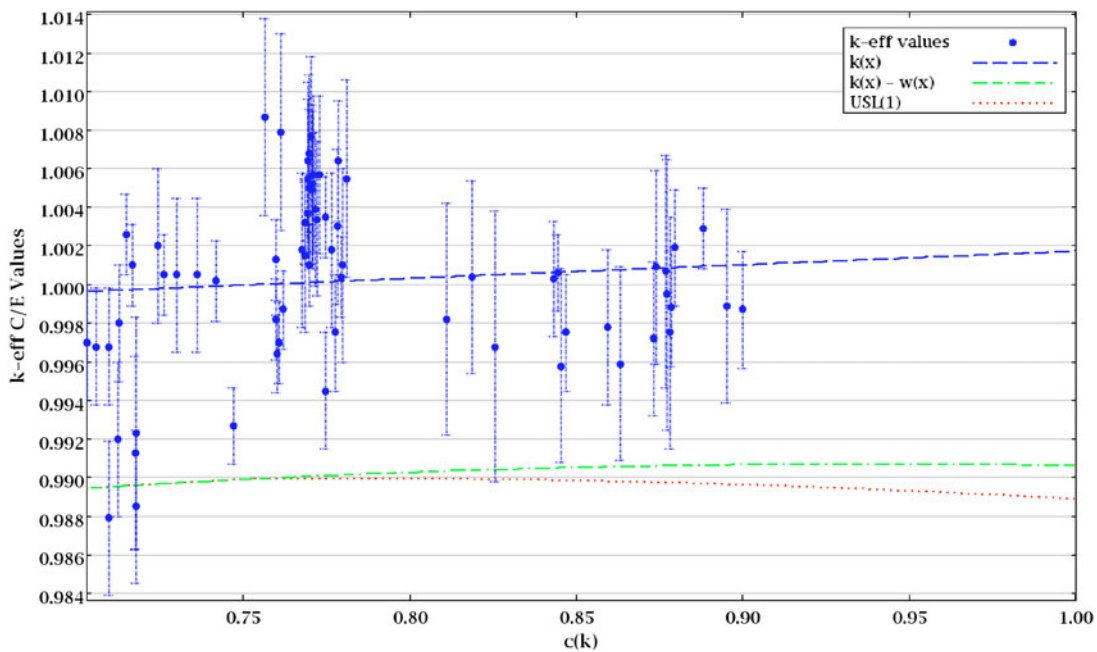


Fig. 11. Trend plot for GBC-32 cask for experiments with  $c_k \geq 0.70$ .

TABLE VIII  
 Penalty in  $k_{eff}$  of GBC-32 Due to Cross-Section  
 Uncertainties After Inclusion of Experiments  
 with  $c_k \geq 0.70$

Covariance Matrix		Penalty % $\Delta k/k$
Nuclide-Reaction	Nuclide-Reaction	
$^{235}\text{U } \bar{p}$	$^{235}\text{U } \bar{p}$	9.10E-02 <sup>a</sup>
$^{235}\text{U } n, \gamma$	$^{235}\text{U } n, \gamma$	4.94E-02
$^{235}\text{U}$ fission	$^{235}\text{U}$ fission	4.09E-02
$^{235}\text{U}$ fission	$^{235}\text{U } n, \gamma$	3.95E-02
$^{56}\text{Fe}$ elastic	$^{56}\text{Fe}$ elastic	3.76E-02
$^{143}\text{Nd } n, \gamma$	$^{143}\text{Nd } n, \gamma$	3.48E-02
$^{149}\text{Sm } n, \gamma$	$^{149}\text{Sm } n, \gamma$	2.16E-02
$^{103}\text{Rh } n, \gamma$	$^{103}\text{Rh } n, \gamma$	2.13E-02
$^{133}\text{Cs } n, \gamma$	$^{133}\text{Cs } n, \gamma$	1.72E-02
$^{145}\text{Nd } n, \gamma$	$^{145}\text{Nd } n, \gamma$	1.72E-02
$^{151}\text{Sm } n, \gamma$	$^{151}\text{Sm } n, \gamma$	1.28E-02
$^{236}\text{U } n, \gamma$	$^{236}\text{U } n, \gamma$	1.03E-02
$^{236}\text{U}$ fission	$^{236}\text{U}$ fission	9.47E-03
$^{237}\text{Np } n, \gamma$	$^{237}\text{Np } n, \gamma$	8.16E-03
$^{101}\text{Ru } n, \gamma$	$^{101}\text{Ru } n, \gamma$	8.14E-03
$^{99}\text{Tc } n, \gamma$	$^{99}\text{Tc } n, \gamma$	7.56E-03
$^{153}\text{Eu } n, \gamma$	$^{153}\text{Eu } n, \gamma$	7.49E-03
$^{235}\text{U } \chi$	$^{235}\text{U } \chi$	7.00E-03
$^{152}\text{Sm } n, \gamma$	$^{152}\text{Sm } n, \gamma$	6.32E-03
$^{147}\text{Sm } n, \gamma$	$^{147}\text{Sm } n, \gamma$	5.61E-03
$^{150}\text{Sm } n, \gamma$	$^{150}\text{Sm } n, \gamma$	5.50E-03
$^{241}\text{Am } n, \gamma$	$^{241}\text{Am } n, \gamma$	4.94E-03
$^{155}\text{Gd } n, \gamma$	$^{155}\text{Gd } n, \gamma$	4.26E-03
$^{58}\text{Ni}$ elastic	$^{58}\text{Ni}$ elastic	3.68E-03
$^{236}\text{U } \bar{p}$	$^{236}\text{U } \bar{p}$	2.60E-03

<sup>a</sup>Read as  $9.10 \times 10^{-2}$ .

benchmarks are at least as sensitive as the GBC-32 to Pu nuclide-reaction pairs at all energies. The U uncertainties are reduced but still rank high as sources of penalty. The uncertainties for structural material such as Fe are only slightly reduced, and uncertainties for fission products such as  $^{143}\text{Nd}$ ,  $^{103}\text{Rh}$ , and  $^{149}\text{Sm}$  are unchanged.

Some experiments in the selected benchmarks contain fission products such as  $^{149}\text{Sm}$  in LEU-COMP-THERM-050 and  $^{103}\text{Rh}$  in LEU-COMP-THERM-079. However, the  $c_k$  values of these experiments are  $\sim 0.45$ , and their usefulness in trending-based bias assessment is limited because of their overall lack of similarity to the GBC-32 application.

Because the fission products are not represented in the benchmark suite and other materials are underrepresented, the penalty of 0.14%  $\Delta k/k$  can be applied as an additional margin or treated as a component of the administrative margin for remaining cross-section uncertainties. As the penalty is a  $1\sigma$  quantity, twice the penalty should be applied to obtain a 95% confidence. A plot of the USLSTATS analysis including the penalty of 0.28%

$\Delta k/k$  is shown in Fig. 12. Note that the penalty only affects the USL<sub>1</sub> value, not the regression line or confidence interval. After inclusion of the penalty, the USL<sub>1</sub> value is reduced to 0.986, accounting for a possible unknown bias that could be present because of the uncovered materials. Even though any potential bias could have a positive or negative sign, the penalty must be applied conservatively.

#### IX.H. Bias Assessment with TSURFER Using $k_{eff}$ Sensitivity Data

An initial data adjustment was performed using all experiments previously identified, excluding the fission product experiments, LEU-COMP-THERM-050 and LEU-COMP-THERM-079, which are addressed in Sec. IX.J. As correlations in experimental uncertainties, required for TSURFER analysis, are currently not available in the IHECSBE, a correlation of 0.7 was assumed for experiments within a given evaluation. Careful quantification of the experimental correlations is important for safety calculations. However, for this example of the methodology, the approximate experimental correlations will suffice. The delta chi-square filtering method, described in Sec. VII.B, was applied with a targeted  $\chi^2$  value of 1.2.

The TSURFER  $\chi^2$  filter identified three experiments for omission from the data adjustment procedure. These experiments are MIX-SOL-THERM-001-003, MIX-SOL-THERM-005-005, and MIX-SOL-THERM-005-006. Adjustments in important cross sections that lead to the best consistency in the experimental data are shown in Fig. 13. The magnitudes and shapes of the adjustments are constrained by cross-section-covariance data. Here,  $^{239}\text{Pu } \bar{p}$  is decreased across the entire energy spectrum, indicating that systems with  $^{239}\text{Pu}$  would overestimate  $k_{eff}$ . The  $^{238}\text{U } n, \gamma$  cross section is decreased at thermal and intermediate energies and generally increased at fast energies. This indicates that systems that are sensitive to  $^{238}\text{U}$  at thermal and intermediate energies could be underestimating  $k_{eff}$  and that fast systems could be overestimating  $k_{eff}$ .

The impact of the adjustments on the C/E ratios for the benchmark experiments can be observed in Fig. 14, where the initial and adjusted  $k_{eff}$  C/E ratios are shown. In Fig. 14 the error bars represent  $1\sigma$  due to the initial and adjusted cross-section-covariance data in the respective data series. Note that the TSURFER adjustment procedure forces agreement between the adjusted calculated and adjusted benchmark values, where the values agree within the specified  $\chi^2$  criteria. For experiments omitted from the adjustment procedure by the  $\chi^2$  filter, no adjusted values are shown.

The bias and bias uncertainty values projected to the GBC-32 from this initial data adjustment are given below.

Computational bias,  $\beta = -0.025\% \Delta k/k$

Uncertainty in the bias,  $\Delta\beta = 0.119\% \Delta k/k$

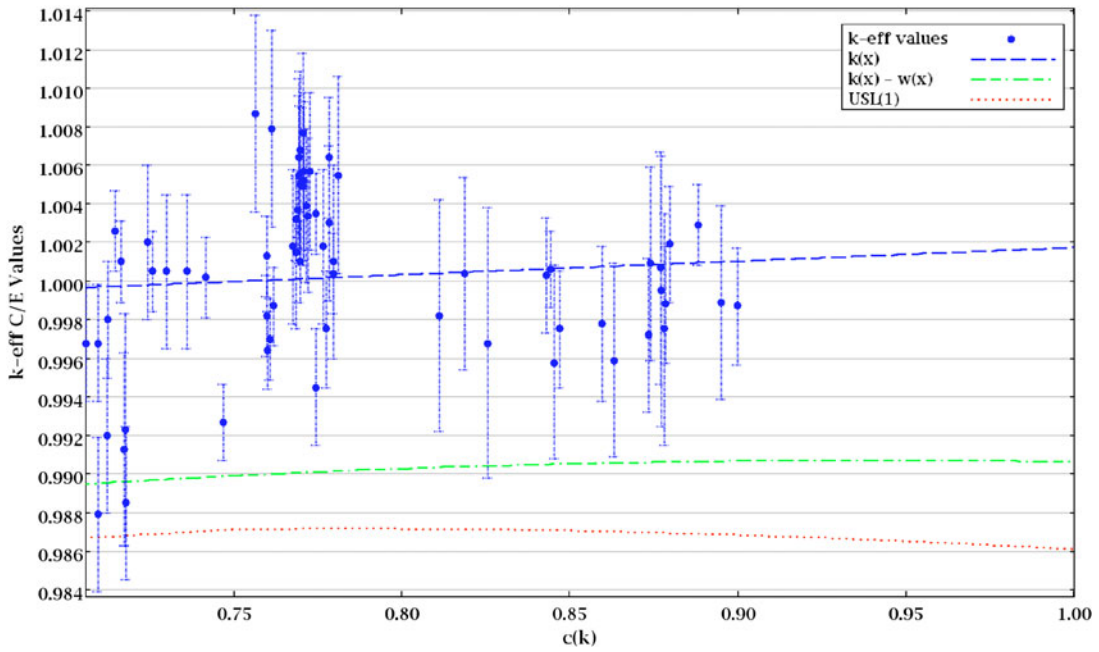


Fig. 12. Trend plot for GBC-32 cask for experiments with  $c_k \geq 0.70$  and penalty.

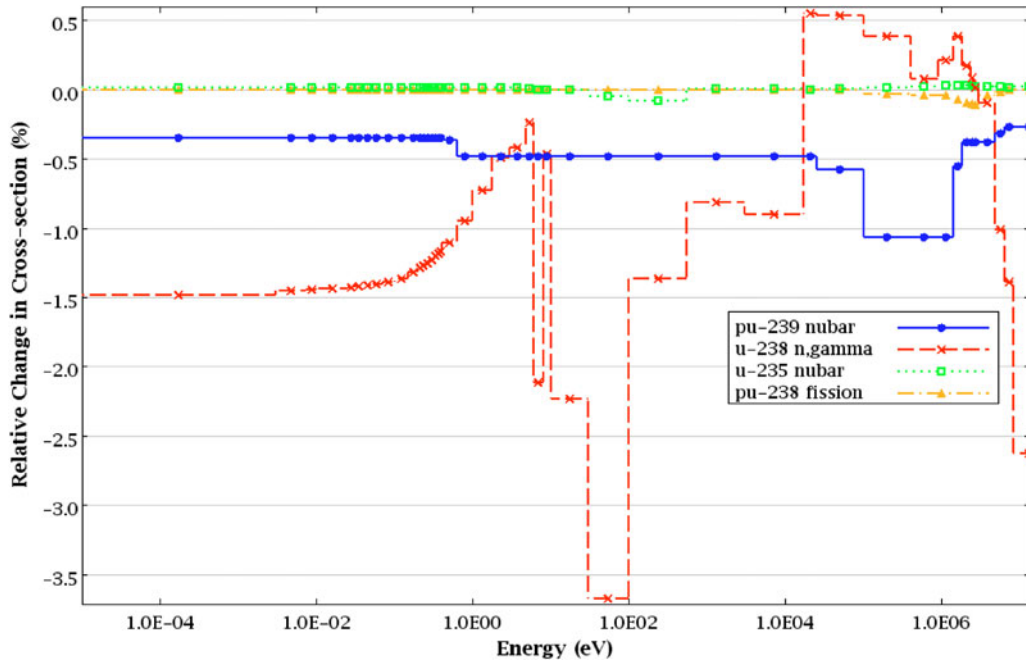


Fig. 13. Cross-section adjustments from initial TSURFER calculation.

Note that the computation bias here is negative, whereas the bias obtained with USLSTATS is positive. However, both values agree within their uncertainties. Where a  $c_k$  filter is applied in TSURFER, including only experiments with  $c_k \geq 0.70$ , and the adjustment is repeated, the following results are found.

Computational bias,  $\beta = 0.077\% \Delta k/k$

Uncertainty in the bias,  $\Delta\beta = 0.229\% \Delta k/k$

Using the same data sets, USLSTATS and TSURFER predict small positive computational biases that agree

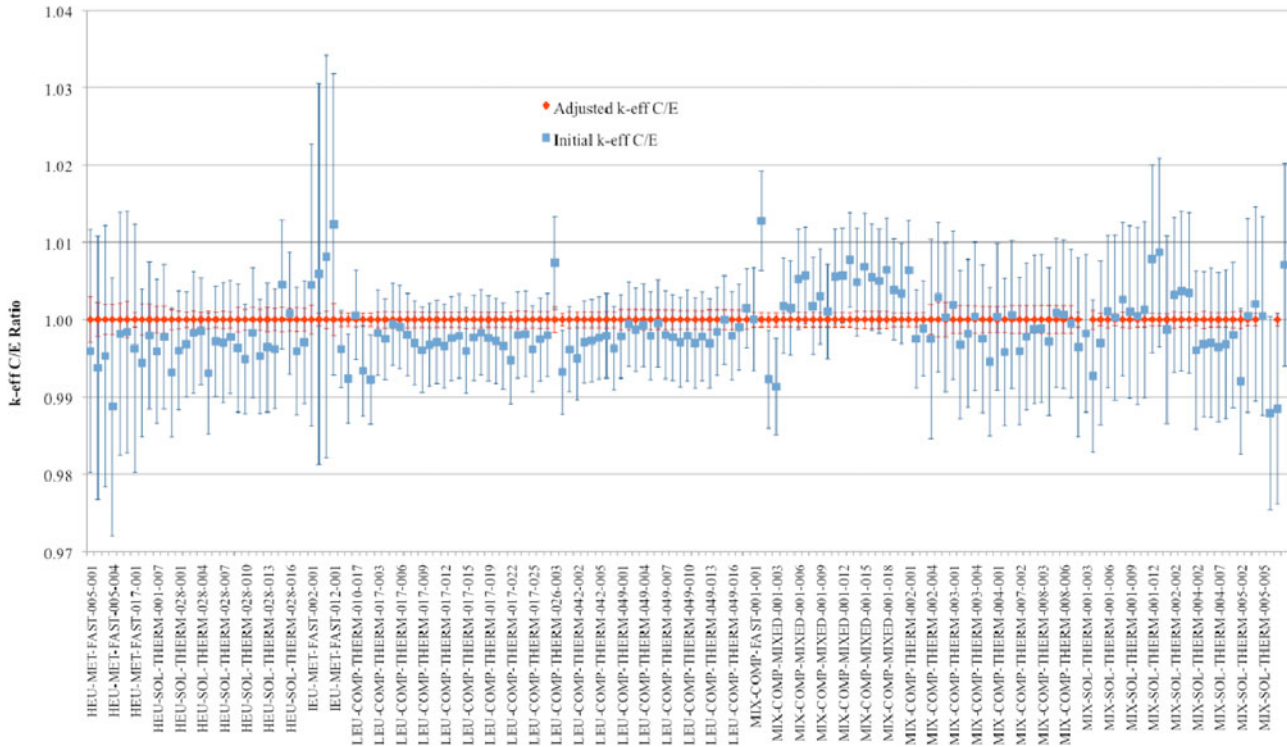


Fig. 14. Initial and adjusted  $k_{eff}$  C/E ratio values from initial TSURFER calculation.

within 0.1%  $\Delta k/k$  and within far less than  $1\sigma$ . The initial TSURFER calculation, including benchmarks that are dissimilar in terms of  $c_k$ , produces a small negative bias that still agrees with the previously computed values within  $1\sigma$ . However, where more benchmarks are included, the precision of the calculation is improved, as quantified by the reduced bias uncertainty.

It is important to note that the TSURFER procedure for bias and bias uncertainty assessment is quite different from interpolation or extrapolation of a trend line with a confidence band treating uncertainties in the data as well as uncertainties in the trend line itself. Instead of trending the data, TSURFER assimilates individual data components, rejecting inconsistent components. In this way, biases comparable to those obtained through other means are obtained, but the uncertainty in the bias will typically be much smaller.

The USL can be determined to a 95% confidence by applying twice the bias uncertainty. An additional administrative margin can be applied but is set to 0.0 in this example. From the initial TSURFER calculation, the following results are found:

$$USL = 0.997.$$

This USL value accounts for uncertainties in the experimental data and uncertainties in the cross-section data. However, like the USL values presented in the previous

section, it does not account for uncertainties in the application itself, which must be considered separately.

### IX.I. Detailed Bias and Bias Uncertainty Assessment with TSURFER

A unique feature of TSURFER is the ability to provide a detailed assessment of sources of the computational bias by multiplying the individual sensitivities of the application by the cross-section adjustments. The processes that are the top 25 contributors to bias in the GBC-32 are shown in Table IX. Because individual nuclide-reaction pairs can provide both positive and negative bias as a function of energy, it is useful to rank sources of biases based on the absolute values of the groupwise contributions. The biases shown in Table IX are listed in descending order according to their L1-norm value, defined as

$$f_x = \frac{\sum_g |S_{x,g} \Delta\alpha_{x,g}|}{\sum_{x'} \sum_g |S_{x',g} \Delta\alpha_{x',g}|} \quad (93)$$

From this bias assessment, positive biases from Pu are offset by the negative biases from U, resulting in a small overall bias.

TABLE IX

Contributions to Bias by Individual Nuclide-Reaction Pairs from Initial TSURFER Calculation

Nuclide	Reaction	Contribution to Bias (% $\Delta k/k$ )	Fraction of L1 Norm
<sup>238</sup> U	<i>n, γ</i>	-2.11E-01 <sup>a</sup>	3.56E-01
<sup>239</sup> Pu	$\bar{v}$	1.28E-01	2.08E-01
<sup>239</sup> Pu	Fission	3.99E-02	6.48E-02
<sup>16</sup> O	Elastic	3.22E-02	5.40E-02
<sup>235</sup> U	Fission	-2.58E-02	4.43E-02
<sup>239</sup> Pu	$\chi$	1.02E-02	3.02E-02
<sup>235</sup> U	$\chi$	2.99E-04	2.94E-02
<sup>56</sup> Fe	<i>n, γ</i>	1.72E-02	2.79E-02
<sup>235</sup> U	Fission	-1.24E-02	2.35E-02
<sup>240</sup> Pu	<i>n, γ</i>	-1.32E-02	2.20E-02
<sup>238</sup> U	Elastic	2.77E-03	2.09E-02
<sup>235</sup> U	<i>n, γ</i>	1.06E-03	1.80E-02
<sup>1</sup> H	Elastic	2.73E-03	1.80E-02
<sup>238</sup> U	<i>n, n'</i>	-6.90E-03	1.24E-02
<sup>235</sup> U	$\bar{v}$	-4.13E-03	1.13E-02
<sup>56</sup> Fe	Elastic	-6.01E-03	9.99E-03
<sup>1</sup> H	<i>n, γ</i>	4.19E-03	6.81E-03
<sup>238</sup> U	$\bar{v}$	3.14E-03	6.09E-03
<sup>241</sup> Am	<i>n, γ</i>	2.70E-03	5.11E-03
<sup>10</sup> B	<i>n, alpha</i>	2.97E-03	4.84E-03
<sup>53</sup> Cr	<i>n, γ</i>	2.23E-03	3.63E-03
<sup>241</sup> Pu	Fission	-1.93E-03	3.29E-03
<sup>58</sup> Ni	<i>n, γ</i>	1.46E-03	2.37E-03
<sup>92</sup> Zr	<i>n, γ</i>	1.35E-03	2.20E-03
<sup>238</sup> U	<i>n, 2n</i>	1.13E-03	1.84E-03

<sup>a</sup>Read as  $-2.11 \times 10^{-1}$ .

The energy-dependent bias can be determined by multiplying the application sensitivity profiles, such as those shown in Fig. 7, by the cross-section adjustments and multiplying by -1. The energy-dependent bias for the GBC-32 for select nuclide-reaction pairs is shown in Fig. 15. The energy-dependence of the bias reflects the energy-dependent structure of the sensitivity data as well the shape of the data adjustments.

Additionally, the uncertainty in the bias can be viewed according to its contributions from the adjusted cross-section-covariance matrices, as shown in Table X. After the adjustment procedure, the remaining unvalidated components of the cross-section data are correlated because they were adjusted using the same set of experimental data. A number of anticorrelations appear in the data, which reduce the overall uncertainty in the bias. Fission products <sup>149</sup>Sm and <sup>103</sup>Rh have bias uncertainty contributions of 0.022 and 0.021%  $\Delta k/k$ , respectively, consistent with the original uncertainties shown in Table V and the penalty values shown in Table VIII. The bias uncertainty values demonstrate that TSURFER made no changes to the cross sections for <sup>149</sup>Sm or <sup>103</sup>Rh because of the

TABLE X

Contribution to the Bias Uncertainty by Covariance Matrix from Initial TSURFER Calculation

Covariance Matrix		Contribution to Bias Uncertainty (% $\Delta k/k$ )
<sup>239</sup> Pu fission	<sup>239</sup> Pu $\bar{v}$	-0.173
<sup>239</sup> Pu $\bar{v}$	<sup>239</sup> Pu $\bar{v}$	0.167
<sup>239</sup> Pu <i>n, γ</i>	<sup>239</sup> Pu $\bar{v}$	-0.137
<sup>238</sup> U <i>n, γ</i>	<sup>238</sup> U <i>n, γ</i>	0.124
<sup>235</sup> U $\bar{v}$	<sup>235</sup> U $\bar{v}$	0.120
<sup>239</sup> Pu fission	<sup>239</sup> Pu fission	0.108
<sup>235</sup> U $\bar{v}$	<sup>238</sup> U <i>n, γ</i>	-0.093
<sup>239</sup> Pu fission	<sup>239</sup> Pu <i>n, γ</i>	0.087
<sup>235</sup> U <i>n, γ</i>	<sup>235</sup> U $\bar{v}$	-0.086
<sup>239</sup> Pu <i>n, γ</i>	<sup>239</sup> Pu <i>n, γ</i>	0.083
<sup>235</sup> U fission	<sup>235</sup> U $\bar{v}$	-0.079
<sup>235</sup> U <i>n, γ</i>	<sup>235</sup> U <i>n, γ</i>	0.071
<sup>238</sup> U <i>n, γ</i>	<sup>239</sup> Pu nubar	-0.068
<sup>235</sup> U fission	<sup>235</sup> U fission	0.065
<sup>238</sup> U <i>n, γ</i>	<sup>238</sup> U $\bar{v}$	-0.064
<sup>235</sup> U <i>n, γ</i>	<sup>238</sup> U <i>n, γ</i>	-0.057
<sup>238</sup> U $\bar{v}$	<sup>238</sup> U $\bar{v}$	0.057
<sup>235</sup> U $\bar{v}$	<sup>239</sup> Pu $\bar{v}$	0.052
<sup>235</sup> U fission	<sup>235</sup> U <i>n, γ</i>	0.050
<sup>1</sup> H elastic	<sup>1</sup> H elastic	0.044
<sup>239</sup> Pu $\bar{v}$	<sup>240</sup> Pu <i>n, γ</i>	-0.043
<sup>238</sup> U <i>n, γ</i>	<sup>239</sup> Pu <i>n, γ</i>	-0.042
<sup>240</sup> Pu <i>n, γ</i>	<sup>240</sup> Pu <i>n, γ</i>	0.042
<sup>235</sup> U fission	<sup>238</sup> U <i>n, γ</i>	-0.041
<sup>56</sup> Fe elastic	<sup>56</sup> Fe elastic	0.041
...	...	...
<sup>149</sup> Sm <i>n, γ</i>	<sup>149</sup> Sm <i>n, γ</i>	0.022
<sup>103</sup> Rh <i>n, γ</i>	<sup>103</sup> Rh <i>n, γ</i>	0.021

exclusion of benchmark experiments containing these nuclides, and they indicate a consistency between the penalty calculation and the TSURFER methodology for processes without experimental coverage.

**IX.J. Bias Assessment with TSURFER Using  $k_{eff}$  Reactivity Sensitivity Data**

The fission product experiments were excluded from the initial TSURFER calculation because even with TSURFER, it may be difficult to examine a single experiment and differentiate bias due to a test material from that due to other materials such as fuel and moderator. An alternative method is to examine two experiments from the same critical assembly, one with and one without the test material, and examine differences in the biases due to the introduction of the test material. TSURFER can provide high-quality biases with low uncertainties only where appropriate experimental data are available. For replacement measurements for test materials, such as the fission

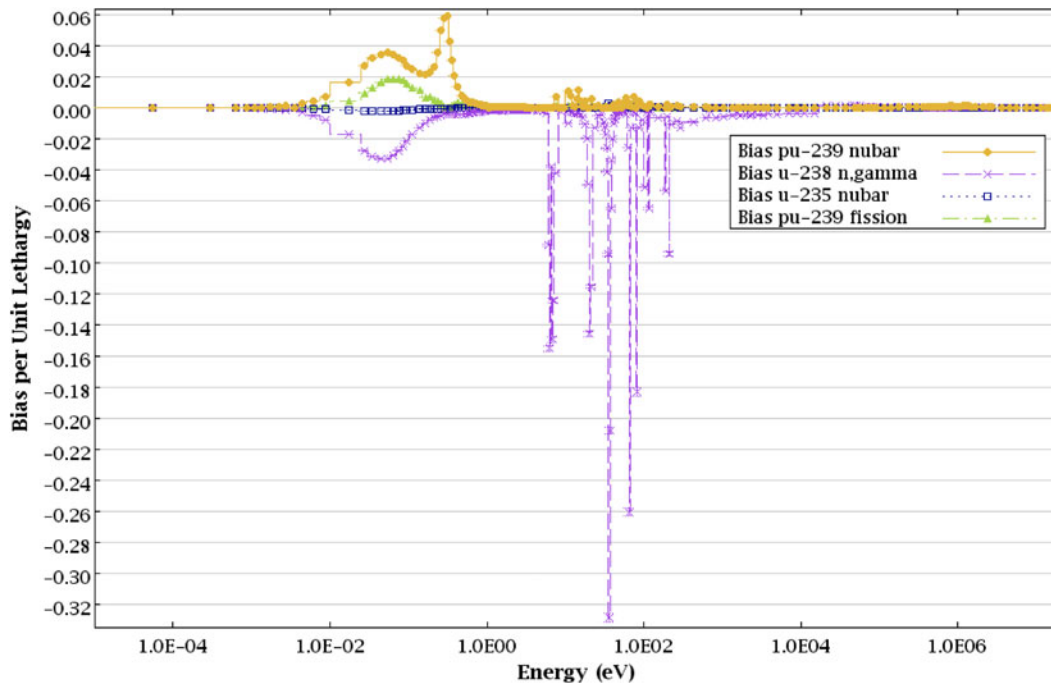


Fig. 15. Energy-dependent bias for GBC-32 from initial TSURFER calculation.

products in LEU-COMP-THERM-050 and LEU-COMP-THERM-079, it is advantageous to employ a means of emphasizing the test material through the use of two highly correlated experiments, one with the test material and one without. Since both experiments are critical, the change in  $k_{eff}$  between the two systems (the reactivity difference) would be zero, within experimental uncertainties. However, if there were a computational bias due to the test material, the computed reactivity between the two experiments would not be zero, as the experiment with the test material would have a different computational bias from the experiment without the test material. This replacement technique magnifies the effect of the test material because all other materials are nearly the same, and sources of uncertainty between the two experiments are highly correlated. The primary difference between the two measurements is the test material itself.

To utilize the measured bias of the test material, TSUNAMI  $k_{eff}$  sensitivity data are generated for each pair of experiments, and TSAR is applied to determine the sensitivity of the reactivity between the two systems to the cross-section data. TSAR determines on a nuclide-reaction and energy-dependent basis the sensitivity of changes in computed  $k_{eff}$  between two systems to the cross-section data. Thus, if the primary difference between two critical measurements is the test material, TSAR determines, on an energy-dependent basis, how sensitive the bias is to the test material. TSURFER then determines the sources of bias, using not only  $k_{eff}$  sensitivity data but also reactivity sensitivity data. For the test ma-

terial, TSURFER applies its data adjustment procedure to obtain a consistency between the computed and measured reactivity changes for each pair of systems, determining the best-estimate cross-section adjustments for the test material. The measured bias due to the test material is then projected to a bias in the application by multiplying the cross-section adjustments that eliminate the bias in the experiments by the application's  $k_{eff}$  sensitivity coefficients for the same material. This product gives the relative bias in the application's computed  $k_{eff}$  value due to the test material.

#### IX.J.1. Fission Product Replacement-Worth Experiments

The LEU-COMP-THERM-050 series of experiments consists of a water-moderated and reflected low-enriched  $\text{UO}_2$  (4.738 wt%  $^{235}\text{U}$ ) fuel rod array surrounding a Zircaloy tank containing  $^{149}\text{Sm}$  solution. For each configuration, the approach to critical was conducted with variable water height. The evaluation documents 11 benchmark experiments containing  $^{149}\text{Sm}$  and two reference configurations where the central Zircaloy tank is filled with water. Some information regarding the cases examined for this work is shown in Table XI.

The LEU-COMP-THERM-079 series of experiments consists of a water-moderated and reflected low-enriched  $\text{UO}_2$  (4.31 wt%  $^{235}\text{U}$ ) fuel rod array with thin foils of  $^{103}\text{Rh}$  inserted between the fuel pellets of some fuel rods. For each configuration, the approach to critical

TABLE XI  
LEU-COMP-THERM-050 Cases

Case	Solution Characteristics			Geometry		<sup>149</sup> Sm Similarity with GBC-32	
	Type	Poison Concentration (g/ℓ)	Acidity (N)	Driver Array	Critical Height (cm)	g	Individual $c_k$
1	H <sub>2</sub> O		0.014	23x23-25	61.381	0.000	0.000
8	Sm	0.1048	0.0149	23x25-25	62.663	0.935	1.000
12	Sm	0.2148	0.0155	25x23-35	80.776	0.996	1.000
13	Sm	0.2148	0.0155	25x23-43	87.577	0.995	1.000
14	Sm	0.6262	0.0190	25x25-39	83.948	1.000	1.000
15	Sm	0.6262	0.0190	25x25-43	88.935	1.000	1.000
16	Sm	0.6262	0.0190	25x25-45	84.553	1.000	1.000
17	Sm	0.6262	0.0190	25x25-49	86.302	1.000	1.000
18	Sm	0.6262	0.0190	25x25-53	88.415	1.000	1.000

was conducted adding fuel rods. The evaluation documents 10 benchmark experiments at two different pitches where three benchmarks at each pitch contain <sup>103</sup>Rh foils. Some information regarding the benchmarks is provided in Table XII.

Although the LEU-COMP-THERM-050 and LEU-COMP-THERM-079 experiments exhibit  $c_k$  values of ~0.45 when compared to the GBC-32 cask, many configurations do have similar sensitivity profiles for the tested fission products. The <sup>149</sup>Sm sensitivities for the GBC-32 and two experiments, LEU-COMP-THERM-050-008 and LEU-COMP-THERM-050-018, are shown in Fig. 16, where the sensitivity profiles are quite similar, as confirmed by the  $g$  and individual  $c_k$  values shown in Table XI.

Sensitivity profiles for <sup>103</sup>Rh for the GBC-32 and LEU-COMP-THERM-079-003, LEU-COMP-THERM-079-005, and LEU-COMP-THERM-079-010 are shown in Fig. 17, where the energy axis is zoomed to highlight important aspects of the sensitivity profiles. None of the experiments demonstrate sensitivity with as great of a magnitude as the GBC-32 for the resonance near 1.25 eV. Experiments 005 and 010 demonstrate a reduction in sensitivity at energies near the resonance peak because of the spatial self-shielding of the 100- $\mu$ m-thick foils and demonstrate more <sup>103</sup>Rh sensitivity at thermal energies than the GBC-32. The <sup>103</sup>Rh  $g$  and individual  $c_k$  values for these experiments relative to the GBC-32 are shown in Table XII. Note that the  $g$  values are in the range of 0.699 to 0.762,

TABLE XII  
LEU-COMP-THERM-079 Cases

Case	Geometry					<sup>103</sup> Rh Similarity with GBC-32	
	Fuel Element Pitch (cm)	Number of Driver Elements	Number of Experiment Elements	Number of <sup>103</sup> Rh Foils/Rod	Nominal Thickness of <sup>103</sup> Rh Foils ( $\mu$ m)	g	Individual $c_k$
1	2.0	257	0	—	—	0.000	0.000
2	2.0	221	36	0	—	0.000	0.000
3	2.0	234	36	31	25	0.747	0.997
4	2.0	243	36	31	50	0.762	0.987
5	2.0	258	36	31	100	0.710	0.959
6	2.8	131	0	—	—	0.000	0.000
7	2.8	95	36	0	—	0.000	0.000
8	2.8	104	36	31	25	0.759	0.947
9	2.8	110	36	31	50	0.744	0.891
10	2.8	122	36	31	100	0.699	0.799

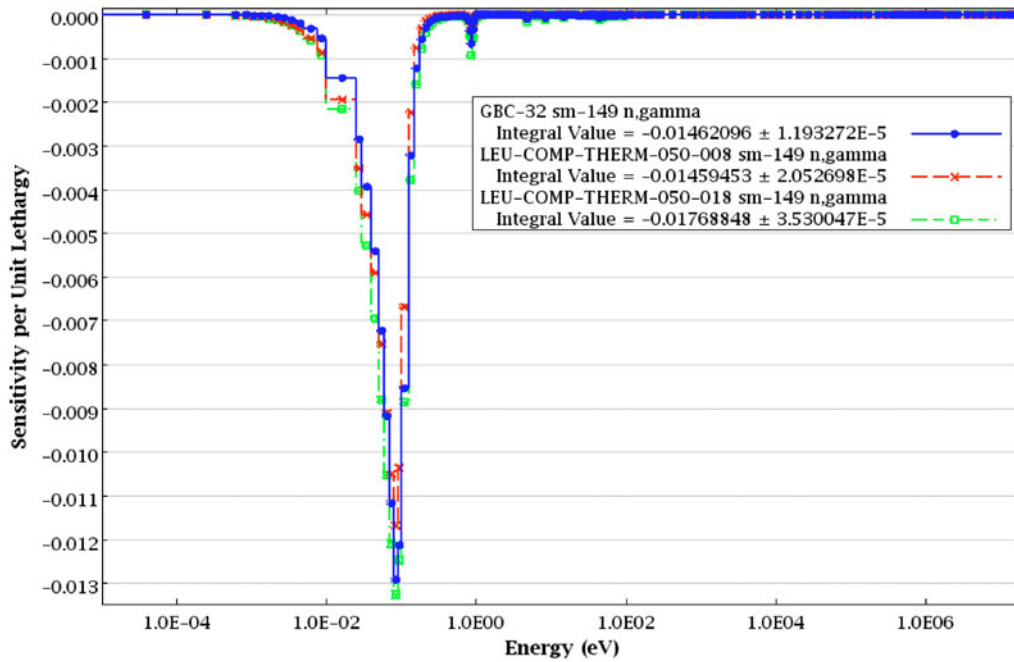


Fig. 16. Sensitivity of  $k_{eff}$  to  $^{149}\text{Sm}$  for GBC-32 and LEU-COMP-THERM-050-008 and -018.

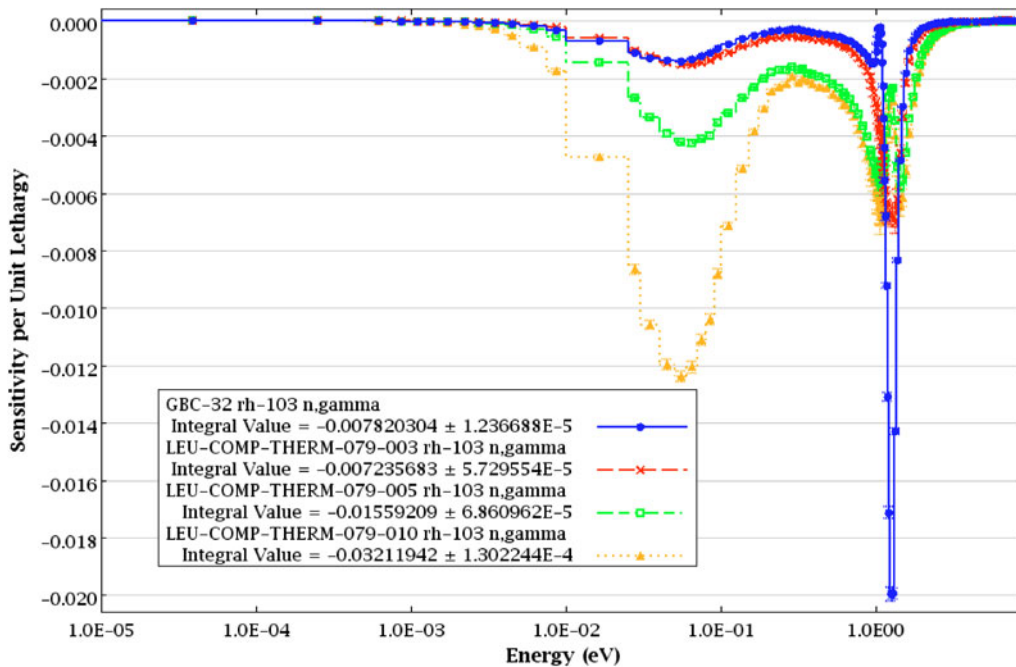


Fig. 17. Sensitivity of  $k_{eff}$  to  $^{103}\text{Rh}$  for GBC-32 and LEU-COMP-THERM-079-003, -005, and -010.

indicating that the experiments provide <80% coverage of the GBC-32 sensitivity, consistent with sensitivity profiles shown in Fig. 17. However, individual  $c_k$  values are much higher, up to 0.997. The individual  $c_k$  assesses similarity in terms of shared uncertainty using not only the

sensitivity data but also the cross-section-covariance data for the process of interest.

The uncertainties in the  $^{149}\text{Sm}$  and  $^{103}\text{Rh}$   $n, \gamma$  cross sections from the SCALE 6 covariance library are shown in Fig. 18. Covariance data for both  $^{149}\text{Sm}$  and  $^{103}\text{Rh}$

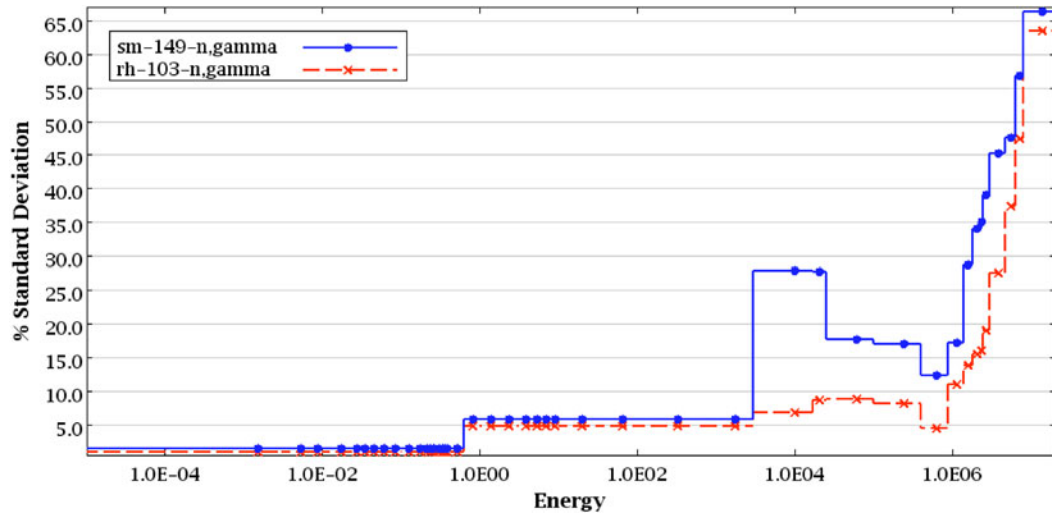


Fig. 18. Uncertainties in  $^{149}\text{Sm}$  and  $^{103}\text{Rh}$   $n, \gamma$  cross sections.

are BLO approximate data, with full correlations within the thermal and intermediate energy ranges, respectively. Although LEU-COMP-THERM-079-003 demonstrates only 75% coverage from the  $g$  assessment, it demonstrates a 99.7% similarity from the covariance-weighted individual  $c_k$ . Although the sensitivity of the experiment is not as great as that of the GBC-32, its uncertainties in each energy range, thermal and intermediate, are highly correlated to those of the GBC-32 because it demonstrates sensitivities at energies similar to those of the GBC-32. Thus, the data from LEU-COMP-THERM-079 can be applicable to the validation of the GBC-32 if appropriate techniques are applied.

#### IX.J.2. Identification of Fission Product Biases

An indication that there is a computation bias due to the test material is that the computed reactivity difference  $\rho_{1 \rightarrow 2}^c$  differs from measured reactivity difference  $\rho_{1 \rightarrow 2}^m$ . The uncertainties must also be considered in these calculations. The uncertainty in the measured reactivity difference is derived from the individual experimental uncertainties and their correlations as

$$\sigma_{\rho_{1 \rightarrow 2}^m} = (\sigma_{k_1^m}^2 + \sigma_{k_2^m}^2 - 2c_{12}\sigma_{k_1^m}\sigma_{k_2^m})^{1/2}, \quad (94)$$

where  $c_{12}$  is the correlation coefficient between the uncertainties of experiments 1 and 2 and the benchmark  $k_{eff}$  uncertainties,  $\sigma_{k_1^m}$  and  $\sigma_{k_2^m}$ , are obtained from the experiment evaluation.

Because the experiments are designed to be similar, the uncertainties due to the fuel, moderator, and other common components will be highly correlated. For the purposes of this study, correlation coefficients of 0.90 were assumed in computing the uncertainties in the measured reactivity differences for LEU-COMP-THERM-

050 configurations and LEU-COMP-THERM-079 configurations. The measured and computed reactivity differences between configurations of the critical experiments are shown in Table XIII in units of percent-milli-rho (pcm), or  $\Delta k_{eff} \times 10^5$ . The uncertainty in the reactivity differences due to cross-section-covariance data is also shown. Because the measured and computed reactivity differences vary, it is possible that there is a bias due to the test material in each series of experiments. However, the level of precision to which these biases can be quantified is limited by the consistency of the observed bias and the uncertainties in the individual results.

The  $k_{eff}$  sensitivities for  $^{235}\text{U}$  fission,  $^{238}\text{U}(n, \gamma)$ , and  $^{149}\text{Sm}(n, \gamma)$  from LEU-COMP-THERM-050 cases 001, 008, and 018 are shown in Fig. 19. Here it can be observed that the  $^{235}\text{U}$  fission and  $^{238}\text{U}(n, \gamma)$  sensitivities are quite similar between all cases. It can also be observed that the  $^{149}\text{Sm}$  sensitivities are an order of magnitude smaller than the other sensitivities. Note that case 001 does not contain samarium solution and thus does not have  $^{149}\text{Sm}$  sensitivity. The  $k_{eff}$  sensitivities for  $^1\text{H}$  elastic scattering for these same three experiments are shown in Fig. 20. Note that small differences can be observed between the three cases, especially between cases 001 and 018, where the high concentration of samarium necessitated a  $\sim 50\%$  increase in the critical water height to compensate for the high negative reactivity of the samarium. These two cases will exhibit different neutron leakages, which affect the  $^1\text{H}$  sensitivity profiles.

The  $k_{eff}$  sensitivities for  $^{235}\text{U}$  fission,  $^{238}\text{U}(n, \gamma)$ , and  $^{103}\text{Rh}(n, \gamma)$  from LEU-COMP-THERM-079 cases 002, 003, and 005 are shown in Fig. 21. As with LEU-COMP-THERM-050, the  $^{235}\text{U}$  fission and  $^{238}\text{U}(n, \gamma)$  sensitivity profiles are similar for all three cases. Here, the rhodium

TABLE XIII  
Reactivity Differences

Evaluation	States	Measured Reactivity Difference (pcm)	Computed Reactivity Difference (pcm)	Uncertainty in Reactivity Due to Covariance Data
LEU-COMP-THERM-050	1 → 8	0 ± 45	-196	34
	1 → 12	0 ± 45	-11	60
	1 → 13	0 ± 45	29	64
	1 → 14	0 ± 45	-16	73
	1 → 15	0 ± 45	31	74
	1 → 16	0 ± 45	142	71
	1 → 17	0 ± 45	125	74
	1 → 18	0 ± 45	118	76
LEU-COMP-THERM-079	2 → 3	30 ± 72	5	23
	2 → 4	20 ± 72	32	35
	2 → 5	20 ± 72	92	47
	7 → 8	50 ± 36	68	22
	7 → 9	0 ± 36	60	34
	7 → 10	60 ± 36	164	55

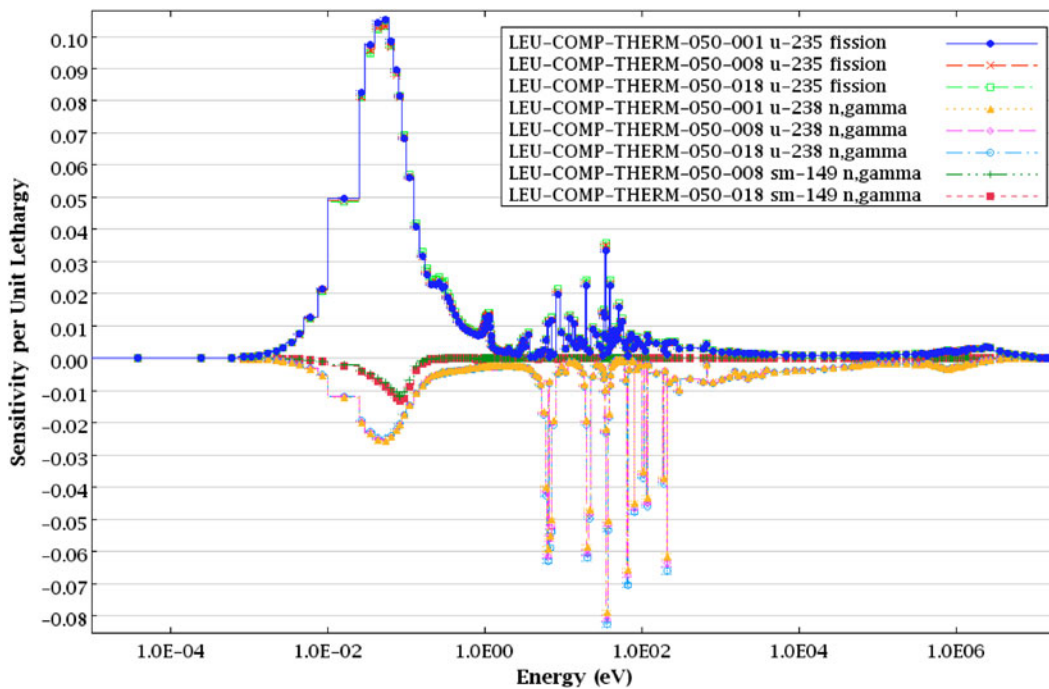


Fig. 19. The  $k_{eff}$  sensitivities for  $^{235}\text{U}$  fission,  $^{238}\text{U}$   $n, \gamma$ , and  $^{149}\text{Sm}$   $n, \gamma$  from LEU-COMP-THERM-050 cases 001, 008, and 018.

sensitivities are much smaller than those of the other nuclides. The  $k_{eff}$  sensitivities for  $^1\text{H}$  elastic scattering for these same three experiments are shown in Fig. 22. Here, the sensitivity profiles are mostly similar for all three cases, except that cases 003 and 005 exhibit a peak in the sensitivity just above 1 eV, corresponding to the

$^{103}\text{Rh}$  resonance. In these experiments,  $^1\text{H}$  elastic scattering in that energy range becomes more important because of the positive reactivity effect of escaping capture in  $^{103}\text{Rh}$ .

The sensitivities of the computed reactivity difference between the pairs of experiments noted in Table XIII

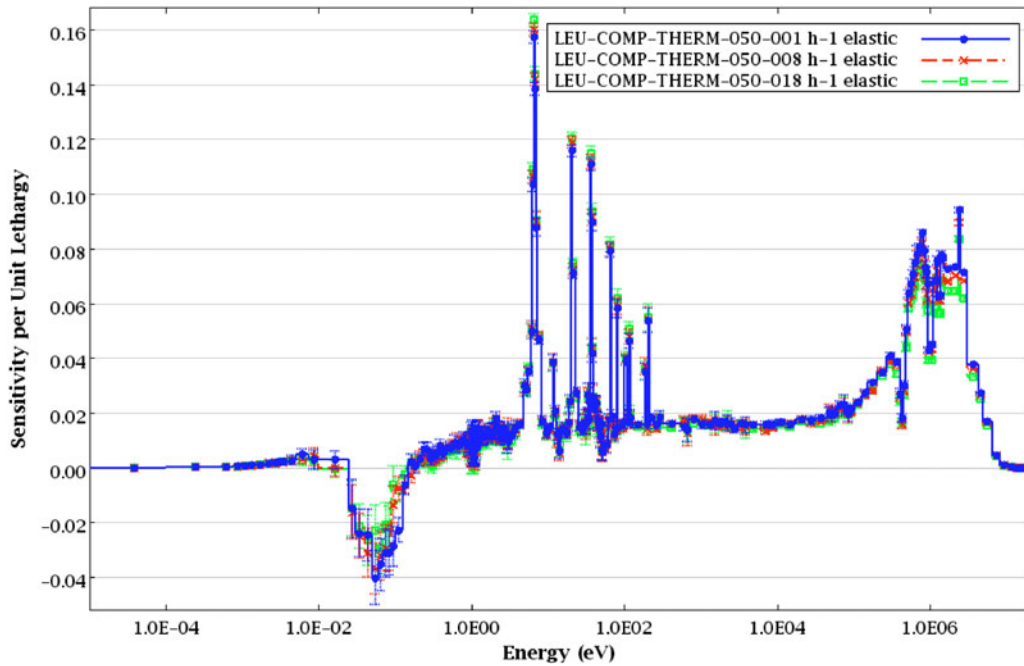


Fig. 20. The  $k_{eff}$  sensitivities for  $^1\text{H}$  elastic scattering from LEU-COMP-THERM-050 cases 001, 008, and 018.

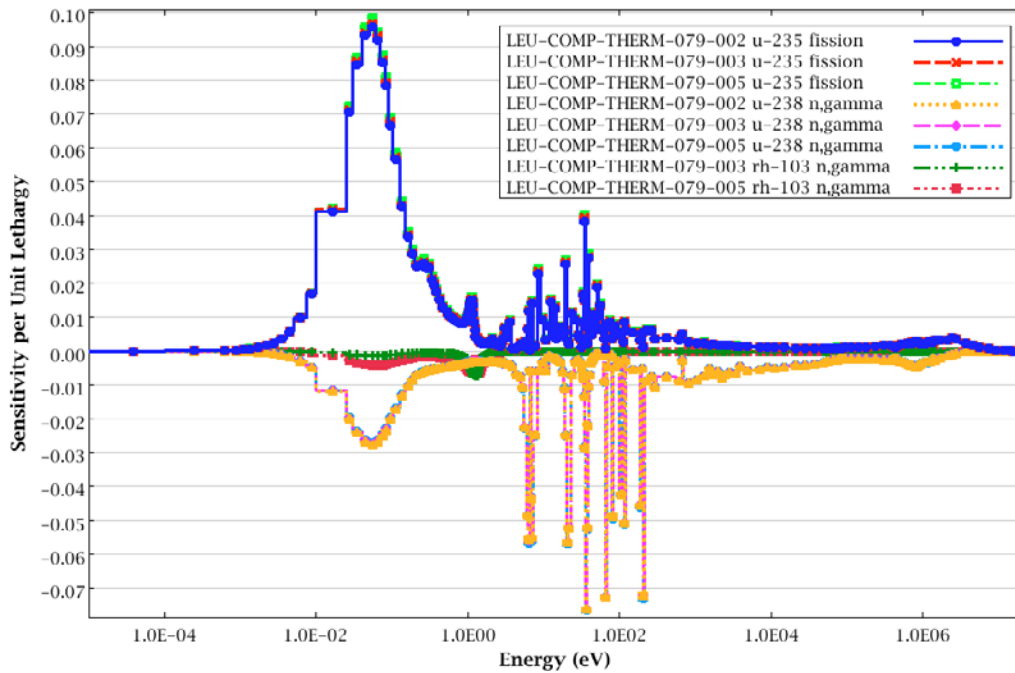


Fig. 21. The  $k_{eff}$  sensitivities for  $^{235}\text{U}$  fission,  $^{238}\text{U}$   $n, \gamma$ , and  $^{103}\text{Rh}$   $n, \gamma$  from LEU-COMP-THERM-079 cases 002, 003, and 005.

were computed with TSAR. The  $\rho$  sensitivities for  $^{235}\text{U}$  fission,  $^{238}\text{U}(n, \gamma)$ , and  $^{149}\text{Sm}(n, \gamma)$  from LEU-COMP-THERM-050 cases 001  $\rightarrow$  008 are shown in Fig. 23. Because the  $^{235}\text{U}$  fission and  $^{238}\text{U}(n, \gamma)$  sensitivity profiles are quite similar between these two cases,  $^{149}\text{Sm}(n, \gamma)$

sensitivity is emphasized in the reactivity sensitivity coefficients. Because the reactivity change between the two cases is not very sensitive to  $^{235}\text{U}$  fission or  $^{238}\text{U}(n, \gamma)$ , the  $-196$  pcm reactivity difference shown in Table XIII is more likely due to  $^{149}\text{Sm}(n, \gamma)$ . However, as shown in

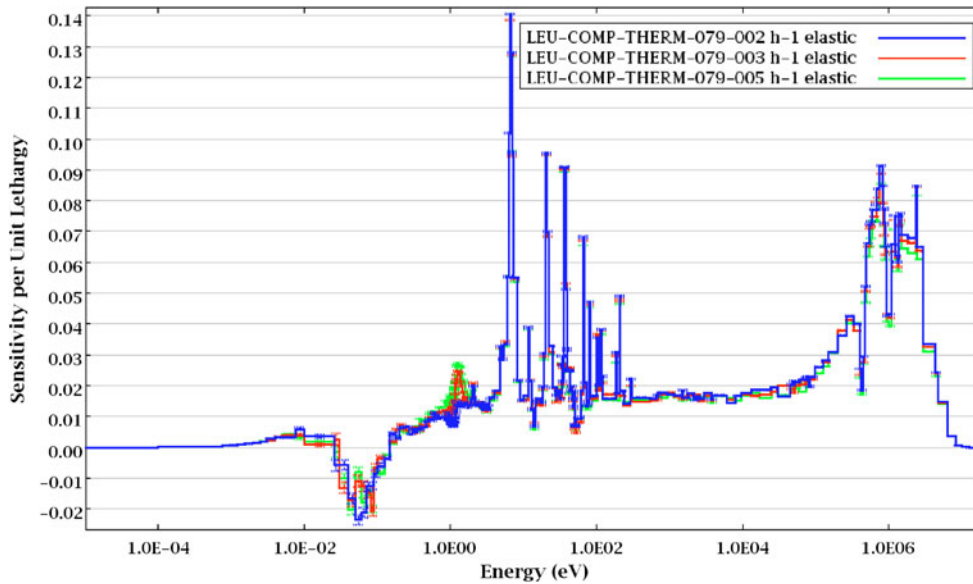


Fig. 22. The  $k_{eff}$  sensitivities for  $^1\text{H}$  elastic scattering from LEU-COMP-THERM-079 cases 002, 003, and 005.

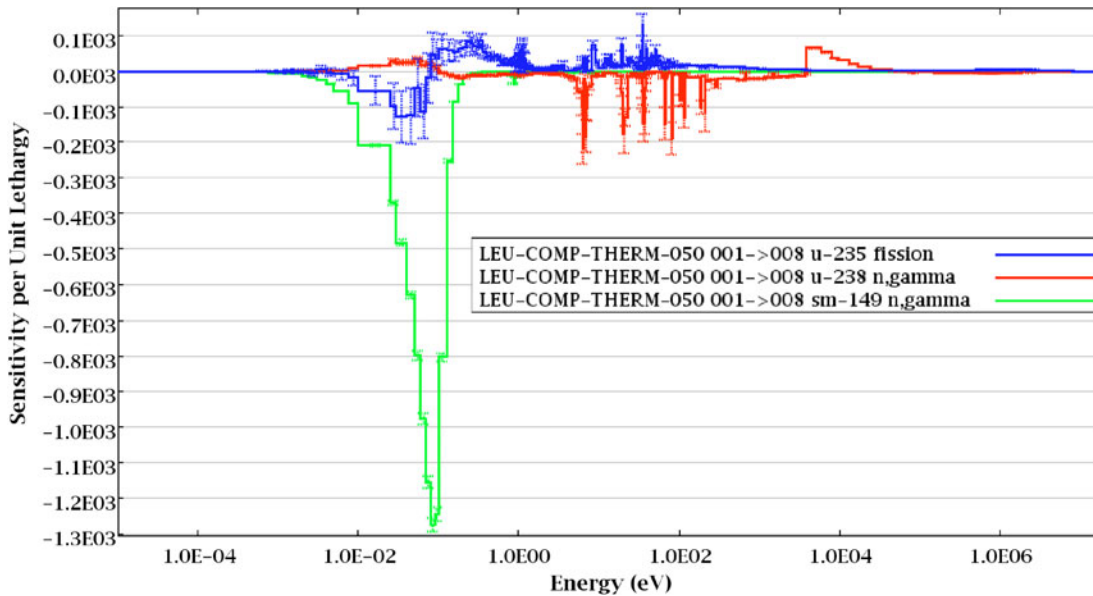


Fig. 23. Reactivity sensitivities for  $^{235}\text{U}$  fission,  $^{238}\text{U} n, \gamma$ , and  $^{149}\text{Sm} n, \gamma$  between LEU-COMP-THERM-050 cases 008 and 001.

Fig. 24, the  $^1\text{H}$  elastic scattering differences between cases 001 and 008 do lead to reactivity sensitivities on the same order of magnitude as the  $^{149}\text{Sm}$  sensitivities. Thus, it is possible that the reactivity difference is due to some combination of  $^1\text{H}$  and  $^{149}\text{Sm}$ .

The  $\rho$  sensitivities for  $^{235}\text{U}$  fission,  $^{238}\text{U}(n, \gamma)$ , and  $^{103}\text{Rh}(n, \gamma)$  from LEU-COMP-THERM-079 cases 002  $\rightarrow$  005 are shown in Fig. 25. Because the  $^{235}\text{U}$  fission and  $^{238}\text{U}(n, \gamma)$  sensitivity profiles are similar between these two cases, the  $^{103}\text{Rh}(n, \gamma)$  sensitivity is emphasized in the

reactivity sensitivity coefficients. However, the reactivity is somewhat sensitive to  $^{235}\text{U}$  fission, indicating a shift in the  $^{235}\text{U}$  fission sensitivities in the  $k_{eff}$  data. As shown in Fig. 26, the  $^1\text{H}$  elastic scattering differences between cases 002 and 005 do lead to reactivity sensitivities that exceed the magnitude of the  $^{103}\text{Rh}$  sensitivities. Thus, it is possible that the reactivity differences are due to some combination of effects from  $^1\text{H}$ ,  $^{103}\text{Rh}$ , and  $^{235}\text{U}$ .

As the reactivity differences for these cases exhibit sensitivities to cross sections other than for the fission

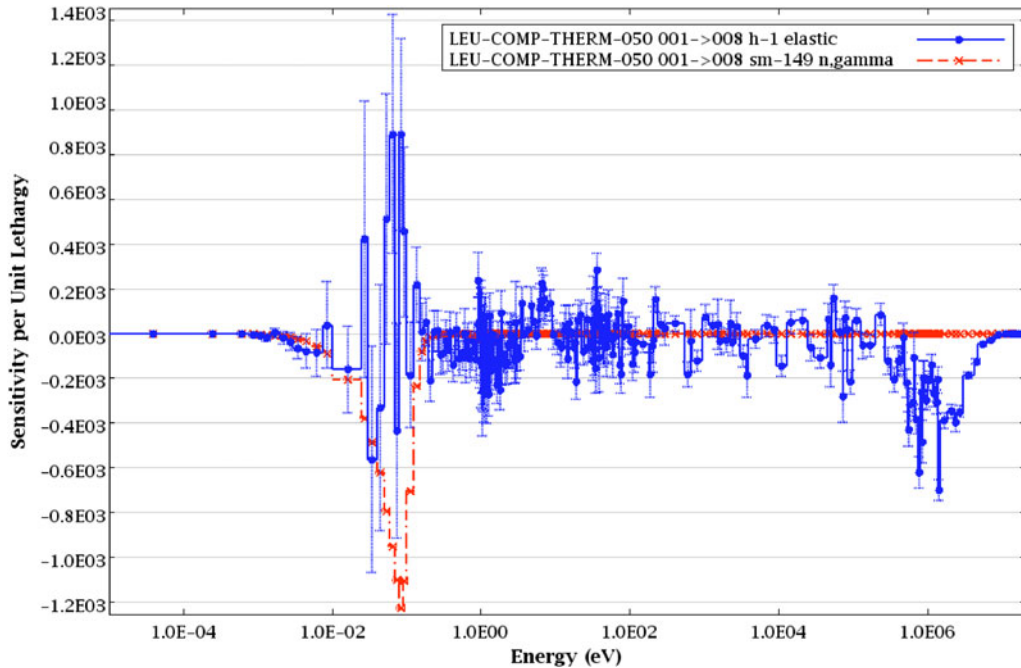


Fig. 24. Reactivity sensitivities for  $^1\text{H}$  elastic scattering and  $^{149}\text{Sm}$   $n, \gamma$  between LEU-COMP-THERM-050 cases 008 and 001.

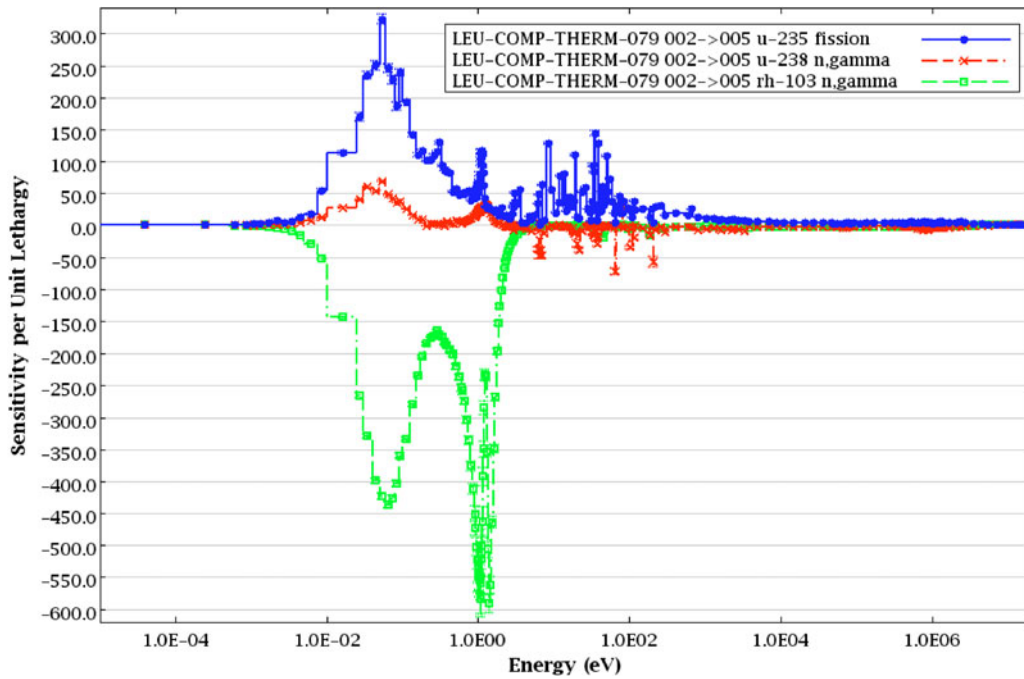


Fig. 25. Reactivity sensitivities for  $^{235}\text{U}$  fission,  $^{238}\text{U}$   $n, \gamma$ , and  $^{103}\text{Rh}$   $n, \gamma$  between LEU-COMP-THERM-079 cases 002  $\rightarrow$  005.

products, the other experiments included in the initial data adjustment will impact the reactivity of the fission product experiments as they are introduced into a subsequent TSURFER calculation. These cross-section ad-

justments from their initial calculation were applied to determine adjusted calculated  $k_{eff}$  values for the LEU-COMP-THERM-050 and -079 experiments. The original and adjusted  $k_{eff}$  values are shown in Fig. 27, where the

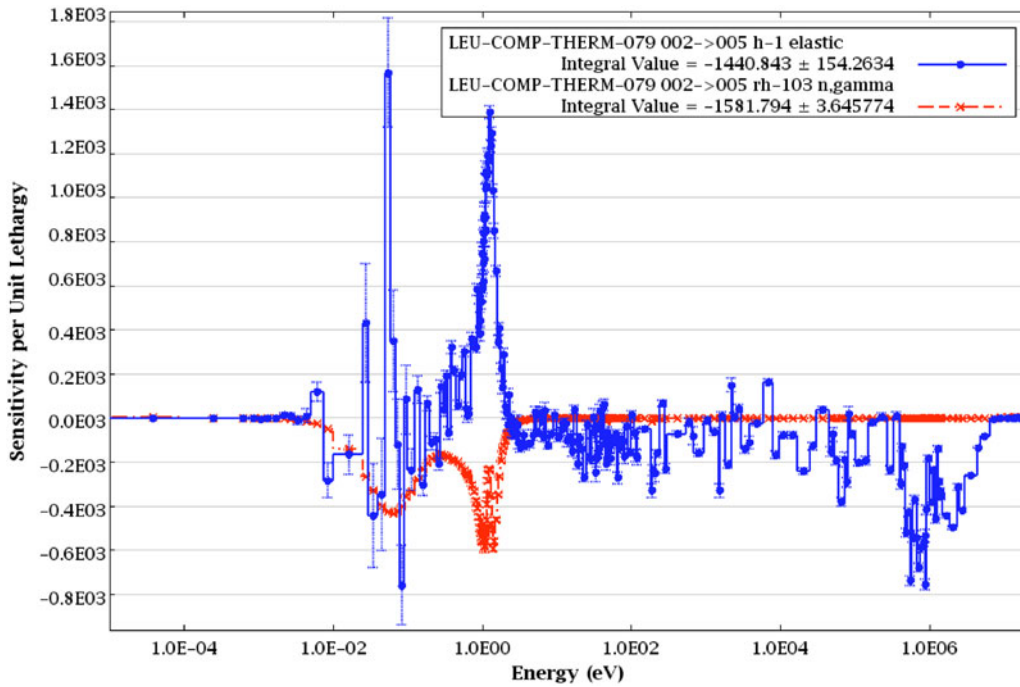


Fig. 26. Reactivity sensitivities for  $^1\text{H}$  elastic scattering and  $^{103}\text{Rh}$   $n, \gamma$  between LEU-COMP-THERM-079 cases 002 and 005.

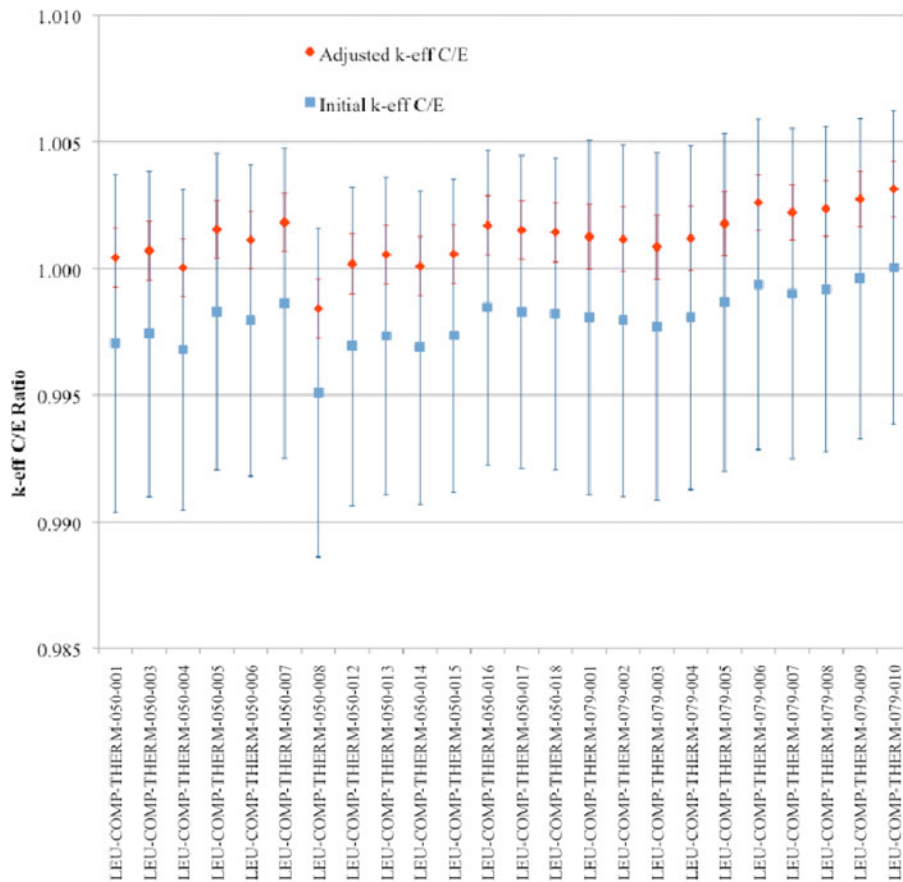


Fig. 27. Initial and adjusted  $k_{eff}$  C/E ratio values for fission product experiments based on adjustments from initial TSURFER calculation.

TABLE XIV  
Reactivity Differences After  $k_{eff}$  Adjustments

Evaluation	States	Adjusted Reactivity Difference (pcm)	Uncertainty in Reactivity Due to Covariance Data (pcm)
LEU-COMP-THERM-050	1 → 8	-203	24
	1 → 12	-29	33
	1 → 13	8	33
	1 → 14	-39	32
	1 → 15	9	33
	1 → 16	123	32
	1 → 17	104	33
	1 → 18	95	33
LEU-COMP-THERM-079	2 → 3	-31	17
	2 → 4	2	22
	2 → 5	59	28
	7 → 8	13	17
	7 → 9	50	23
	7 → 10	86	33

error bars represent the original and adjusted uncertainty in  $k_{eff}$  due to cross-section-covariance data, respectively. The uncertainty due to cross-section-covariance data for each of these experiments was reduced from  $\sim 0.6\% \Delta k/k$  to  $\sim 0.1\% \Delta k/k$ , indicating significant coverage by the

experiments active in the adjustment procedure for processes important to the fission products experiments. The initial adjustment should remove most sources of bias, except for biases caused by the fission products. The C/E ratios for all experiments changed from slightly less than one before the adjustment to slightly more than one after the adjustment is applied. However, the differences between the individual experiments are largely unchanged, indicating that the reactivity differences are due to components that were not adjusted (i.e., the fission products).

The reactivity differences after the initial  $k_{eff}$  adjustment are shown in Table XIV, along with the uncertainties in the adjusted values due to the adjusted covariance data. Although only minor changes in the reactivity differences are realized, the uncertainties are reduced by more than 50% in some cases.

IX.J.3.  $k_{eff}$  and Reactivity Data Adjustment

A subsequent data adjustment was performed including the reactivity sensitivity data from TSAR in the active adjustment. Because the nuclides other than the fission products were constrained by the other active experiments in the adjustment, only small additional changes in those cross sections were introduced by adding the reactivity data into the adjustment. The adjustments previously shown in Fig. 13 using  $k_{eff}$  data and the adjustments using both  $k_{eff}$  and reactivity are very similar, as shown in Fig. 28. The most notable difference is that the  $^{238}\text{U}(n, \gamma)$

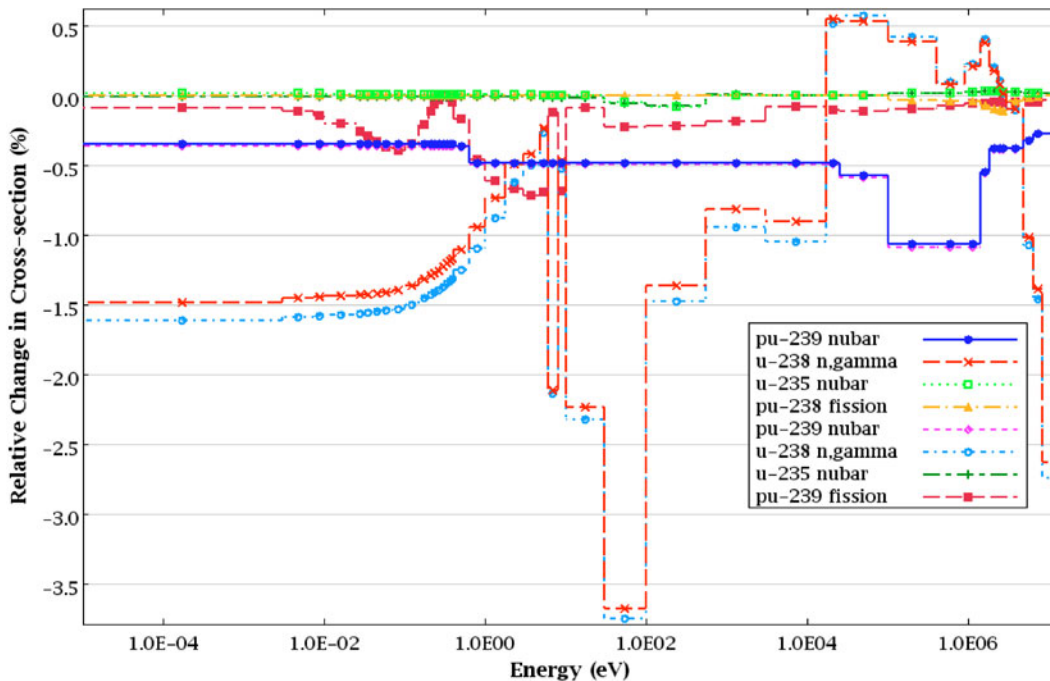


Fig. 28. Cross-section adjustments from  $k_{eff}$ -only and  $k_{eff}$  and  $\rho$  TSURFER calculations.

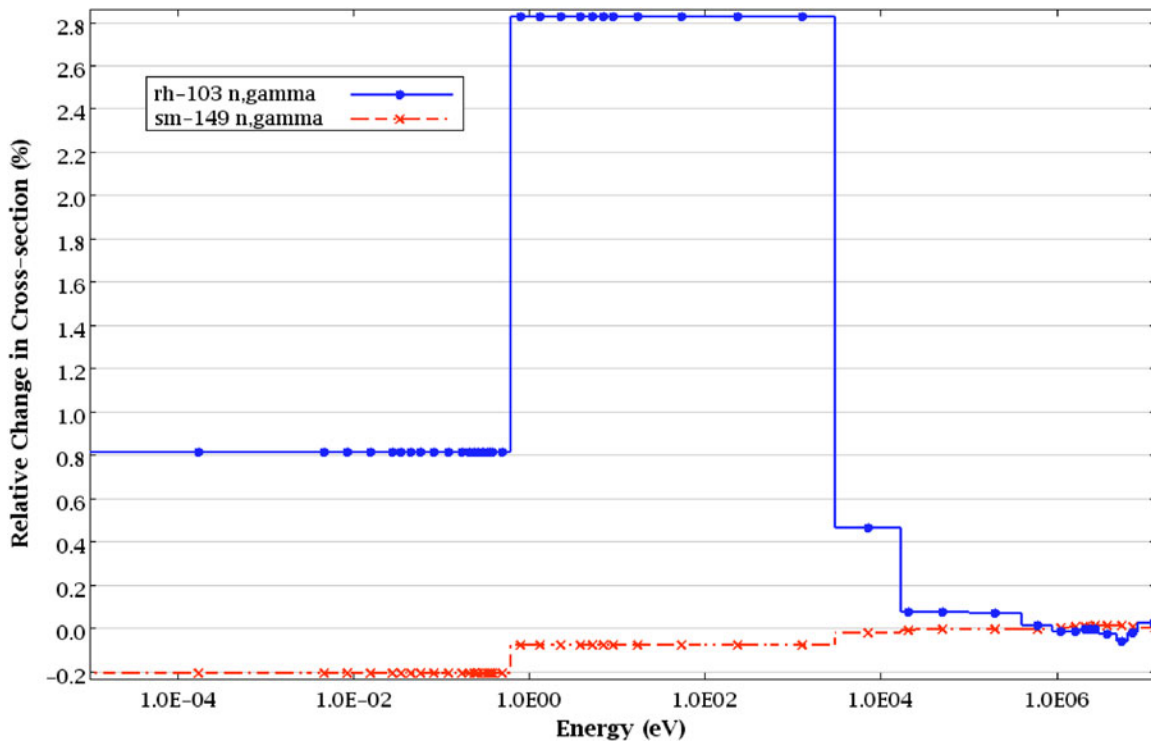


Fig. 29. Fission product cross-section adjustments from  $k_{eff}$  and  $\rho$  TSURFER calculation.

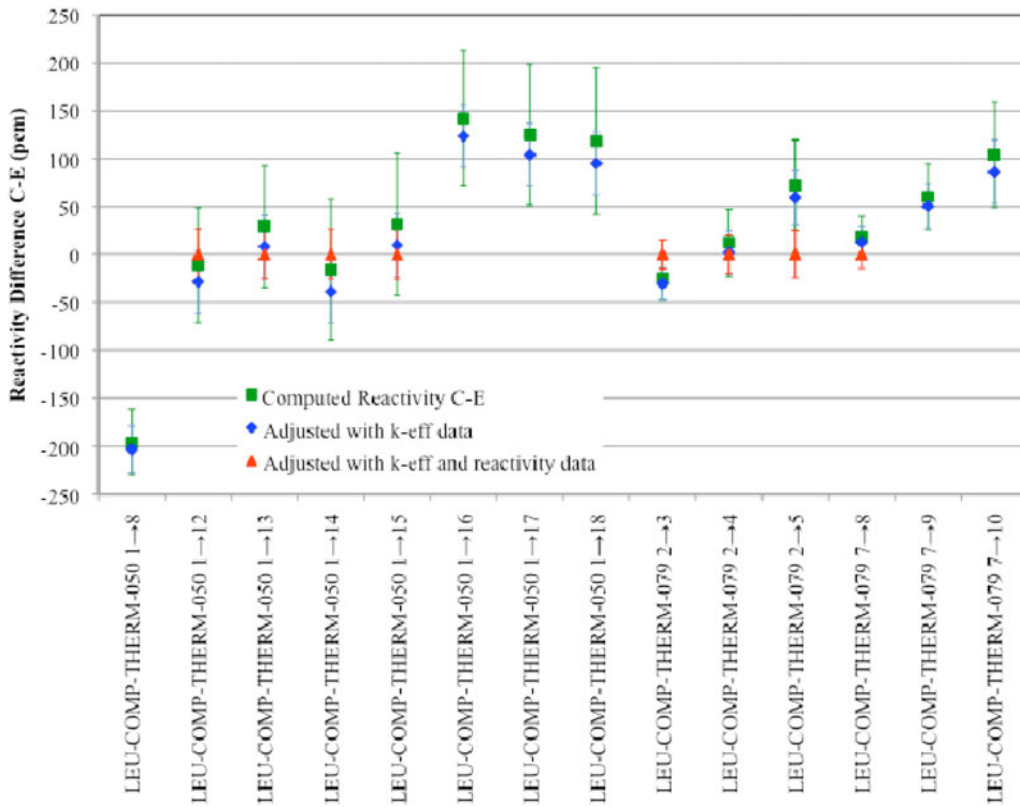


Fig. 30. Reactivity difference C/E values.

cross section is adjusted  $\sim 0.1\%$  lower in the thermal and intermediate energies. The adjustments for the fission product nuclides are shown in Fig. 29. Note that the broad uniform changes in the cross sections across the thermal- and intermediate-energy regions are due to correlations in the SCALE cross-section-covariance data for  $^{103}\text{Rh}$  and  $^{149}\text{Sm}(n, \gamma)$  reactions, which are both BLO evaluations. A small reduction in the  $^{149}\text{Sm}(n, \gamma)$  cross section and a substantial increase in the  $^{103}\text{Rh}$  cross section are observed.

The reactivity difference C/E values for LEU-COMP-THERM-050 and LEU-COMP-THERM-079 are shown in Fig. 30 for the initially computed values, the values after the initial TSURFER  $k_{eff}$  calculation, and the values after the TSURFER  $k_{eff}$  and reactivity calculation. The error bars represent a standard deviation in reactivity difference due to the initial or adjusted cross-section-covariance data for each data set, respectively. The  $\chi^2$  filter of TSURFER rejected 6 of the 14 reactivity assessments as inconsistent when they were included as experiments in the TSURFER calculation. The remaining systems were active in the data adjustment process, which produces C/E values of 0.0, with associated reduced uncertainties.

After the second adjustment, including the  $k_{eff}$  sensitivity data from the initial adjustment and the fission product reactivity sensitivity data, a slightly smaller bias with a smaller bias uncertainty was computed for the GBC-32 application.

Computational bias,  $\beta = -0.004\% \Delta k/k$

Uncertainty in the bias,  $\Delta\beta = 0.114\% \Delta k/k$

The processes that are the top 25 contributors to bias in the GBC-32 from this analysis are shown in Table XV, sorted in descending order according to their L1-norm values. The bias values are similar to those from the initial adjustment shown in Table IX, except that they now include bias values for  $^{103}\text{Rh}$  and  $^{149}\text{Sm}$  of 0.015 and  $-0.003\% \Delta k/k$ , respectively.

The energy-dependent bias for the GBC-32 for the two fission products is shown in Fig. 31. When multiplying the broad changes in the cross section by the specific sensitivity data for the GBC-32, it is evident that the bias for  $^{103}\text{Rh}$  is due primarily to the strong resonance near 1 eV.

This example has illustrated many of the unique features of TSUNAMI for sensitivity analysis and uncertainty quantification: assessment of the similarity of benchmark experiments to the targeted application; determination of computational bias, bias uncertainty, and penalties for trending analysis; and determination of computational bias and bias uncertainties through data adjustment techniques including experimental data either directly from  $k_{eff}$  benchmarks or from a pair of benchmarks with reactivity differencing.

TABLE XV

Contributions to GBC-32 Bias by Individual Nuclide-Reaction Pairs from  $k_{eff}$  and  $\rho$  TSURFER Calculation

Nuclide	Reaction	Contribution to Bias (% $\Delta k/k$ )	Fraction of L1 Norm
$^{238}\text{U}$	$n, \gamma$	$-2.25\text{E}-01^a$	$3.65\text{E}-01$
$^{239}\text{Pu}$	$\bar{\nu}$	$1.32\text{E}-01$	$2.06\text{E}-01$
$^{239}\text{Pu}$	Fission	$3.97\text{E}-02$	$6.22\text{E}-02$
$^{16}\text{O}$	Elastic	$3.22\text{E}-02$	$5.20\text{E}-02$
$^{239}\text{Pu}$	$n, \gamma$	$-2.47\text{E}-02$	$4.08\text{E}-02$
$^{235}\text{U}$	$\chi$	$2.76\text{E}-04$	$2.95\text{E}-02$
$^{239}\text{Pu}$	$\chi$	$1.02\text{E}-02$	$2.88\text{E}-02$
$^{56}\text{Fe}$	$n, \gamma$	$1.78\text{E}-02$	$2.78\text{E}-02$
$^{103}\text{Rh}$	$n, \gamma$	$1.50\text{E}-02$	$2.34\text{E}-02$
$^{238}\text{U}$	Elastic	$2.78\text{E}-03$	$2.02\text{E}-02$
$^{240}\text{Pu}$	$n, \gamma$	$-1.25\text{E}-02$	$2.00\text{E}-02$
$^{235}\text{U}$	$n, \gamma$	$3.39\text{E}-03$	$1.42\text{E}-02$
$^{235}\text{U}$	Fission	$-5.96\text{E}-03$	$1.31\text{E}-02$
$^1\text{H}$	Elastic	$-3.87\text{E}-05$	$1.19\text{E}-02$
$^{238}\text{U}$	$n, n'$	$-6.23\text{E}-03$	$1.18\text{E}-02$
$^{235}\text{U}$	Nubar	$6.89\text{E}-03$	$1.13\text{E}-02$
$^{56}\text{Fe}$	Elastic	$-6.51\text{E}-03$	$1.03\text{E}-02$
$^{238}\text{U}$	$\bar{\nu}$	$2.43\text{E}-03$	$5.02\text{E}-03$
$^{241}\text{Am}$	$n, \gamma$	$2.67\text{E}-03$	$4.87\text{E}-03$
$^{149}\text{Sm}$	$n, \gamma$	$-3.03\text{E}-03$	$4.73\text{E}-03$
$^{10}\text{B}$	$n, \alpha$	$2.87\text{E}-03$	$4.50\text{E}-03$
$^1\text{H}$	$n, \gamma$	$2.44\text{E}-03$	$3.81\text{E}-03$
$^{53}\text{Cr}$	$n, 2n$	$2.31\text{E}-03$	$3.61\text{E}-03$
$^{92}\text{Zr}$	Elastic	$2.31\text{E}-03$	$3.61\text{E}-03$
$^{241}\text{Pu}$	Fission	$-1.80\text{E}-03$	$2.94\text{E}-03$

<sup>a</sup>Read as  $-2.25 \times 10^{-1}$ .

## X. AVAILABILITY OF SENSITIVITY DATA

The validation of diverse sets of applications requires potentially thousands of data files to be maintained and organized by the user, and a growing number of these files are available through the IHECSBE. For 2009 the IHECSBE included 419 SDFs generated by ORNL using SCALE 6 with the 238-group ENDF/B-VII.0 cross-section library. Many of the files distributed with the IHECSBE were generated as part of a study published as "Application of the SCALE TSUNAMI Tools for the Validation of Criticality Safety Calculations Involving  $^{233}\text{U}$ " (Ref. 41), and primarily consist of critical configurations of  $^{233}\text{U}$ , as shown in Table XVI.

Additional input files have been generated as part of an effort jointly supported by the U.S. Department of Energy Nuclear Criticality Safety Program and the U.S. Nuclear Regulatory Commission. For this project, a new SCALE procedure was created to guide the development of Models and Derived Data (MADD). The MADD procedure requires input models to match the description

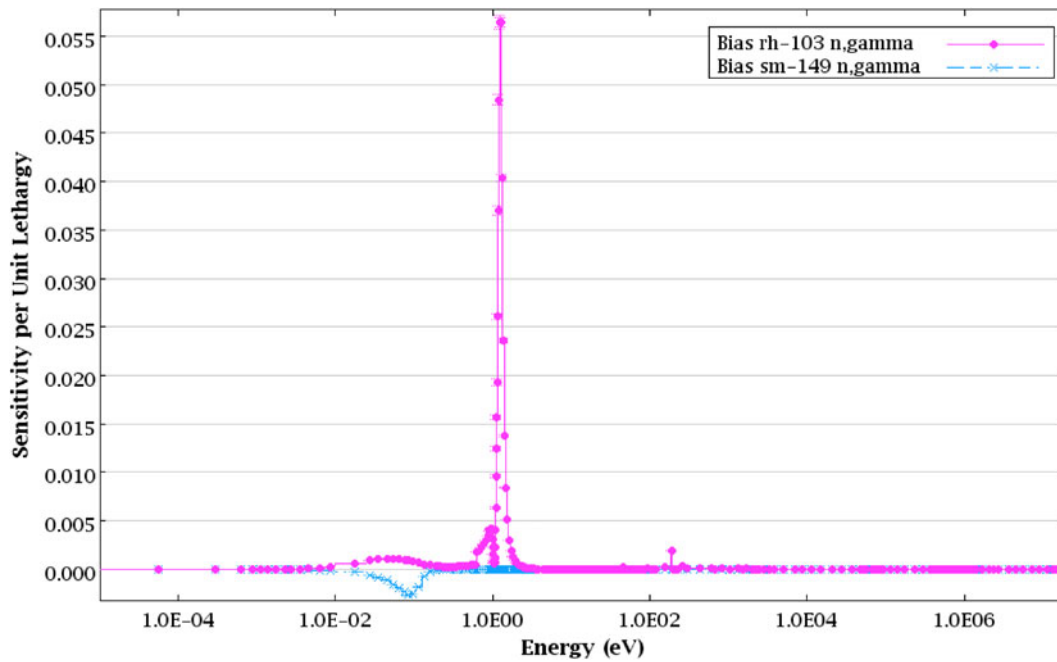


Fig. 31. Energy-dependent bias for <sup>149</sup>Sm and <sup>103</sup>Rh in GBC-32 from *k<sub>eff</sub>* and ρ TSURFER calculation.

TABLE XVI

Evaluations with TSUNAMI Sensitivity Data from ORNL/TM-2008-196\* Distributed in the 2009 IHECSBE

Evaluation	Cases
LEU-COMP-THERM-049	1-18
MIX-COMP-FAST-001	1
U233-COMP-THERM-001	2-4
U233-MET-FAST-001	1
U233-MET-FAST-002	1, 2
U233-MET-FAST-003	1, 2
U233-MET-FAST-005	1, 2
U233-MET-FAST-006	1
U233-SOL-INTER-001	1-13, 15, 17-27, 29, 31-33
U233-SOL-MIXED-001	14, 26, 30
U233-SOL-MIXED-002	3, 5, 6, 8, 9
U233-SOL-THERM-001	1-5
U233-SOL-THERM-002	1-17
U233-SOL-THERM-003	1-10
U233-SOL-THERM-004	1-8
U233-SOL-THERM-005	1, 2
U233-SOL-THERM-006	1-25
U233-SOL-THERM-008	1
U233-SOL-THERM-009	1-4
U233-SOL-THERM-011	28
U233-SOL-THERM-012	1-8
U233-SOL-THERM-013	1-21
U233-SOL-THERM-014	1-16
U233-SOL-THERM-015	1, 2, 4, 7, 10-31
U233-SOL-THERM-016	1-4, 6-33
U233-SOL-THERM-017	1-7

\*Ref. 41.

provided in Section 3 of an IHECSBE benchmark evaluation to the extent possible using multigroup cross sections and 3-D modeling with KENO V.a or KENO-VI. The models are generated by a qualified originator and independently checked by a qualified reviewer. Additionally, the sensitivity data generated through TSUNAMI calculations are rigorously checked with direct perturbation calculations to ensure that the data are accurate. Models are often refined after direct perturbation results reveal inadequate resonance self-shielding models or inadequate spatial resolution of the flux solution through the use of mesh flux accumulators. The input models and sensitivity results are accepted into the MADD archive only after they have passed this rigorous assessment of quality by the originator and reviewer. ORNL does not provide any guarantee that these models are completely free from errors, but they are believed to be of very high quality. For 2009, 170 SDFs were generated under the MADD procedure and were distributed in IHECSBE. The benchmark cases are summarized in Table XVII.

## XI. CONCLUSIONS

In SCALE 6, the TSUNAMI codes calculate the sensitivity of *k<sub>eff</sub>* or reactivity difference to variations of the neutron cross-section data on an energy-dependent, nuclide-reaction-specific basis. They also provide uncertainty quantification, using the comprehensive neutron cross-section-covariance data from SCALE 6, and use the sensitivity and uncertainty data to produce correlation

TABLE XVII  
Evaluations with MADD TSUNAMI Sensitivity  
Data Distributed in 2009 IHECSBE

Evaluation	Cases
HEU-MET-FAST-005	1-6
HEU-MET-FAST-008	1
HEU-MET-FAST-009	1, 2
HEU-MET-FAST-010	1, 2
HEU-MET-FAST-011	1
HEU-MET-FAST-013	1
HEU-MET-FAST-016	1, 2
HEU-MET-FAST-017	1
HEU-MET-FAST-018	1
HEU-MET-FAST-019	1
HEU-MET-FAST-020	1
HEU-MET-FAST-021	1
HEU-MET-FAST-024	1
HEU-MET-FAST-030	1
HEU-MET-FAST-038	1, 2
HEU-SOL-THERM-001	1-10
HEU-SOL-THERM-013	1-4
HEU-SOL-THERM-014	1-3
HEU-SOL-THERM-016	1-3
HEU-SOL-THERM-028	1-18
HEU-SOL-THERM-029	1-7
HEU-SOL-THERM-030	1-7
IEU-MET-FAST-003	1
IEU-MET-FAST-004	1
IEU-MET-FAST-005	1
IEU-MET-FAST-009	1
LEU-COMP-THERM-001	1-8
LEU-COMP-THERM-002	1-5
LEU-SOL-THERM-002	1-3
LEU-SOL-THERM-003	1-9
LEU-SOL-THERM-004	1-7
MIX-COMP-THERM-001	1-4
MIX-COMP-THERM-004	1-11
PU-MET-FAST-001	1
PU-MET-FAST-002	1
PU-MET-FAST-006	1
PU-MET-FAST-008	1
PU-MET-FAST-010	1
PU-MET-FAST-018	1
PU-MET-FAST-022	1
PU-MET-FAST-023	1
PU-MET-FAST-024	1
PU-SOL-THERM-001	1-6
PU-SOL-THERM-002	1-7
PU-SOL-THERM-003	1-8
PU-SOL-THERM-004	1-13

coefficients and other relational parameters that quantify the similarity of benchmark experiments to application systems for code validation purposes. Bias and bias uncertainties are quantified using parametric trending analysis or data adjustment techniques, providing detailed assessments of sources of biases and their uncertainties

and quantifying gaps in experimental data available for validation. An example of the GBC-32 shipping cask has demonstrated many of these techniques.

## REFERENCES

1. "SCALE: A Modular Code System for Performing Standardized Computer Analyses for Licensing Evaluation," Version 6, Vols. I-III, ORNL/TM-2005/39, Oak Ridge National Laboratory (Jan. 2009).
2. S. GOLUOGLU, L. M. PETRIE, Jr., M. E. DUNN, D. F. HOLLENBACH, and B. T. REARDEN, "Monte Carlo Criticality Methods and Analysis Capabilities in KENO," *Nucl. Technol.*, **174**, 214 (2011).
3. ANSI/ANS-8.1-1998, "American National Standard for Nuclear Criticality Safety in Operations with Fissionable Materials Outside Reactors," American Nuclear Society, La Grange Park, Illinois.
4. ANSI/ANS-8.24-2007, "American National Standard for Validation of Neutron Transport Methods for Nuclear Criticality Safety Calculations," American Nuclear Society, La Grange Park, Illinois.
5. B. L. BROADHEAD, B. T. REARDEN, C. M. HOPPER, J. J. WAGSCHAL, and C. V. PARKS, "Sensitivity- and Uncertainty-Based Criticality Safety Validation Techniques," *Nucl. Sci. Eng.*, **146**, 340 (2004).
6. J. J. LICHTENWALTER et al., "Criticality Benchmark Guide for Light-Water-Reactor Fuel in Transportation and Storage Packages," NUREG/CR-6361, ORNL/TM-13211, Oak Ridge National Laboratory (1997).
7. P. R. BEVINGTON, *Data Reduction and Error Analysis for the Physical Sciences*, McGraw-Hill Book Company, New York (1969).
8. E. M. OBLow, "Sensitivity Theory from a Differential Viewpoint," *Nucl. Sci. Eng.*, **59**, 187 (1976).
9. W. M. STACEY, Jr., "Variational Estimates and Generalized Perturbation Theory for the Ratios of Linear and Bilinear Functionals," *J. Math. Phys.*, **13**, 1119 (1972); see also W. M. STACEY, Jr., "Variational Estimates of Reactivity Worths and Reaction Rate Ratios in Critical Nuclear Reactors," *Nucl. Sci. Eng.*, **48**, 444 (1972).
10. L. N. USACHEV, "Perturbation Theory for the Breeding Ratio and for Other Number Ratios Pertaining to Various Reactor Processes," *J. Nucl. Energy A/B*, **18**, 571 (1964).
11. A. GANDINI, "A Generalized Perturbation Method for Bilinear Functionals of the Real and Adjoint Neutron Fluxes," *J. Nucl. Energy*, **21**, 755 (1967).
12. A. HARA, T. TAKEDA, and Y. KIKUCHI, "SAGEP: Two-Dimensional Sensitivity Analysis Code Based on Generalized Perturbation Theory," JAERI-M 84-027, Japan Atomic Energy Research Institute (1984).
13. M. L. WILLIAMS, B. L. BROADHEAD, and C. V. PARKS, "Eigenvalue Sensitivity Theory for Resonance-Shielded Cross Sections," *Nucl. Sci. Eng.*, **138**, 177 (2001).

14. P. R. BEVINGTON, *Data Reduction and Error Analysis for the Physical Sciences*, McGraw-Hill Book Company, New York (1969).
15. "ENDF-6 Formats Manual: Data Formats and Procedures for the Evaluated Nuclear Data File ENDF/B-VI and ENDF/B-VII," ENDF-102, Brookhaven National Laboratory (2009).
16. B. T. REARDEN, "Perturbation Theory Eigenvalue Sensitivity Analysis with Monte Carlo Techniques," *Nucl. Sci. Eng.*, **146**, 367 (2004).
17. M. L. WILLIAMS, J. C. GEHIN, and K. T. CLARNO, "Sensitivity Analysis of Reactivity Responses Using One-Dimensional Discrete Ordinates and Three-Dimensional Monte Carlo Methods," *Proc. Topl. Mtg. Reactor Physics: Advances in Nuclear Analysis and Simulation (PHYSOR-2006)*, Vancouver, British Columbia, Canada, September 10–14, 2006, C135, American Nuclear Society (2006) (CD-ROM).
18. M. L. WILLIAMS, "Sensitivity and Uncertainty Analysis for Eigenvalue-Difference Responses," *Nucl. Sci. Eng.*, **155**, 18 (2007).
19. "International Handbook of Evaluated Criticality Safety Benchmark Experiments," NEA/NSC/DOC(95)03, Organisation for Economic Co-operation and Development/Nuclear Energy Agency (Sep. 2009).
20. T. T. IVANOVA, M. N. NIKOLAEV, K. F. RASKACH, E. V. ROZHNIKIN, and A. M. TSIBOULIA, "Influence of the Correlations of Experimental Uncertainties on Criticality Prediction," *Nucl. Sci. Eng.*, **145**, 97 (2003).
21. L. WILLIAMS and B. T. REARDEN, "SCALE-6 Sensitivity/Uncertainty Methods and Covariance Data," *Nucl. Data Sheets*, **109**, 12, 2796 (2008).
22. D. WIARDA and M. E. DUNN, "PUFF-IV: A Code for Processing ENDF Uncertainty Data into Multigroup Covariance Matrices," ORNL/TM-2006/147, Oak Ridge National Laboratory (2006).
23. N. M. LARSON, L. C. LEAL, H. DERRIEN, G. ARBANAS, R. O. SAWYER, and D. WIARDA, "A Systematic Description of the Generation of Covariance Matrices," *Proc. Topl. Mtg. Reactor Physics: Advances in Nuclear Analysis and Simulation (PHYSOR-2006)*, Vancouver, British Columbia, Canada, September 10–14, 2006, C061, American Nuclear Society (2006) (CD-ROM).
24. R. LITTLE et al., "Low-Fidelity Covariance Project," *Nucl. Data Sheets*, **109**, 12, 2828 (2008).
25. M. L. WILLIAMS, B. L. BROADHEAD, M. E. DUNN, and B. T. REARDEN, "Approximate Techniques for Representing Nuclear Data Uncertainties," *Proc. Eighth Int. Topl. Mtg. Nuclear Applications and Utilization of Accelerators (ACCAPP '07)*, Pocatello, Idaho, July 30–August 2, 2007 (2007).
26. S. F. MUGHABGHAB, *Atlas of Neutron Resonances: Resonance Parameters and Thermal Cross Sections*, Elsevier, Amsterdam (2006).
27. M. T. PIGNI, M. HERMAN, and P. OBLOŽINSKÝ, "Extensive Set of Cross-Section Covariance Estimates in the Fast Neutron Region," *Nucl. Sci. Eng.*, **162**, 25 (2009).
28. D. ROCHMAN, M. HERMAN, P. OBLOZINSKY, and S. F. MUGHABGHAB, "Preliminary Cross Section and Nubar Covariances for WPEC Subgroup 26," BNL-77407-2007-IR, Brookhaven National Laboratory (2007).
29. T. KAWANO, P. TALOU, P. G. YOUNG, G. HALE, M. B. CHADWICK, and R. C. LITTLE, "Evaluation of Covariances for Actinides and Light Elements at LANL," *Nucl. Data Sheets*, **109**, 12, 2817 (2008).
30. G. HALE, "Covariances from Light-Element R-Matrix Analyses," *Nucl. Data Sheets*, **109**, 12, 2812 (2008).
31. L. C. LEAL, D. WIARDA, B. T. REARDEN, and H. DERRIEN, "<sup>233</sup>U Cross-Section and Covariance Data Update for SCALE 5.1 Libraries," ORNL/TM-2007/115, Oak Ridge National Laboratory (Feb. 2008).
32. S. F. MUGHABGHAB, "Thermal Neutron Capture Cross Sections Resonance Integrals and G-Factors," INDC (NDS)-440, International Atomic Energy Agency (Feb. 2003).
33. B. L. BROADHEAD and J. J. WAGSCHAL, "The Fission Spectrum Uncertainty," *Proc. PHYSOR 2004—The Physics of Fuel Cycles and Advanced Nuclear Systems: Global Developments*, Chicago, Illinois, April 25–29, 2004, 95821, American Nuclear Society (2004) (CD-ROM).
34. ANSI/ANS-8.17, "American National Standard for Criticality Safety Criteria for the Handling, Storage, and Transportation of LWR Fuel Outside Reactors," American Nuclear Society, La Grange Park, Illinois (1984).
35. H. R. DYER and C. V. PARKS, "Recommendations for Preparing the Criticality Safety Evaluation of Transport Packages," NUREG/CR-5661, ORNL/TM-11936, Oak Ridge National Laboratory (1997).
36. Y. YEIVIN, J. J. WAGSCHAL, J. H. MARABLE, and C. R. WEISBIN, "Relative Consistency of ENDF/B-IV and -V with Fast Reactor Benchmarks," *Proc. Int. Conf. Nuclear Cross Sections for Technology*, J. L. FOWLER, C. H. JOHNSON, and C. D. BOWMAN, Eds., NBS SP 594 (1980).
37. B. T. REARDEN, W. J. ANDERSON, and G. A. HARMS, "Use of Sensitivity and Uncertainty Analysis in the Design of Reactor Physics and Criticality Benchmark Experiments for Advanced Nuclear Fuel," *Nucl. Technol.*, **151**, 133 (2005).
38. J. C. WAGNER, "Computational Benchmark for Estimation of Reactivity Margin from Fission Products and Minor Actinides in PWR Burnup Credit," NUREG/CR-6747, ORNL/TM-2000/306, Oak Ridge National Laboratory (Oct. 2001).
39. D. E. MUELLER and B. T. REARDEN, "Sensitivity Coefficient Generation for a Burnup Credit Cask Model Using TSUNAMI-3D," *Proc. NCSD Topl. Mtg.*, Knoxville, Tennessee, September 19–22, 2005, American Nuclear Society (2005) (CD-ROM).
40. *International Handbook of Evaluated Criticality Safety Benchmark Experiments*, NEA/NSC/DOC(95)03, Organisation for Economic Co-operation and Development—Nuclear Energy Agency (2008).
41. D. E. MUELLER, B. T. REARDEN, and D. F. HOLLENBACH, "Application of the SCALE TSUNAMI Tools for the Validation of Criticality Safety Calculations Involving <sup>233</sup>U," ORNL/TM-2008-196, Oak Ridge National Laboratory (Jan. 2009).